# Charge inversion and DNA condensation by multivalent ions

# Charge inversion and DNA condensation by multivalent ions

**Proefschrift**

ter verkrijging van de graad van doctor
aan de Technische Universiteit Delft,
op gezag van de Rector Magnificus prof.dr.ir. J.T. Fokkema,
voorzitter van het College voor Promoties,
in het openbaar te verdedigen op dinsdag 19 december 2006 om 12.30 uur

door


## Koen BESTEMAN

natuurkunding ingenieur
geboren te Den Haag.

Dit proefschrift is goedgekeurd door de promotor:
Prof. dr. C. Dekker

Toegevoegd promotor:
Dr. S.G. Lemay

Samenstelling van de promotiecommissie:

| | |
|---|---|
| Rector Magnificus, | voorzitter |
| Prof. dr. C. Dekker | Technische Universiteit Delft, promotor |
| Dr. S.G. Lemay | Technische Universiteit Delft, toegevoegd promotor |
| Prof. dr. ir. J.E. Mooij | Technische Universiteit Delft |
| Prof. dr. J. Lyklema | Wageningen Universiteit |
| Prof. dr. H. Schiessel | Universiteit Leiden |
| Prof. dr. A. Travesset | Iowa State University, USA |
| Dr. ir. S.J.T. van Noort | Universiteit Leiden |
| Prof. dr. ir. G.E.W. Bauer | Technische Universiteit Delft, reservelid |


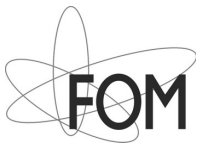


*printed by:* Gildeprint Drukkerijen, www.gildeprint.nl

Casimir Ph.D. Series, Delft-Leiden, 2006
ISBN-10: 90-8593-022-7
ISBN-13: 978-90-8593-022-8

Keywords: charge inversion, DNA condensation, multivalent ions, ion correlations, atomic force microscope, magnetic tweezers

Cover design: Koen Besteman and Thijn van der Heijden



Printed in the Netherlands

# Contents

# Chapter 1

# Introduction

This thesis describes the results of a four-year experimental study on the phenomena of charge inversion and DNA condensation induced by multivalent ions. This first chapter gives an introduction on electrostatic screening in electrolytes in general and by multivalent ions in particular. The chapter ends with a short outline of the thesis.

*"Overcharging, also called charge reversal or charge inversion, is the occurrence of electric double layers in which, [...] there is more countercharge than charge on the surface." "For the interpretation of this phenomenon disparate explanations have been forwarded and elaborated that, briefly, can be distinguished as 'chemical' (specific adsorption,...) and 'physical' (ion correlations,...)." "In the literature, there is not only a disparity between the 'chemical' and 'physical' approach with respect to the underlying science but also an almost complete ignorance of each other's achievements." "This is an unfortunate situation because in real systems 'chemical' and 'physical' phenomena can both occur so that relevant insights and relevant experiments have been overlooked."*

From J. Lyklema, *Overcharging, Charge reversal: Chemistry or Physics?*, Colloids and Surfaces A, *in press*

## 1.1 The electric double layer

Charged particles in solution and the interactions between them are a major focus of such diverse fields as biophysics, colloid science and polymer physics. For example, most of the proteins and nucleic acids contained in a cell are highly charged. The interactions between these molecules, determined in large part by electrostatics, form the basis of life.

Electrostatics in solution is however more subtle than in vacuum. The charge of an object is normally screened by mobile ions in the surrounding electrolyte. Coions (ions with the same sign of charge) are repelled from the surroundings of the object. Counterions (ions with opposite charge) are electrostatically attracted to the object but gain entropy by moving away from it. Their spatial distribution is a compromise between these two opposite tendencies. The resulting arrangement of screening charges around the object is known as the electric double layer. Its structure has a major impact on interactions between charged objects in solution. It is therefore crucial to understand it in detail before more complicated cellular processes such as DNA compaction can be fully understood.

### 1.1.1 Mean-field theory

The screening ions around a charged object have been described in a mean-field approach since the pioneering work of Debye, Gouy and Chapman [1–3]. The point-like ions are assumed to distribute themselves in the mean potential resulting from the object and all ions. Combining the Poisson equation and the Boltzmann distribution, both of which relate the charge and potential distributions, results in the so-called Poisson-Bolzmann (PB) equation (see for example [4])

$$\nabla^2\varphi(\boldsymbol{r}) = -\frac{e}{\epsilon\epsilon_0}\sum_i n_i^0 Z_i \exp\left(\frac{-Z_i e\varphi(\boldsymbol{r})}{kT}\right), \tag{1.1}$$

where $\varphi(\boldsymbol{r})$ is the electrostatic potential at position $\boldsymbol{r}$, $Z_i$ is the valence (including sign) of ion species i, $n_i^0$ is the number density at a reference position (for example in the bulk) of ion species $i$, $-e$ is the electron charge, $\epsilon_0$ is the permitivity of free space, $\epsilon$ is the dielectric constant of the solvent, and $kT$ is the thermal energy. In this model the ions form a diffuse charged cloud that screens the charge of the object, the so-called diffuse layer.

For low surface-charge densities or far from any charged object, where the electrostatic potential energy with respect to the bulk solution is smaller than the thermal energy $kT$, the PB-equation can be linearized. In the presence of a

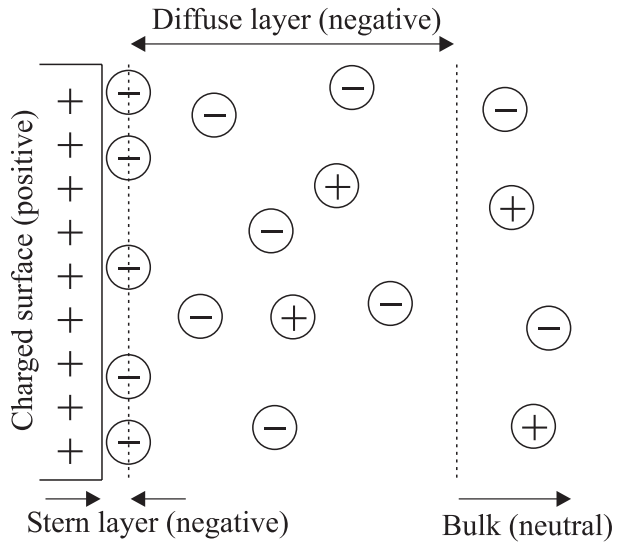


**Figure 1.1:** Illustration of the electric double layer at a positively charged surface in the presence of a monovalent salt.

bulk electrolyte (excess positive and negative ions) this results in the so-called Debye-Hückel approximation [1]. The resulting potential decays exponentially with distance from the surface towards the bulk value. The characteristic decay length, the Debye length $\lambda_d$, is given by

$$\lambda_d = \left( \sum_i \frac{n_i^\infty Z_i^2 e^2}{\epsilon \epsilon_0 kT} \right)^{-1/2}, \tag{1.2}$$

where $n_i^\infty$ is the number density of ion specie $i$ in the bulk. The Debye length is a measure for the thickness of the diffuse layer.

At smaller distances from charged surfaces, where the electrostatic potential energy with respect to the bulk is larger than $kT$, this linearization does not hold and the potential distribution departs from simple exponential decay. The full PB equation can only be solved analytically for simple cases such as a charged plane in a symmetrical electrolyte (where counterions and coions have the same valence). In this case a second characteristic length scale comes into play, the Gouy-Chapman length $l_{gc}$, that is inversely proportional to the surface charge. $l_{gc}$ is a measure of how far the ions can move away from an unscreened, charged planar surface given thermal energy $kT$.

The PB-equation breaks down near such highly charged surfaces that the Gouy-Chapman length becomes smaller than the ion size. This corresponds to a pronounced accumulation of counterions at a distance from the surface that is smaller than their actual radius, which is unphysical. To account for this

breakdown due to finite ion size, Stern suggested that the center of the ions should be constrained to remain a finite distance from the surface [5]. This resulted in the introduction of what is now known as the Stern layer in models of the double layer. The Stern layer consists of a two-dimensional layer of ions located a distance $d_s$ from the surface, where $d_s$ should be at least as large as the ionic radius. A schematic picture of the electric double layer around a charged surface that consists of a Stern layer and a diffuse layer is shown in Fig. 1.1.

### 1.1.2 Surface geometry

The delicate interplay between electrostatics and entropy that gives rise to the electric double layer is influenced by the geometry of the charged object. We consider three different object geometries, planar, spherical, and cylindrical, first concentrating on solutions containing only counterions.

In the case of a planar charged surface with only counterions present, the electrostatic attraction of the counterions to the surface dominates over the entropy gained by moving them to infinity. Gouy and Chapman solved the PB-equation for this case at the beginning of the twentieth century [2, 3] and showed that the counterions concentrations decay monotonically with distance from the surface, with a large part of the ions residing within a distance $l_{gc}$ from the surface.

The opposite holds for a charged spherical object in the presence of only counterions. In this case, the entropy gain for moving a counterion away from the surface always exceeds the electrostatic attraction to the surface. Therefore all counterions move away from the surface towards infinity.

For an infinitely-long charged cylindrical object (which is important in biology since it resembles the shape of a DNA molecule) in the presence of only counterions, Manning showed that there is an interesting balance between entropy and electrostatics. For low surface-charge densities, the entropic free energy gained by a counterion by moving away from the surface towards infinity exceeds the electrostatic attraction to the surface. But when the surface-charge density becomes higher than a threshold value, electrostatic attraction instead dominates over the entropy gain. Therefore, for highly charged cylindrical objects, part of the counterions become "Manning condensed"on the surface while the remaining counterions reside away from the surface [6].

The above holds in the presence of only counterions. In the presence of a bulk electrolyte (excess positive and negative ions), electrostatic interactions are screened within distances of the order of the Debye length. The geometry of the object in such case is only relevant when its radius of curvature is smaller than the Debye length, otherwise it can be approximated by a flat plane. Note that a

DNA molecule has a radius of only 1 nm and therefore its cylindrical geometry needs to be accounted for in most circumstances.

### 1.1.3 Breakdown of mean-field theory

For moderate surface charge and low-valence electrolytes, the mean-field approach gives a good working description of the electric double layer. But in more complicated situations, such as high surface charge and high-valence ions, this microscopic picture of screening starts to break down and several experimental observations remain poorly understood. In this study we focus on two startling phenomena that are induced by multivalent ions: the sign-reversal of the effective charge of an object known as charge inversion, and the electrostatic attraction between like-charged objects, in particular between DNA molecules.

## 1.2 Charge inversion

Charge inversion occurs when the total charge of screening ions in the Stern layer exceeds that of the object being screened, thereby inverting the sign of the effective surface charge (charge of the surface plus charge of ions in the Stern layer). Charge inversion is an important phenomenon since it can dramatically change the interaction between charged objects such as colloid particles and most biomolecules, turning attraction into repulsion and vise versa. It has been observed experimentally using electrophoresis and force spectroscopy [7–9].

Interestingly, charge inversion cannot be described in the framework of a purely electrostatic mean-field theory, which predicts that the absolute value of the electrostatic potential decreases monotonically away from a charged surface towards the bulk value. Instead it was originally explained by specific adsorption of multivalent ions (or multivalent-ion complexes) to the charged surface [7, 8, 10]. In these models, specific interactions induce an additional affinity between the multivalent ions and the surface. As a consequence more ions can be positioned at the surface than needed to entirely screen the surface charge, leading to charge inversion.

It has since been suggested that charge inversion can also occur in the absence of chemical specificity. The corresponding theoretical description takes into account spatial correlations between multivalent ions at the charged surface, which are ignored in mean field theories [11]. It is argued that, even at room temperature, multivalent ions assemble into a highly ordered structure on the surface being screened. This structure resembles a two-dimensional Wigner crystal but exhibits only short-range order [12] (Fig. 1.2(a)). For low bulk concentrations of

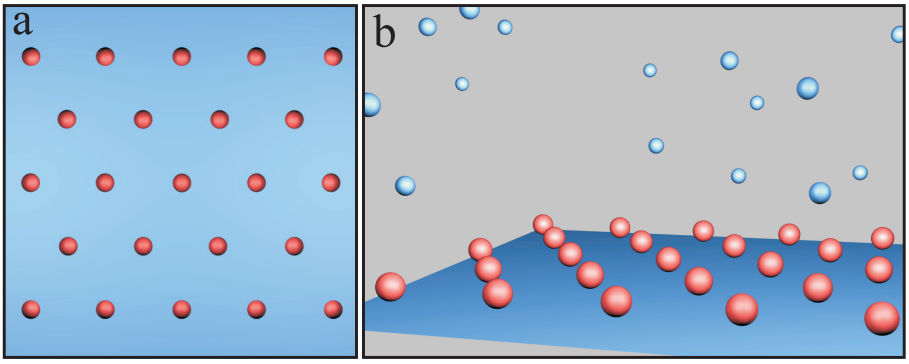


**Figure 1.2:** (a) Illustration of a charged surface with a Wigner crystal structure of multivalent counterions. (b) Illustration of charge inversion in the SCL model. The diffuse layer mostly consists of coions (light balls away from the surface).

multivalent ions, only part of the surface charge is screened by this strongly correlated liquid (SCL). At a certain bulk concentration, the so-called charge-inversion concentration, the SCL screens the totality of the surface charge. Above this concentration more ions are packed in the SCL than needed to screen the surface charge and charge inversion has occurred (Fig. 1.2(b)).

At the start of this thesis research, most experimental observations of charge inversion were seemingly adequately explained by specific interactions between ions and the surface. We set out to directly probe the charge-inversion concentration and its dependence on several system parameters in order to test the prediction that charge inversion can be a consequence of correlations and in particular to test the SCL model described above.

## 1.3 DNA condensation

In every human cell, about 2 m of DNA is packed in the nucleus that has a diameter of order 10 $\mu$m. The fact that DNA in solution is one of the most highly charged polymers known greatly complicates this tight packing. In somatic cells (as opposed to germline cells) the human genome is packed into chromosomes by wrapping the DNA around positively charged proteins called histones [13]. This very complicated system leaves the possibility of gene expression while achieving a great degree of compaction. Even more dramatically, during spermiogenesis (last stage in the formation of a sperm cell), histones are replaced by small arginine-rich proteins, called protamines, resulting in highly-packed, transcriptionally-inactive chromatin where the DNA strands are positioned side by side [14, 15]. Despite their importance, relatively little is known about the structure and dynamics of

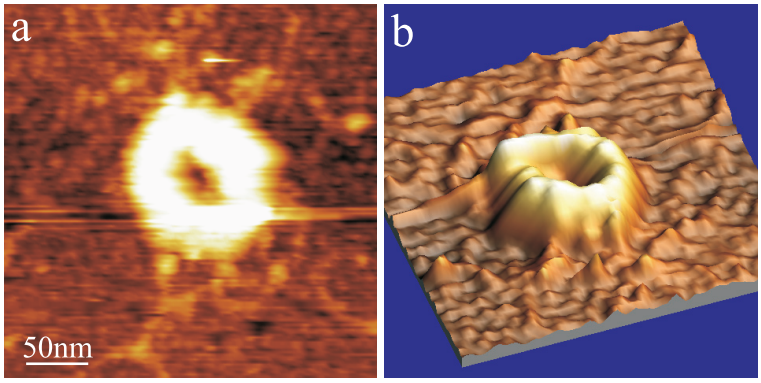


**Figure 1.3:** Atomic Force Microscopy images (same image in 2D (a) and 3D (b)) of a torroidal shaped DNA condensate obtained with 0.25 mM spermidine on oxygen-plasma-treated graphite.

these chromatin structures *in vivo*

Surprisingly, DNA compaction is also observed *in vitro* in the presence of small amounts of multivalent cations [16]. The packing density and condensate structure observed *in vitro* by multivalent ions [17, 18] (Fig. 1.3) is very similar to that observed *in vivo* in sperm cells by protamines [19, 20] and in certain viruses [21]. In addition, DNA compaction occurs in the presence of the naturally occurring polyamines spermine [22] and spermidine [17], which have been implicated in a broad range of cellular processes and are believed to be involved in DNA compaction *in vivo* [23, 24]. As a result, this DNA condensation by multivalent ions, a form of like-charge attraction, has received a lot of attention the last few decades both experimentally and theoretically.

In addition to bettering our understanding of chromatin structure and like-charge attraction, a potential application for DNA condensation by polyamines and other condensing agents lies in gene delivery. Here, a certain gene has to be transported into a target cell for therapeutic reasons. To pass by the negatively charged cell wall using endocytosis, the DNA needs to be compacted and its negative effective charge has to be reduced significantly. Is has been shown experimentally that both these criteria can be met by condensing DNA with a range of (positively charged) condensing agents [25].

For DNA condensation by multivalent ions to occur, not only does the electrostatic repulsion between the like-charged DNA molecules have to be reduced by screening, but also an attraction has to be induced at short range. It is mostly believed that positional correlations between counterions at the DNA surface are responsible for this attraction [26–32]. Such positional correlations result in an alternating charge pattern along the DNA molecule, resulting in a short-range

attractive force.

There are several theoretical proposals for the origin of the positional correlations between the multivalent ions at the DNA surface. Repulsive interactions between multivalent counterions at the DNA surface (in the Stern layer), resulting in the formation of a SCL, are one possibility [27, 29]. It has also been argued that dynamic fluctuations of multivalent counterions can result in positional correlations and attractive forces, in a manner reminiscent of van der Waals forces [30, 31]. Lastly, they could be caused by the helical structure of the DNA [32]. If for example multivalent ions have a high affinity to position themselves in the major groove of the DNA, charge separation of the negative phosphate groups on the backbone and the positive ions takes place, resulting in a periodic modulation of the charge.

Despite a large body of splendid experimental and theoretical research on DNA condensation by cationic species, both the microscopic mechanism driving DNA condensation and the condensation dynamics remain unclear. This is in part due to the small length and time scales involved. Most of our experimental knowledge on DNA condensation comes from bulk measurements using techniques such as light scattering and electron microscopy [16, 33]. These techniques only probe such microscopic interactions and short-time dynamics in an indirect manner.

Recent developments in single-molecule approaches have opened new ways to study the condensation of a single DNA molecule in real time and learn about the dynamics of the process. In addition, a recent theoretical proposal on the microscopic mechanism driving DNA condensation was made, that is particularly amenable to experimental testing by relating charge inversion to DNA condensation [34]. It has previously been observed that DNA de-condenses at high multivalent-ion concentration [35]. Nguyen *et al* [34] proposed that this so-called reentrant condensation is caused by charge inversion of the DNA. Above the charge inversion concentration the net charge of the DNA increases, eventually causing the electrostatic repulsion to overcome the short range attraction leading to reentrant condensation. Both charge inversion and reentrant condensation, as well as their putative correspondence, are phenomena that are amenable to direct experimental testing.

## 1.4 This thesis

This thesis describes experimental research on charge inversion and DNA condensation that was performed by several researchers including myself over a time

span of four years in the Molecular Biophysics Group at the Delft University of Technology. The thesis consists of a collection of published and "to be published" articles. Since every chapter is presented as a stand-alone article, some repetition occurs between chapters.

Experimental research on charge inversion of macroscopic surfaces by different multivalent ions is described in **chapters 2** and **3**. We investigated charge inversion by measuring forces between charged surfaces in the presence of multivalent ions using an Atomic Force Microscope (AFM). We directly probed the sign of the effective surface charge and thereby the charge-inversion concentration. Our results support the hypothesis that spatial correlations between multivalent ions at the charged surface can drive charge inversion.

We then steered our research towards DNA condensation. We first visualized DNA condensates attached to mica surfaces using AFM, a widely used method for probing the condensate structure. To our surprise, most structures of DNA condensates that we observed on mica were two-dimensional and didn't resemble the typical torroidal and rod-like structures observed by other methods. **Chapter 4** of this thesis describes our findings concerning the influence of the imaging surface in AFM on the morphology of DNA condensed with multivalent ions.

We studied the condensation dynamics of DNA by employing a single-molecule technique, magnetic tweezers. For the first time we observed a single DNA molecule condense in real time in the presence of multivalent cations. Our findings, discussed in **chapter 5**, indicate that the condensation of a DNA molecule under tension is nucleation limited and that the transition state consists of a loop. This in contrast to previous explanations of experimental observations on the condensation of a single DNA molecule, where the condensation was interpreted as a transition between equilibrium phases.

In **chapter 6** we experimentally relate DNA condensation to charge inversion, coming full circle to our measurements of chapters 2 and 3. For the first time we observed charge inversion of multivalent-ions-induced DNA condensates using dynamic light scattering. With the magnetic tweezers we studied reentrant condensation on the single-molecule level and compared the results to the charge-inversion data. We propose a model for our observations that is based on the nucleation-limited behavior that we observed.

Finally, we observed the real-time condensation of a single DNA molecule induced by protamines. **Chapter 7** describes our findings on the influence of protamine concentration and twist on the condensation, and the charge inversion of the DNA-protamine complex.

# Bibliography


[1] P. Debye and E. Hückel, Phys. Z. **24**, 185 (1923).

[2] G. Gouy, J. Phys. Radium **9**, 457 (1910).

[3] D. L. Chapman, Phil. Mag. **25**, 475 (1913).

[4] J. Lyklema, Fundamentals of Interface and Colloid Science **Volume I** (1991).

[5] O. Stern, Z. Elektrochem. **30**, 508 (1924).

[6] G. S. Manning, J. Chem. Phys. **51**, 924 (1969).

[7] R. O. James and T. W. Healey, J. Coll. Int. Sci. **40**, 42 (1972); J. Coll. Int. Sci. **40**, 53 (1972); J. Coll. Int. Sci. **40**, 65 (1972).

[8] R. M. Pashley, J. Coll. Int. Sci. **102**, 23 (1984).

[9] A. Martín-Molina, M. Quesada-Pérez, F. Galisteo-González, and R. Hidalgo-Álvarez, J. Chem. Phys. **118**, 4183 (2003).

[10] K. B. Agashe and J. R. Regalbuto, J. Coll. Int. Sci. **185**, 174 (1996).

[11] For comprehensive reviews see A. Yu. Grosberg, T. T. Nguyen, and B. I. Shklovskii, Rev. Mod. Phys. **74**, 329 (2002); Y. Levin, Rep. Prog. Phys. **65**, 1577 (2002); M. Quesada-Pérez *et al.*, Chem. Phys. Chem. **4**, 234 (2003).

[12] B. I. Shklovskii, Phys. Rev. E **60**, 5802 (1999).

[13] B. Alberts, A. Johnson, J. Lewis, M. Raff, K. Roberts, and P. Walter, *Molecular Biology of the Cell* (Garland Science, New York, 4th edition, 2002).

[14] J. D. Lewis, Y. Song, M. E. de Jong, S. M. Bagha, and J. Ausió, Chromosoma **111**, 473 (2003).

[15] W. S. Ward and D. S. Coffey, Biol. Reprod. **44**, 569 (1991).

[16] V. A. Bloomfield, Biopolymers **44**, 269 (1997).

[17] L. C. Gosule and J. A. Schellman, Nature **259**, 333 (1976).

[18] N. V. Hud and K. H. Downing, Proc. Natl. Acad. Sci. USA **98**, 14925 (2001).

[19] N. V. Hud, M. J. Allen, K. H. Downing, J. Lee, and R. Balhorn, Biochem. Biophys. Res. Commun. **193**, 1347 (1993).

[20] M. J. Allen, E. M. Bradbury, and R. Balhorn, Nucleic Acids Res. **25**, 2221 (1997).

[21] M. E. Cerritelli, N. Cheng, A. H. Rosenberg, C. E. McPherson, F. P. Booy, and A. C. Steven, Cell **91**, 271 (1997).

[22] D. K. Chattoraj, L. C. Gosule, and J. A. Schellman, J. Mol. Biol. **121**, 327 (1978).

[23] T. Thomas and T. J. Thomas, Cell. Mol. Life Sci. **58**, 244 (2001).

[24] D. Hougaard, Int. Rev. Cytol. **138**, 51 (1992).

[25] V. Vijayanathan, T. Thomas, and T. J. Thomas, Biochemistry **41**, 14085 (2002).

[26] W. M. Gelbart, R. F. Bruinsma, P. A. Pincus, and V. A. Parsegian, Physics Today **53**, 38 (2000).

[27] I. Rouzina and V. A. Bloomfield, J. Phys. Chem. **100**, 9977 (1996).

[28] N. Grønbech-Jensen, R. J. Mashl, R. F. Bruinsma, and W. M. Gelbart, Phys. Rev. Lett. **78**, 2477 (1997).

[29] B. I. Shklovskii, Phys. Rev. Lett. **82**, 3268 (1999).

[30] F. Oosawa, Biopolymers **6**, 1633 (1968).

[31] R. Golestanian and T. B. Liverpool, Phys. Rev. E **66**, 051802 (2002).

[32] A. A. Kornyshev and S. Leikin, Phys. Rev. Lett. **82**, 4138 (1999).

[33] N. V. Hud and I. D. Vilfan, Annu. Rev. Biophys. Biomol. Struct. **34**, 295 (2005).

[34] T. T. Nguyen, I. Rouzina, and B. I. Shklovskii, J. Chem. Phys. **112**, 2562 (2000).

[35] J. Pelta, F. Livolant, and J.-L. Sikorav, J. Biol. Chem. **271**, 5656 (1996).

# Chapter 2

# Direct observation of charge inversion by multivalent ions as a universal electrostatic phenomenon

**K. Besteman, M. A. G. Zevenbergen, H. A. Heering, and S. G. Lemay**

We have directly observed reversal of the polarity of charged surfaces in water upon the addition of tri- and quadrivalent ions using atomic force microscopy. The bulk concentration of multivalent ions at which charge inversion reversibly occurs depends only very weakly on the chemical composition, surface structure, size and lipophilicity of the ions, but is very sensitive to their valence. These results support the theoretical proposal that spatial correlations between ions are the driving mechanism behind charge inversion.

This chapter has been published in Physical Review Letters **93**, 170802 (2004).

## 2.1 Introduction

Understanding screening due to mobile ions in liquid is a key theme of such diverse fields as polymer physics, nanofluidics, colloid science and molecular biophysics. Several counter-intuitive phenomena occur at high concentrations of multivalent ions. Examples include attraction between like-charged macromolecules such as DNA [1] or actin filaments [2] and reversal of the sign of the electrophoretic mobility of charged colloids [3, 4]. The latter effect has become known as charge inversion.

The conventional paradigm for describing screening in liquid divides the screening ions into two components: (1) the so-called Stern layer, consisting of ions confined to the surface, and (2) a diffuse component described by the Poisson-Boltzmann (PB) equation that decays exponentially with distance far from the charged object. Charge inversion can be accounted for by introducing a "chemical" binding constant that reduces the free energy of multivalent ions situated in the Stern layer, reflecting an assumed specific interaction between these ions and the surface being screened. This binding constant is expected to depend on properties of the ions such as their size, chemical composition, surface structure, lipophilicity and valence. While this approach has been successful in *describing* experimental data [3, 5–7], it usually provides little insight into the underlying binding mechanism and lacks significant predictive power.

A universal mechanism for charge inversion based predominantly on electrostatic interactions has been proposed [8]. It was noted that the predicted chemical potential of the Stern layer can be significantly lowered if spatial correlations between discrete ions are accounted for. At room temperature, the loss of entropy entailed by the formation of a highly-correlated ionic system is substantial. For multivalent counterions and sufficiently high surface-charge densities, however, this is more than compensated by the corresponding gain in electrostatic energy, leading to charge inversion [9]. To date, these theories have remained untested by experiments.

Here we present direct measurements of charge inversion and its dependence on the properties of the screening ions. Using an atomic force microscope (AFM), we measured the force between two oppositely-charged surfaces. This approach circumvents the main limitations of previous measurements, namely, reliance on modelling of hydrodynamic effects [3, 4] and the need to disentangle phenomena at two similarly-charged surfaces [5, 7]. We observe that in the presence of a sufficiently high concentration of tri- and quadrivalent ions, the force reversibly changes sign. The bulk concentration at which charge inversion occurs, $c_0$, depends almost exclusively on the valence of the ions, consistent with the universal

predictions of ion-correlation theories.

## 2.2 Materials and Methods

Positively charged amine-terminated surfaces were prepared under argon atmosphere by immersing silicon wafers with 200-500 nm thermally-grown oxide in a 0.1% solution of 1-trichlorosilyl-11-cyanoundecane (Gelest) in toluene for 30 minutes, then in a 20 % solution of Red Al (Sigma-Aldrich) in toluene for 5 hours. Negatively charged surfaces were prepared by gluing 10 $\mu$m diameter silica spheres (G. Kisker Gbr) with epoxy resin to AFM cantilevers (ThermoMicroscope Microlevers, nominal force constant 0.03 N/m) using the method of Ducker *et al* [10], as illustrated in Fig. 2.1(a). Force spectroscopy measurements were performed using a Digital Instrument NanoScope IV AFM to yield the force $F$ on the silica bead versus the bead-surface separation $d$ [10].

At separations $d$ greater than the Debye length $\lambda$ of the solution, the force $F$ decays exponentially with $d$:

$$F = F_0 \exp(-d/\lambda), \qquad d > \lambda. \tag{2.1}$$

The parameter $F_0$ is proportional to the so-called renormalized surface-charge densities of both the silica bead and the amine-terminated surface, $\sigma_b^\star$ and $\sigma_s^\star$ respectively. The values of $\sigma_{b,s}^\star$ are related by the PB equation to the net surface-charge densities $\sigma_b$ and $\sigma_s$ (including both the bare surface charge and the charge in the Stern layer). At low net surface-charge densities $|\sigma_{b,s}| < \sigma_{\max}$, the renormalized charge densities are simply equal to the net charge densities: $\sigma_{b,s}^\star = \sigma_{b,s}$. Here $\sigma_{\max} \approx 4\ kT\epsilon/e\lambda$, where $k$ is the Boltzmann constant, $T$ is the temperature, $\epsilon$ is the dielectric constant of water and $-e$ is the electron charge. At higher net charge densities, $\sigma_{b,s}^\star$ saturates at $\sigma_{\max}$. Because we use oppositely charged surfaces and $Z$:1 electrolytes, where $Z$ is the valence of the multivalent ions, correlation effects are only relevant at one of the surfaces. The other surface can thus be thought of as a constant probe [11]. Near charge inversion, $F_0$ is approximately proportional to the net surface-charge density of the surface being screened by multivalent ions, $\sigma_b$ or $\sigma_s$, and the sign of the force unambiguously yields the polarity of this net surface charge.

For $d \lesssim \lambda$, the PB equation predicts a more complicated form than Eq. (2.1). Van der Waals forces, regulation of the surface charge and depletion forces can also become important. We therefore concentrate our analysis on the regime where both $d > \lambda$ and van der Waals forces are small ($d > 10$ nm), where we can reliably fit to Eq. (2.1).

Three positive trivalent ions were investigated. Lanthanum $La^{3+}$ is a metal ion with a first hydration shell consisting of 8–9 water molecules (radius $r$ of the complex 398 pm [12–15]). Ruthenium(III) hexammine $[Ru(NH_3)_6]^{3+}$ contains a Ru(III) core surrounded by six $NH_3$ groups ($r$ = 364 pm [12–14]). Cobalt(III) sepulchrate $[CoC_{12}H_{30}N_8]^{3+}$ is a caged cobalt complex with $CH_2$ groups exposed to the solvent ($r$ = 445 pm [16]), making it less hydrophillic than the other two.

## 2.3 Results

Figure 2.1 shows the measured force-distance relation $F(d)$ as a function of multivalent-ion concentration $c$ for the multivalent salts $LaCl_3$ (b), $CoC_{12}H_{30}N_8Cl_3$ (c) and $Ru(NH_3)_6Cl_3$ (d). A force measurement with only supporting electrolyte ($LaCl_3$: [17], $CoC_{12}H_{30}N_8Cl_3$ and $Ru(NH_3)_6Cl_3$: [18]) was first performed (squares), showing an attractive interaction between the surfaces. Solutions with increasing concentrations of multivalent ions in addition to the monovalent supporting electrolyte were then pumped through the AFM fluid cell of 50 $\mu$l volume at a rate 0.15–0.2 ml/min for at least 5 minutes per solution. This allowed the surface to equilibrate with the bulk electrolyte and insured that $c$ was not diminished by ions screening the surface. Consecutive measurements of $F(d)$ at multivalent-ion concentrations $c$ = 10 $\mu$M, 100 $\mu$M and 1 mM are shown in Fig. 2.1. At the end of the experiment, the measurement with $c$ = 10 $\mu$M was repeated (open circles). The $CoC_{12}H_{30}N_8Cl_3$ and $Ru(NH_3)_6Cl_3$ measurements were carried out consecutively using the same silica bead.

We interpret these observations as follows. The positive multivalent ions adsorb on the negative silica bead, reducing $\sigma_b$ and thus the magnitude of the force. Near 1 mM, the screening charge in the Stern layer overcompensates for the bare surface charge; $\sigma_b$ becomes positive and the force becomes repulsive. The last measurement with $c$ = 10 $\mu$M, which shows a recovery to the force measured at the beginning of the experiment, indicates that charge inversion reflects reversible equilibrium between the surface and the bulk electrolyte.

We fitted each $F(d)$ curve to Eq. (2.1) for $d > \lambda$. Because it is difficult to accurately fit $\lambda$ when the force is very small, its value was fitted for the curve with $c = 0$ (e.g. $\lambda$ = 18 nm for the data of Fig. 2.1(c,d)) and corrected using the standard expression for $\lambda$ when $c > 0$ (e.g. $\lambda$ = 4 nm for the 1 mM data in Fig. 2.1(c,d)).

Figure 2.2(a) shows the fitted normalized force extrapolated to zero separation, $F_{N0}(c) = F_0(c)/F_0(0)$, for the $[CoC_{12}H_{30}N_8]^{3+}$ and $[Ru(NH_3)_6]^{3+}$ data of Fig. 2.1(c,d). Similarly, Fig. 2.2(b) shows $F_{N0}(c)$ for consecutive measurements

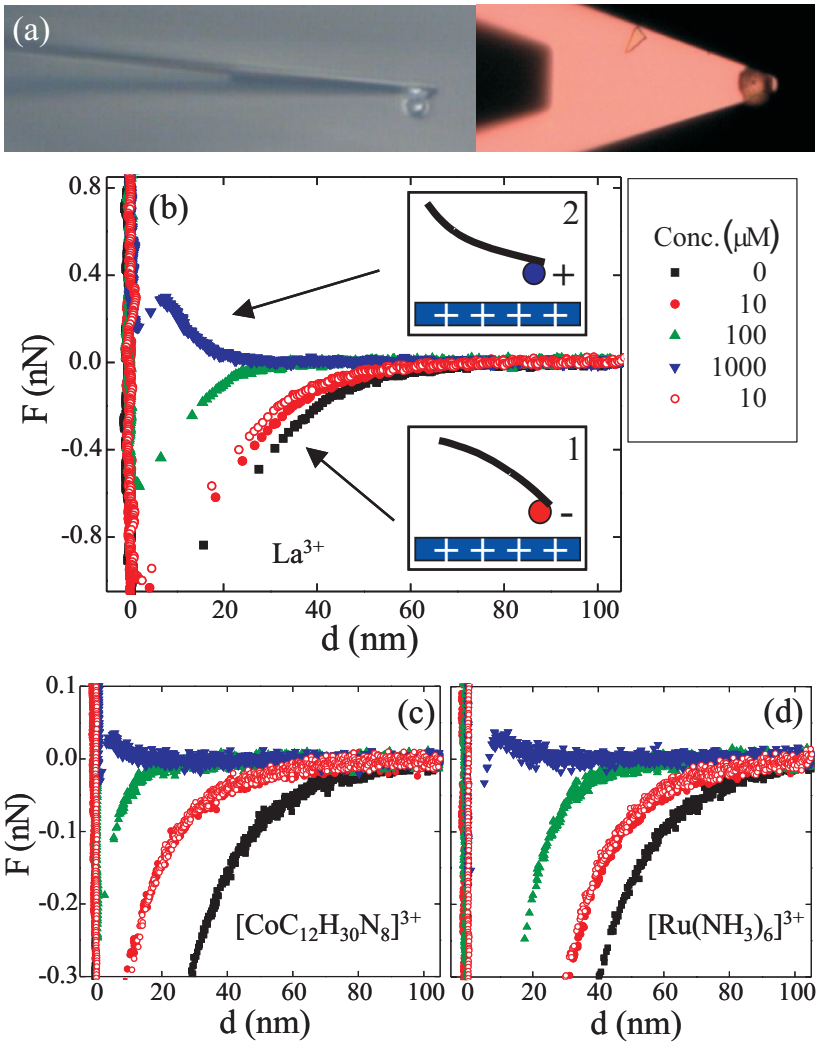


**Figure 2.1:** (a) Optical microscope images of the side (left) and top (right) of a cantilever with a silica sphere. Force versus separation measurements in different concentrations of (b) $LaCl_3$, (c) $CoC_{12}H_{30}N_8Cl_3$ and (d) $Ru(NH_3)_6Cl_3$. Insets illustrate schematically the attractive (1) and repulsive (2) forces between the silica bead and the amine-terminated surface. The legend applies to all three graphs.

using the same silica bead on $La^{3+}$ (data from Fig. 2.1(b)) and $[Ru(NH_3)_6]^{3+}$ ($F(d)$ curves not shown). We estimate the charge-inversion concentration $c_0$ by linearly interpolating between the data points immediately above and below $F_{N0} = 0$ on the lin-log scale. In both sets of measurements, the observed values of $c_0$ differ by a factor $\sim 2$. More generally, we find that the charge-inversion concentrations of silica for the three chemically different trivalent ions $La^{3+}$, $[Ru(NH_3)_6]^{3+}$ and $[CoC_{12}H_{30}N_8]^{3+}$ differ by at most a factor of 2.1, as

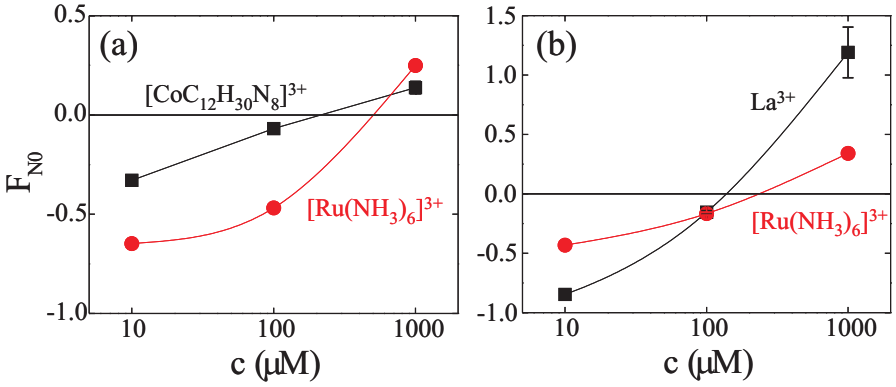


**Figure 2.2:** Normalized force extrapolated to zero separation obtained from fits to Eq. (2.1), versus multivalent-ion concentration $c$ for (a) $CoC_{12}H_{30}N_8Cl_3$ (squares) and $Ru(NH_3)_6Cl_3$ (circles) and for (b) $LaCl_3$ (squares) and $Ru(NH_3)_6Cl_3$ (circles). In each case the data were obtained consecutively using the same silica bead. Lines are guides to the eye.

summarized in Table 2.1. This is comparable to the variation observed between measurements for the same ion and pH using different, nominally identical beads and surfaces. Although the charge-inversion concentrations of the three positive trivalent ions are similar, there are differences in the observed $F(d)$ curves. In particular, $La^{3+}$ is less effective in reducing the absolute force at low concentrations, but it exhibits the largest magnitude of the force for $c \gg c_0$.

Figure 2.3 shows measurements where the same amine-terminated surface was consecutively charge inverted by a molecule in two different charge states, iron(II) hexacyanide $[Fe(CN)_6]^{4-}$ ($r = 443$ pm) and iron(III) hexacyanide $[Fe(CN)_6]^{3-}$ ($r = 437$ pm) [12–14], ensuring that essentially the only difference between the two measurements is the valence of the ions. Figure 2.3(c) shows $F_{N0}$ versus $c$ for both ions [19]. The charge-inversion concentrations for the two ions differ by a factor $\sim 50$.

Measurements using $[Fe(CN)_6]^{4-}$ and ruthenium(II) hexacyanide $[Ru(CN)_6]^{4-}$ ($r = 456$ pm [12–14]), two ions with the same chemical groups exposed to solution and differing only by their core atom, gave nearly identical $F(d)$ curves at all concentrations.

Two divalent ions, $Ca^{2+}$ and $Mg^{2+}$ [15] did not show charge inversion at a concentration of 1 mM on a silica bead that showed charge inversion at 1 mM $La^{3+}$. Thus divalent ions, if they can charge invert a silica bead at all, do so at higher concentrations than trivalent ions. Concentrations higher than 1mM were not investigated because $\lambda$ then becomes so short that other effects mask the electrostatic interaction between the surfaces.

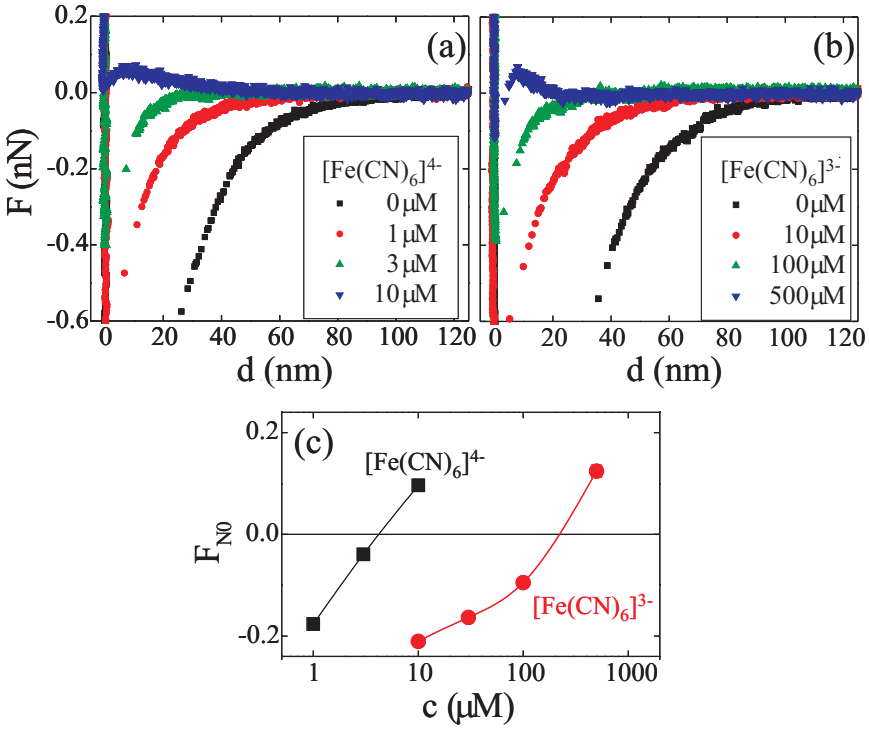


**Figure 2.3:** Force versus separation measurements in different concentrations of (a) $K_4Fe(CN)_6$ and (b) $K_3Fe(CN)_6$. (c) Normalized force at zero separation versus multivalent-ion concentration $c$ for $K_4Fe(CN)_6$ (squares) and $K_3Fe(CN)_6$ (circles). Lines are guides to the eye.

Additional experiments were performed with positively charged surfaces made by chemically modifying a silicon dioxide surface with 3-aminopropyltriethoxysilane (APTES) and by adsorbing poly-L-lysine on mica. The main results are summarized in Table 2.1

## 2.4 Discussion and Conclusions

In terms of a chemical-binding description, our measurements indicate that the binding constants for $La^{3+}$, $[Ru(NH_3)_6]^{3+}$ and $[CoC_{12}H_{30}N_8]^{3+}$ on silica differ by at most a factor $\sim 2$, despite the fact that these ions have significantly different chemical composition, surface structure, size and lipophilicity. The binding constant differs by more than a factor of 10 for the same molecule in two different charge states on amine-terminated surfaces. These observations strongly suggest that specific chemical interactions are not responsible for charge inversion in our measurements and that the mechanism for adsorption is predominantly electrostatic.

**Table 2.1:** Summary of measurements in which the same surface was charge inverted by two different ions. The column se shows the supporting electrolyte.

| surface | probe | se | ion(1) | ion(2) | $c_0^{(1)}$ $\mu$M | $c_0^{(2)}$ $\mu$M | $\frac{c_0^{(high)}}{c_0^{(low)}}$ |
|---|---|---|---|---|---|---|---|
| chlorosilane | silica bead | [19] | $[Fe(CN)_6]^{4-}$ | $[Fe(CN)_6]^{3-}$ | 4 | 200 | 50 |
| chlorosilane | silica bead | [19] | $[Fe(CN)_6]^{4-}$ | $[Fe(CN)_6]^{3-}$ | 6 | 450 | 75 |
| APTES | silica bead | [20] | $[Fe(CN)_6]^{4-}$ | $[Fe(CN)_6]^{3-}$ | 13 | 170 | 13 |
| APTES | silica bead | [20] | $[Ru(CN)_6]^{4-}$ | $[Fe(CN)_6]^{4-}$ | 11 | 13 | 1.2 |
| silica bead | APTES | [20] | $La^{3+}$ | $[Ru(NH_3)]^{3+}$ | 560 | 730 | 1.3 |
| silica bead | poly-L-lysine | [17] | $[CoC_{12}H_{30}N_8]^{3+}$ | $La^{3+}$ | 190 | 120 | 1.6 |
| silica bead | poly-L-lysine | [17] | $[CoC_{12}H_{30}N_8]^{3+}$ | $La^{3+}$ | 170 | 180 | 1.1 |
| silica bead | chlorosilane | [17] | $La^{3+}$ | $[Ru(NH_3)]^{3+}$ | 130 | 210 | 1.6 |
| silica bead | chlorosilane | [18] | $[CoC_{12}H_{30}N_8]^{3+}$ | $[Ru(NH_3)]^{3+}$ | 210 | 450 | 2.1 |
| poly-L-lysine | silica bead | [20] | $[Ru(CN)_6]^{4-}$ | | 22 | | |

We compare our results with ion-correlation theories using the formalism of Shklovskii [9], in which the multivalent counterions in the Stern layer are assumed to form a strongly correlated liquid with short-range correlations resembling those of a Wigner crystal. This theory provides a simple analytical prediction for $c_0$:

$$c_0 = \left|\frac{\sigma_{\text{bare}}}{2rZe}\right| \exp\left(\frac{\mu_c}{kT}\right) \exp\left(\frac{\Delta\mu^0}{kT}\right) \tag{2.2}$$

Here $\sigma_{\text{bare}}$ is the bare surface-charge density, $\Delta\mu^0$ is the standard energy of adsorption of an ion and $\mu_c$ is the chemical potential of the strongly correlated liquid. The latter can be approximated by the value for a Wigner crystal: $\mu_c \propto \sigma_{\text{bare}}^{1/2} Z^{3/2}$. In the calculations we use the full expression for $\mu_c$ [9].

In the absence of hydration effects and specific chemical interactions, $\Delta\mu^0 = 0$ and $\mu_c$ is solely responsible for charge inversion. In this case charge inversion is a universal electrostatic effect and $c_0$ depends very sensitively on $Z$ but is independent of the chemical structure of the ions. This is in good qualitative agreement with our observations.

Equation (2.2) has two unknowns, $\sigma_{\text{bare}}$ and $\Delta\mu^0$, which can be deduced from consecutive measurements using $[Fe(CN)_6]^{4-}$ and $[Fe(CN)_6]^{3-}$ on the same surface. From rows 1 and 2 in Table 2.1 we extract values of $\sigma_{\text{bare}} = +0.45$ and $+0.55$ $e/\text{nm}^2$, and $\Delta\mu^0 = -1.4kT$ and $-0.1kT$ respectively. The calculation assumes that $\Delta\mu^0$ and $\sigma_{\text{bare}}$ are the same for both measurements. The corresponding values of $\mu_c$ are $-9.4kT$ and $-10.6kT$ for $Z = 4$ and $-5.8kT$ and $-6.5kT$ for $Z = 3$. The observation that $|\mu_c| \gg |\Delta\mu^0| \lesssim kT$ indicates that specific interactions are negligible and that ion correlations are the dominant mechanism behind charge inversion in this system.

The same calculation for the APTES measurements in Table 2.1 (row 3) yields $\sigma_{\rm bare} = +0.2\ e/{\rm nm}^2$, $\Delta\mu^0 = -3.0kT$, and $\mu_c = -5.8kT$ and $-3.5kT$ for $Z = 4$ and 3, respectively. This suggests that specific adsorption plays a larger role in this case. However, the value of $|\mu_c|$ for APTES and $Z = 3$ corresponds to the lower end of the range of validity of Eq. (2.2) [9], which may be responsible for the difference. In addition, the surface charge was modelled as being uniformly distributed whereas real surfaces consist of discrete chemical groups. This disorder is expected to facilitate charge inversion, and its relative importance should be greater for APTES with its smaller $\sigma_{\rm bare}$. Elucidating the interplay between disorder and correlations remains an important theoretical challenge.

Taking $\Delta\mu^0 = 0$ and $c_0 = 200\ \mu$M for $[CoC_{12}H_{30}N_8]^{3+}$ screening silica gives $\sigma_{\rm bare} = -0.75\ e/{\rm nm}^2$, consistent with commonly accepted values [21].

These experiments are among the first systematic steps toward understanding the fundamentals of screening of real surfaces by multivalent ions. Specific binding does not provide an adequate explanation for our observations. An alternative description based on ion correlations yields qualitative and semi-quantitative agreement.

**Acknowledgement:** We thank J. Lyklema for useful discussions and C. Dekker for general support and useful discussions.

# Bibliography

[1] V. A. Bloomfield, Biopolymers **44**, 269 (1997).

[2] T. E. Angelini, H. Liang, W. Wriggers, and G. C. L. Wong, Proc. Nat. Acad. Sci. USA **100**, 8634 (2003).

[3] R. O. James and T. W. Healey, J. Colloid Interface Sci. **40**, 42 (1972); **40**, 53 (1972); **40**, 65 (1972).

[4] A. Martín-Molina, M. Quesada-Pérez, F. Galisteo-González, and R. Hidalgo-Álvarez, J. Chem. Phys. **118**, 4183 (2003).

[5] R. M. Pashley, J. Colloid Interface Sci. **102**, 23 (1984).

[6] K. B. Agashe and J. R. Regalbuto, J. Colloid Interface Sci. **185**, 174 (1996).

[7] V. Vithayaveroj, S. Yiacoumi, and C. Tsouris, J. Dispersion Sci. Technol. **24**, 517 (2003).

[8] For comprehensive reviews see A. Yu. Grosberg, T. T. Nguyen, and B. I. Shklovskii, Rev. Mod. Phys. **74**, 329 (2002); Y. Levin, Rep. Prog. Phys. **65**,

1577 (2002); M. Quesada-Pérez, E. González-Tovar, A. Martín-Molina, M. Lozada-Cassou, and R. Hidalgo-Álvarez, Chem.Phys.Chem. **4**, 234 (2003).

[9] B. I. Shklovskii, Phys. Rev. E **60**, 5802 (1999).

[10] W. A. Ducker, T. J. Senden, and R. M. Pashley, Langmuir **8**, 1831 (1992).

[11] The value of $\sigma^\star \approx \sigma_{\max}$ for the probe is not really constant since it depends linearly on $\lambda^{-1}$ and more subtly on the valence of the co-ions; G. Téllez and E. Trizac, Phys. Rev. E **70**, 011404 (2004). This has no influence on the measured sign of the force, however, and the error induced in $c_0$ is of the same order as that from other sources.

[12] Sum of metal ion radius and ligand ($H_2O$, $NH_3$, $CN^-$) diameter. Agrees within 4 % with crystallographic data.

[13] R. D. Shannon, Acta Crystallogr., Sect A: Cryst. Phys., Diffr., Theor. Gen. Crystallogr. **A32**, 751 (1976).

[14] Y. Marcus, *Ion properties* (Marcel Dekker Inc., New York, 1997), Chap. 3.

[15] All measurements were done at pH less than the first hydrolysis constant of the ions; J. Burgess, *Metal ions in solution* (Ellis Horwood, Chichester, England, 1979).

[16] Crystal structure with van der Waals radii; A. Bacchi, F. Ferranti, and G. Pelizzi, Acta Crystallogr., Sect. C: Cryst. Struct. Commun **C49**, 1163 (1993).

[17] Supporting electrolyte was a 1 mM HEPES (4-(2-hydroxyethyl)piperazine-1-ethanesulfonic acid) buffer, pH 7.0±0.3 set by adding KOH.

[18] Supporting electrolyte was a mixture of 0.3 mM KOH and HCl with pH 6.5 ± 0.5.

[19] Supporting electrolyte was the same as [18] with pH 5.8±0.3.

[20] Supporting electrolyte was a 0.1 mM MES (2-morpholinoethanesulfonic acid) buffer, pH 6.0±0.3 set by adding KOH.

[21] R. K. Iler, *The chemistry of silica* (Wiley, New York, 1979).

# Chapter 3

# Charge inversion by multivalent ions: dependence on dielectric constant and surface-charge density

**K. Besteman, M. A. G. Zevenbergen, and S. G. Lemay**

Charge inversion occurs when the effective charge of a surface exposed to solution reverses polarity due to an excess of counterions accumulating in the immediate vicinity of the surface. Using atomic force spectroscopy, we have directly measured the effect on charge inversion of changing the dielectric constant of the solvent and the surface-charge density. Both decreasing the dielectric constant and increasing the bare surface-charge density lower the charge-inversion concentration. These observations are consistent with the theoretical proposal that spatial correlations between ions are the dominant driving mechanism for charge inversion.

This chapter has been published in Physical Review E **72**, 061501 (2005).

## 3.1 Introduction

Screening by mobile ions dominates electrostatic interactions in electrolytes, making it a very important element of polymer physics, nanofluidics, colloid science and molecular biophysics. In the presence of multivalent ions, counterintuitive phenomena occur such as attraction between like-charged molecules [1] and its converse, repulsion between oppositely charged objects [2]. Similarly, the electrophoretic mobility of charged colloids can reverse sign in the presence of multivalent ions [3, 4], a phenomenon known as *charge inversion* or *overcharging*. Charge inversion has also been observed and studied using numerical simulations [5, 6].

Early observations of the charge inversion of oxides by metal ions were interpreted in terms of specific chemical binding between the multivalent ions and the surface being screened [3, 7–9]. This mechanism necessarily relies on the detailed chemical structure of the substances involved, for example the propensity of metal ions to form hydroxides [3, 7–9]. Theory, however, suggests that such specific interactions are not necessary for charge inversion to take place [10]. In particular, it has been argued that spatial correlations, ignored in conventional mean-field descriptions of screening on which much of our intuition is based, are highly relevant for multivalent ions and naturally lead to charge inversion. We indeed recently showed [2] that, for a variety of ions, charge inversion is an equilibrium effect that depends very strongly on the valence $Z$ of the ions but can be largely insensitive to their chemical properties, in agreement with these theoretical predictions.

Here we extend these measurements by exploring the dependence of charge inversion on the dielectric constant of the medium $\epsilon$ and the bare surface-charge density $\sigma_{\text{bare}}$. We compare the results with the predictions from both specific binding and ion-correlation theories.

## 3.2 Theoretical background

Charge inversion occurs when the concentration of multivalent ions in the bulk solution, $c$, exceeds the so-called charge-inversion concentration, $c_0$. We are particularly interested in probing $c_0$ for two related reasons. First, $c_0$ can be determined experimentally without recourse to any particular model. Second, it is a quantity that is particularly amenable to theoretical treatment: since the surface is neutralized at $c = c_0$, fewer assumptions are necessary regarding the structure of the double layer. In this section we first summarize the derivation of a simple, mean-field expression for $c_0$ in terms of specific binding of multivalent ions to

the surface, then indicate how this expression is modified by spatial correlations between multivalent ions at the surface.

Consider a surface with bare charge density $\sigma_{\text{bare}}$ in equilibrium with an electrolyte. For large $\sigma_{\text{bare}}$ the double layer is conventionally divided into two regions: the diffuse layer, in which the Poisson-Boltzmann (PB) equation holds, and, close to the surface, the so-called Stern layer. In our simple model, the latter contains a two-dimensional layer of ions (predominantly multivalent in our case) located a distance $d_s$ away from the surface containing a charge density $\sigma_{\text{Stern}}$. The parameter $d_s$ represents the finite size of the ions. For simplicity the charge density is commonly taken to be zero in the range $0 < x < d_s$, where $x$ is the distance from the surface. It is further assumed that multivalent ions are held in the Stern layer not only by electrostatic interaction with the charged surface, but also by a chemical interaction. Specifically, it is assumed that local interactions between each ion and the surface and/or the solvent contribute a change in free energy $\Delta\mu^{0*}$ upon taking one multivalent from the bulk to the Stern layer. The parameter $\Delta\mu^{0*}$ includes any complex formation between the ion and the surface. It can in general be expected to depend on specific properties of the system such as chemical composition, surface structure and lipophilicity of both the ions and the surface. $\Delta\mu^{0*}$ cannot be predicted reliably at this time: in comparing to data it is typically treated as an empirical fitting parameter.

In equilibrium, the electrochemical potential of the multivalent ions in the bulk is equal to that of multivalent ions in the Stern layer [11]. These electrochemical potentials are respectively $\mu_b = \mu_b^0 + kT\ln(c/c_{\max}) + Ze\psi(\infty)$ and $\mu_s = \mu_s^0 + kT\ln(c_s/c_{s,\max}) + Ze\psi(d_s)$. Here the activity coefficients have been set to unity [11], $\mu_s^0$ and $\mu_b^0$ are constant parameters such that $\mu_s^0 - \mu_b^0 = \Delta\mu^{0*}$, $c$ and $c_{\max}$ are respectively the concentration and maximum concentration of multivalent ions in the bulk, $c_s$ and $c_{s,\max}$ are respectively the two-dimensional concentration and maximum two-dimensional concentration of multivalent ions in the Stern layer, and $\psi(x)$ is the electrostatic potential as a function of the distance $x$ from the surface. $k$, $T$ and $-e$ are the Boltzmann constant, the absolute temperature and the electron charge, respectively. Equilibrium thus requires that

$$kT\ln\left(\frac{c_s}{c_{s,\max}}\right) + \Delta\mu^{0*} + Ze\psi(d_s) = kT\ln\left(\frac{c}{c_{\max}}\right), \tag{3.1}$$

where the potential in the bulk $\psi(\infty)$ was taken as zero.

In the region $0 < x < d_s$ the potential $\psi$ varies linearly with $x$ to the value $\psi(d_s)$. For $x > d_s$, $\psi(x)$ drops to the bulk value according to the PB-equation. Figure 3.1(a) sketches the potential $\psi(x)$ for the cases when the Stern layer almost compensates the surface charge ($c < c_0$, $|\sigma_{\text{Stern}}| < |\sigma_{\text{bare}}|$), fully compensates the

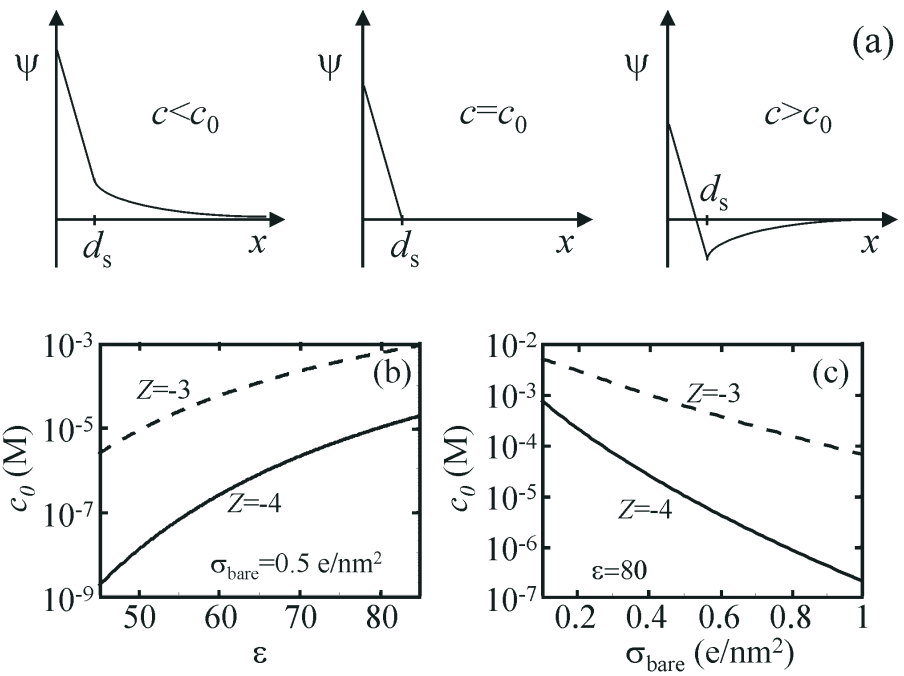


**Figure 3.1:** (a) Sketch of the electrostatic potential $\psi$ as a function of the distance $x$ from a surface with constant $\sigma_{\rm bare}$ for the cases $c < c_0$ (no charge inversion), $c = c_0$ (neutralization of the surface), and $c > c_0$ (charge inversion). (b) Dependence of the charge-inversion concentration $c_0$ on $\epsilon$ as predicted by spatial correlation theory, Eq. (3.3), with $\Delta\mu^0 = 0$, $r = 0.5$ nm and $\sigma_{\rm bare} = 0.5$ e/nm$^2$. (c) Same as (b) for dependence on bare surface-charge density $\sigma_{\rm bare}$ with $\epsilon = 80$.

surface charge ($c = c_0$, $|\sigma_{\rm Stern}| = |\sigma_{\rm bare}|$, $\psi(d_s) = 0$), and overcompensates the surface charge ($c > c_0$, $|\sigma_{\rm Stern}| > |\sigma_{\rm bare}|$).

At $c = c_0$ the bare surface charge is entirely compensated by the charge in the Stern layer, thus $c_s = |\sigma_{\rm bare}/Ze|$ and $\psi(d_s) = 0$. Further taking on geometrical grounds that $c_{s,\max}/c_{\max} = 2r$, where $r$ is the radius of an ion, Eq. (3.1) then yields for the charge-inversion concentration:

$$c_0 = \left|\frac{\sigma_{\rm bare}}{2rZe}\right| \exp\left(\frac{\Delta\mu^{0*}}{kT}\right). \tag{3.2}$$

For specific binding to account for charge inversion, $\Delta\mu^{0*}$ must be negative and several times $kT$ in magnitude.

Real surfaces become charged in an electrolyte by the dissociation of charged groups (ions) from the surface or association of charged groups to the surface [12]. Such chemical equilibrium between surface sites and charge-determining ions renders $\sigma_{\rm bare}$ dependent on the concentration of charge-determining ions at the surface, and thus on the bulk concentration of all ions in the solution including the

multivalent ions. This so-called charge regulation does not affect the condition for charge inversion given by Eq. (3.2), however, and only enters Eq. (3.2) implicitly via $\sigma_{\text{bare}}$. In situations where charge regulation plays a significant role, the value of $\sigma_{\text{bare}}$ must be obtained self-consistently for the condition $\psi(d_s) = 0$ and $c = c_0$. Since experimentally $\sigma_{\text{bare}}(c_0)$ is difficult to determine independently, we will treat it as an unknown parameter.

So far we have discussed the influence of regulation of the bare surface charge due to equilibrium with a bulk reservoir. Additional regulation effects can occur when two surfaces are brought into such proximity to each other that they influence each other's double layers. This effect can even result in a reversal of the force of interaction as a function of the distance between the surfaces [13–15]. Since our experiments mostly focus on long-range interactions (distance greater than $2\lambda$, where $\lambda$ is the Debye length) and that such regulation effects become important at shorter range, we do not consider these effects further here.

Several authors have attempted descriptions beyond the mean-field one outlined above and incorporated the role of spatial correlations between multivalent ions in the Stern layer. Here we concentrate on the formalism introduced by Shklovskii [16], which hinges on the theoretical observation that multivalent ions must form a strongly correlated ionic liquid in the Stern layer of surfaces with high $\sigma_{\text{bare}}$. This formalism leads to simple analytical expressions for the charge-inversion concentration $c_0$. The development parallels that given above, with the additional refinement that $\Delta\mu^{0*}$ is replaced by $\Delta\mu^0 + \mu_c$. Here $\Delta\mu^0$ represents hydration and specific binding effects while $\mu_c$ accounts for spatial interactions between multivalent ions in the Stern layer. The predicted value for the charge-inversion concentration is then

$$c_0 = \left|\frac{\sigma_{\text{bare}}}{2rZe}\right| \exp\left(\frac{\mu_c}{kT}\right) \exp\left(\frac{\Delta\mu^0}{kT}\right) \tag{3.3}$$

with $\mu_c$ given by [16, 17]

$$\mu_c = -kT\left(1.65\Gamma - 2.61\Gamma^{1/4} + 0.26\ln\Gamma + 1.95\right) \tag{3.4}$$

and the interaction parameter $\Gamma$ by

$$\Gamma = \frac{1}{4kT\epsilon\epsilon_0}\sqrt{\left|\frac{e^3Z^3\sigma_{\text{bare}}}{\pi}\right|}, \tag{3.5}$$

where $\epsilon_0$ is the permittivity of free space. This theory holds for $\Gamma \gg 1$ [16, 18], which is typically fulfilled for $Z \geq 3$. For example when $Z = 3$, $\sigma_{\text{bare}} = 0.5$ e/nm$^2$ and $\epsilon = 80$, the value of $\Gamma$ is 4.6. Calculated values of $\Gamma$ from our experiments are

in the range $3 \lesssim \Gamma \lesssim 8$. For $\Gamma \gg 1$, $\mu_c$ is approximately equal to the first term in Eq. (3.4), yielding $\mu_c \propto -\sqrt{|\sigma_{\rm bare} Z^3|}/\epsilon$. Thus while we use the full expression for $\mu_c$ in our calculations, the approximation is expected to correctly predict the qualitative trends. For monovalent salt ($Z = 1$) at room temperature, $\Gamma \lesssim 1$ and correlation effects do not play a significant role [16, 18, 19].

Equation (3.3) predicts that charge inversion can occur even in the absence of specific adsorption ($\Delta\mu^0 = 0$). Correlations are then solely responsible for charge inversion. The dependence of $c_0$ on $Z$, $\epsilon$ and $\sigma_{\rm bare}$ from Eq. (3.3)-(3.5) is plotted in Fig. 3.1.

## 3.3 Materials and Methods

We have determined the charge-inversion concentration through a direct measurement of the electrostatic interaction between two oppositely charged surfaces, as described previously [2]. In short, we used a Digital Instrument NanoScope IV Atomic Force Microscope (AFM) to measure the force $F$ between the surfaces versus their separation $d$ in different concentrations $c$ of an asymmetric $Z$:1 electrolyte. The sign of the force far from contact unambiguously yields the effective polarity of the surface being screened by the multivalent counterion.

The negatively charged surface consisted of a silica bead glued to an AFM cantilever. The AFM cantilever was heated with a soldering iron. Using a micromanipulator, a small amount of epoxy resin (EPI-REZ 3522-W-60) was deposited on the hot tip of the cantilever. Next, a 10 $\mu$m silica sphere (G. Kisker Gbr) was deposited from a glass microscope slide on the tip of the cantilever. Upon cooling, the resin solidified and the bead remained attached to the end of the tip [20]. In contact with water silica gets charged by the dissociation of silanol groups, (Si)OH $\rightleftarrows$ (Si)$O^-$ + $H^+$, where (Si) is a silicon atom at the surface.

The positively charged amine-terminated surface was prepared from a silicon dioxide surface. A silicon substrate with 300-500 nm thermally grown oxide was first immersed in a 3:1 mixture of sulfuric acid and hydrogen peroxide for 15 min and rinsed with deionized Milli-Q filtered water (mq-water). In a glove box containing a nitrogen environment, it was then immersed in a 0.1% solution of 1-trichlorosilyl-11-cyanoundecane ($NC(CH_2)_{11}SiCl_3$) (Gelest) in toluene for 30 min and rinsed in clean toluene. The trichlorosilane group of the molecule binds covalently to the surface. The substrate was then sonicated in toluene, chloroform and again toluene, each for 5 min in an acid hood. Back in the glove box, it was immersed in a 20 % solution of Red Al (Sigma-Aldrich) in toluene for 5 h and afterwards rinsed in clean toluene. The Red Al reduces the cyano group to an

amino group. Finally the substrate was sonicated in respectively toluene, acetone, mq-water, nitric acid (pH 2) and mq-water each for 5 min and blown dry. The substrate was kept under nitrogen atmosphere until used. In contact with water the amino group can take up a proton, (Si)−R−$NH_2$ + $H^+$ ⇄ (Si)−R−$NH_3{}^+$.

The AFM cantilever (ThermoMicroscope Microlever) had a nominal force constant of about 0.03 N/m, as specified by the manufacturer. Absolute values of force shown here are based on this value.

We present results using five different multivalent ions. The same molecule in two different charge states, iron(II) hexacyanide $[Fe(CN)_6]^{4-}$ ($r$ = 443 pm) and iron(III) hexacyanide $[Fe(CN)_6]^{3-}$ ($r$ = 437 pm) [21–23], both with $K^+$ counterions, was used to investigate charge inversion on the positively charged amine-terminated surface. Three positive trivalent ions with a different chemical composition were used to investigate charge inversion on the negatively charged silica bead. All three have $Cl^-$ counterions. Lanthanum $La^{3+}$ is a metal ion with a first hydration shell consisting of 8–9 water molecules (radius $r$ of the complex 398 pm [21–24]). Ruthenium(III) hexamine $[Ru(NH_3)_6]^{3+}$ contains a Ru(III) core surrounded by six $NH_3$ groups ($r$ = 364 pm [21–23]). Cobalt(III) sepulchrate $[CoC_{12}H_{30}N_8]^{3+}$ is a caged cobalt complex with $CH_2$ groups exposed to the solvent ($r$ = 445 pm [25]), and is expected to be less hydrophillic than the other two.

For each series of measurements, $F(d)$ was first measured in a monovalent electrolyte. Consecutive measurements with increasing concentrations of multivalent ions in addition to the monovalent salt were then carried out. Each new solution was pumped through the AFM liquid cell (volume ≈ 50 $\mu$L) at a rate of 0.15 ml/min for 5-15 min before obtaining $F(d)$ curves, thus allowing the surface to equilibrate with the solution and insuring that $c$ was not diminished by ions screening the surface. At the end of each experiment, the lowest concentration of multivalent ions was pumped back into the fluid cell and $F(d)$ curves were once again obtained.

## 3.4 Force-distance curves

Figure 3.2 shows the measured force $F$ versus the distance $d$ between a silica bead and an amine-terminated surface. Three curves are shown that correspond to three different electrolytes. The observed $F(d)$ curves are dramatically different for the three cases.

The curve represented by squares was obtained in a solution containing 0.5 mM monovalent salt. At bead-surface separations less than about 75 nm, an attrac-

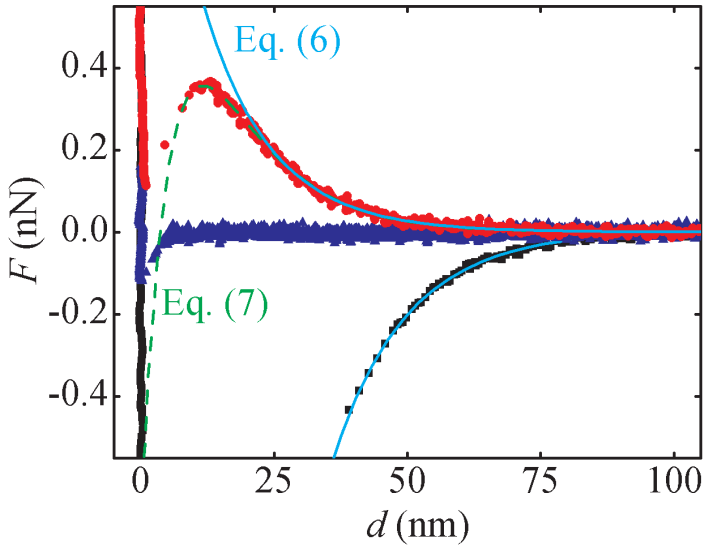


**Figure 3.2:** Measurements of the force $F$ versus separation $d$ in a pH 6 solution with 0.5 mM KCl (squares), after adding 50 $\mu$M $[Fe(CN)_6]^{4-}$ to the 0.5 mM KCl solution (circles), and in a 1 M KCl solution (triangles). The three measurements used the same amine-terminated surface and silica bead. Fits to Eq. (3.6) are shown as solid lines. A fit to Eq. (3.7) is shown as a dashed line.

tive (negative) force was observed that increased in magnitude with decreasing separation. Below about 35 nm separation, the attractive force gradient exceeded the spring constant of the cantilever and the bead snapped to the surface.

The curve represented by circles was obtained in a solution containing 50 $\mu$M -4:+1 salt in addition to the monovalent salt. A repulsive (positive) force was clearly observed below about 55 nm separation, which we interpret as indicating that charge inversion of the positive surface has occurred. The force increased with decreasing distance until $d = 13$ nm. For $d$ in the range 8-13 nm, the force instead decreased with decreasing distance. Below 8 nm snap-in occurred.

The curve represented by triangles was obtained in a solution containing 1 M monovalent salt. The Debye screening length $\lambda$ of this solution is $\approx 0.3$ nm, and hence electrostatic interactions are expected to play no role except at extremely small separations. The observed force remained zero until the distance $d$ was only about 5 nm. Below this distance a weak attractive force was observed which we attribute to van der Waals forces. The data show that van der Waals forces are negligible for $d > 10$ nm.

In order to quantitatively describe the $F(d)$ curves, we distinguish between two main regimes depending on whether the separation $d$ is greater or smaller

than about twice the Debye length $\lambda$ of the solution.

In the regime $d \gtrsim 2\lambda$, the force $F$ between the silica bead and amine-terminated surface is expected from the Poisson-Boltzmann equation to decay exponentially with $d$:

$$F(d) = F_0 \exp(-d/\lambda), \qquad d \gtrsim 2\lambda. \tag{3.6}$$

The parameter $F_0$ is not the real force at zero separation, but rather the value of the force when the functional form valid far from the surface is extrapolated to the surface. Theoretically $F_0 \propto \sigma_b^\star \sigma_s^\star$, where $\sigma_b^\star$ and $\sigma_s^\star$ are the so-called renormalized surface-charge densities of the silica bead and of the amine-terminated surface, respectively. $\sigma_b^\star$ and $\sigma_s^\star$ are related to the net surface-charge densities of the bead and the amine-terminated surface, $\sigma_b$ and $\sigma_s$, which include both the bare surface charge and the charge in the Stern layer. At low net surface-charge density $|\sigma_{b,s}| < \sigma_{\max} \approx 4kT\epsilon\epsilon_0/e\lambda$, the renormalized charge densities are simply equal to the net charge densities: $\sigma_{b,s}^\star = \sigma_{b,s}$. At higher net charge densities, $\sigma_{b,s}^\star$ saturates at $\sigma_{\max}$.

Because we use oppositely charged surfaces and asymmetric $Z$:1 electrolytes and correlation effects are only relevant for $Z > 1$, charge inversion is only expected to occur at one of the surfaces. The other surface, screened predominantly by monovalent ions, can thus be thought of as a constant probe. Near charge inversion, $F_0$ is thus approximately proportional to the net surface-charge density of the surface being screened by multivalent ions, $\sigma_b$ or $\sigma_s$, and the sign of the force unambiguously yields the polarity of this net surface charge. Note that, strictly speaking, the value of $\sigma^\star \approx \sigma_{\max}$ for the probe is not constant since it depends linearly on $\lambda^{-1}$ and more subtly on the valence of the ions [26]. This introduces a small systematic error in the fitted value of $c_0$, but does not affect the measured *sign* of the force.

The solid lines in Fig. 3.2 show fits of the data to Eq. (3.6) in which $F_0$ and $\lambda$ are used as fitting parameters. The fitted values of $\lambda$ are 13.9 and 12.6 nm for the measurements in the monovalent electrolyte and in the electrolyte containing multivalent ions, respectively. The calculated values of $\lambda$ for these electrolytes are 13.6 and 9.6 nm, respectively. Equation (3.6) gives less good quantitative agreement with the data obtained in the charge-inversion regime. It also fails to capture the decrease in $F$ with decreasing $d$ at short range in this case. This is not unreasonable since Eq. (3.6) becomes increasingly inaccurate with decreasing $d$. The leading correction [14] yields

$$F = F_0 \exp(-d/\lambda) + F_1 \exp(-2d/\lambda), \tag{3.7}$$

which reduces to Eq. (3.6) at large enough separations. Here $|F_1| \propto \sigma_b^{\star 2} + \sigma_s^{\star 2}$.

Near charge inversion of one of the two surfaces, the $F_1$ term in Eq. (3.7) becomes much more prevalent. This is because $\sigma^\star$ vanishes at $c_0$ for the surface being charge-inverted while $\sigma^\star$ of the other surface remains $\approx \sigma_{\mathrm{max}}$, leading to a vanishing $F_0$ and a largely unaffected $F_1$. Equation (3.6) can therefore be expected to be less accurate near charge inversion, as observed.

The sign of $F_1$ depends on the boundary conditions of the system: surfaces with constant net surface-charge density give positive values of $F_1$ (repulsive force), while surfaces at constant potential give negative values of $F_1$ (attractive force) [13–15, 20]. A surface whose net surface-charge is strongly regulated behaves as being at constant potential, and this is also the case that is predicted to apply for the net surface charge in the presence of a strongly correlated Stern layer [14].

The dashed line in Fig. 3.2 gives a fit of Eq. (3.7) to the measurement in the presence of multivalent ions, where $F_0$, $F_1$ and $\lambda$ are used as fitting parameters. The fitted value of $F_1$ is negative, implying that the surface screened by multivalent ions indeed behaves as if held at a constant potential. The fitted value of $\lambda$ is 11.6 nm, in better agreement with the expected value than the fit to Eq. (3.6).

In the remainder of this paper we concentrate on the regime where both $d > 2\lambda$ and van der Waals forces are small ($d > 10$ nm), where we can reliably fit to Eq. (3.6). Under these conditions and near charge inversion, $F_0$ is approximately proportional to the net surface-charge density of the surface being screened by multivalent ions and the sign of the force unambiguously yields the polarity of this net surface charge.

## 3.5 Dielectric constant $\epsilon$

We have measured the influence of the dielectric constant of the solvent on the charge-inversion concentration by using water-alcohol mixtures as the solvent. These were prepared by mixing solutions of 2 mM KOH and 2 mM HCl (both in water) to the desired pH value, then diluting with mq-water and/or ethanol to obtain mixtures with dielectric constant $\epsilon = 80$ (only water), 68 (75% water, 25% ethanol) and 54 (50% water, 50% ethanol). The values of the dielectric constant were obtained by interpolating between tabulated values for water-ethanol mixtures [27].

Figure 3.3 shows an experiment where the same amine-terminated surface was charge inverted with $[\mathrm{Fe(CN)_6}]^{4-}$ in electrolytes with different dielectric constants. The same silica bead was used during the entire experiment. After changing the dielectric constant of the solution, a part of the amine-terminated surface

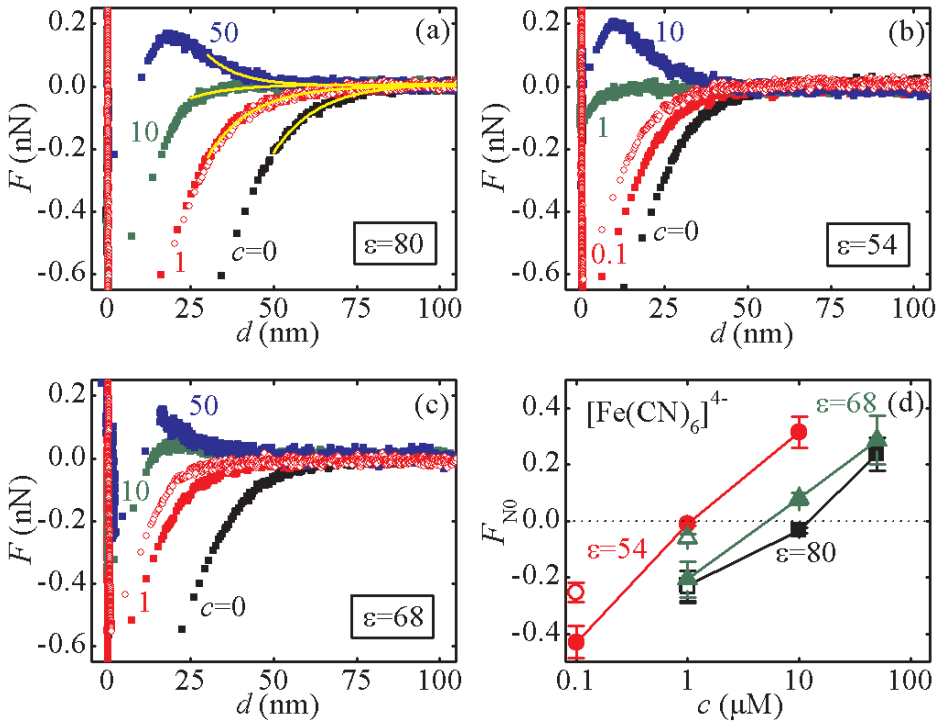


**Figure 3.3:** Measurement of the force $F$ versus separation $d$ in solvents with different dielectric constants: $\epsilon = 80$ (a), $\epsilon = 54$ (b) and $\epsilon = 68$ (c). The electrolyte contained $[Fe(CN)_6]^{4-}$ and 0.5 mM KCl at pH 6.0±0.5 The numbers next to each curve indicate the multivalent ion concentration $c$ in $\mu$M. All measurements were performed with the same amine-terminated surface and silica bead. In (a), fits to Eq. (3.6) are shown as solid lines. (d) Normalized force $F_{N0}$ versus $c$ for $\epsilon = 80$ (squares), $\epsilon = 54$ (circles) and $\epsilon = 68$ (triangles). In each panel the open symbols represent the last measurement performed to check the reversibility of the charge inversion.

that had not been in contact with the electrolyte during the previous measurement was used. The data clearly show that a lower concentration of multivalent ions is required to cause charge inversion when the dielectric constant is reduced.

We fitted $F(d)$ curves to Eq. (3.6) in the range $d > 2\lambda$ and extracted the force $F_0$. Because it is difficult to accurately fit $\lambda$ when the force is very small, the value of $\lambda$ was only fitted for the curve with $c = 0$ and corrected using the standard expression when $c > 0$. Figure 3.3(a) shows such fits to Eq. (3.6) as solid lines through the data.

Figure 3.3(d) shows $F_0$ versus multivalent ion concentration $c$. Each point represents the average of five separate fits. To facilitate comparison between different curves, the value of $F_0$ was normalized to its value when $c = 0$ for each curve: $F_{N0}(c) = F_0(c)/F_0(0)$. We estimate the charge-inversion concentration $c_0$

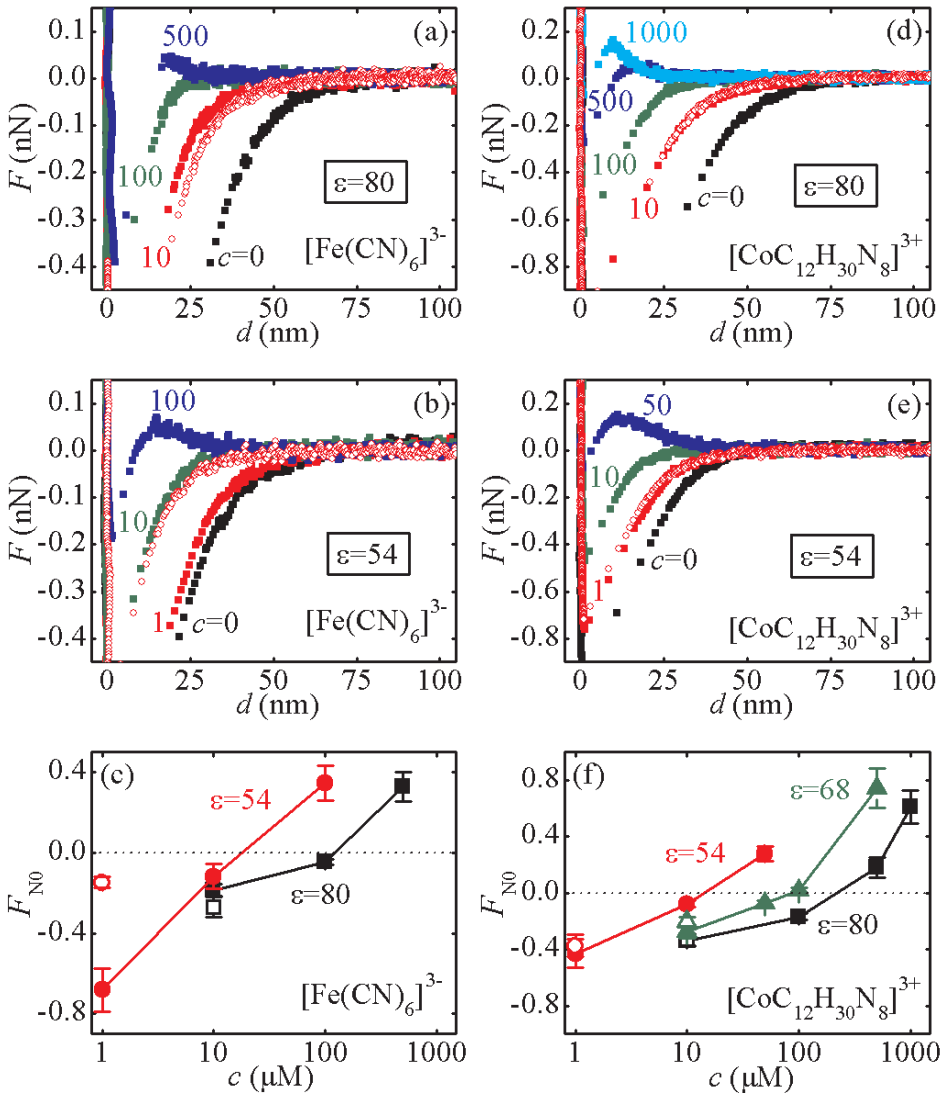


**Figure 3.4:** Force $F$ versus separation $d$ in the presence of $[Fe(CN)_6]^{3-}$ (a,b) or $[CoC_{12}H_{30}N_8]^{3+}$ (d,e) with solvents having dielectric constants $\epsilon = 80$ (a,d) or $\epsilon = 54$ (b,e). The electrolyte contained 0.5 mM ($\epsilon = 80$) or 0.25 mM ($\epsilon = 54$) KCl with pH 6.0±0.5 for the $[Fe(CN)_6]^{3-}$ measurements and 0.5 mM KCl with pH 7.0±0.5 for the $[CoC_{12}H_{30}N_8]^{3+}$ measurements. (c,f) $F_{N0}$ versus $c$ using $[Fe(CN)_6]^{3-}$ (c) and $[CoC_{12}H_{30}N_8]^{3+}$ (f) for $\epsilon = 80$ (squares), $\epsilon = 54$ (circles) and $\epsilon = 68$ (triangles). The values of $c_0$ for $[Fe(CN)_6]^{3-}$ are 120 and 18 $\mu$M for $\epsilon = 80$ and 54, respectively. The values of $c_0$ for $[CoC_{12}H_{30}N_8]^{3+}$ are 220, 88 and 14 $\mu$M for $\epsilon = 80$, 68 and 54, respectively.

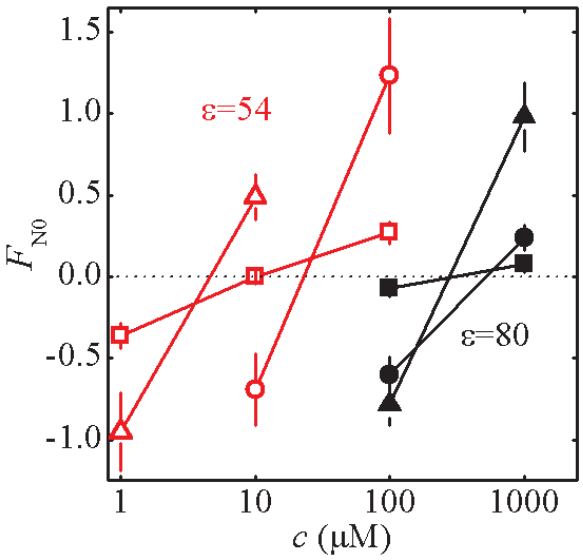


**Figure 3.5:** Normalized force $F_{N0}$ versus multivalent-ion concentration $c$ for three experiments in which a silica bead was charge inverted using the trivalent ions $[CoC_{12}H_{30}N_8]^{3+}$ (squares), $[Ru(NH_3)_6]^{3+}$ (circles) and $La^{3+}$ (triangles). Electrolytes containing 1 mM HEPES of pH 7.3±0.2 with $\epsilon = 80$ (filled symbols) and $\epsilon = 54$ (open symbols) were used. The values of $c_0$ for $\epsilon = 80$ and 54 are 300 and 10 $\mu$M for $[CoC_{12}H_{30}N_8]^{3+}$, 520 and 23 $\mu$M for $[Ru(NH_3)_6]^{3+}$, and 280 and 6 $\mu$M for $La^{3+}$.

by linearly interpolating between the data points immediately above and below $F_{N0} = 0$ on the lin-log scale. The resulting values of $c_0$ are 12, 5 and 1 $\mu$M for $\epsilon = 80$, 68 and 54, respectively. Thus lowering the dielectric constant from 80 to 54 causes a decrease of the charge-inversion concentration by a factor $\approx 10$.

At the end of each experiment, $F(d)$ was measured at the same concentration $c$ of multivalent ions as was used at the beginning of the experiment (open circles in Fig. 3.3). In water, the resulting curve was usually identical to that measured at the beginning of the experiment (see for example Fig. 3.3(a)). In water-ethanol mixtures, however, the magnitude of the force often decreased after prolonged exposure (Fig. 3.3(b,c)). This was also observed in the absence of multivalent ions, indicating that exposure to ethanol induced a slow decrease of the magnitude of the surface charge. To minimize the influence of this on further analysis, we compare data that were obtained on surfaces exposed to solution for approximately the same duration.

Figure 3.4 shows similar experiments using the multivalent ions $[Fe(CN)_6]^{3-}$ and $[CoC_{12}H_{30}N_8]^{3+}$, and 0.5mM KCl as monovalent salt. When decreasing $\epsilon$ from 80 to 54, $c_0$ decreased by a factor 7 for $[Fe(CN)_6]^{3-}$ and 16 for $[CoC_{12}H_{30}N_8]^{3+}$.

Figure 3.5 shows a comparison between the three trivalent positive ions. In each case decreasing $\epsilon$ causes a decrease in $c_0$ irrespective of chemical structure. The values of $c_0$ for the three ions are within a factor of 2 at $\epsilon = 80$ and within a factor of 4 at $\epsilon = 54$. The decrease in $c_0$ when decreasing $\epsilon$ from 80 to 54 is a factor of 23 for $[Ru(NH_3)_6]^{3+}$, 47 for $La^{3+}$, and 30 for $[CoC_{12}H_{30}N_8]^{3+}$ for these particular surfaces. In these measurements HEPES buffer was used as the monovalent salt because of the atypical behavior of $La^{3+}$, namely, the pH of an unbuffered $La^{3+}$ solution decreased from pH 7 to pH 5.5-6.0 upon adding 1 mM $La^{3+}$. At this $La^{3+}$ concentration impurities also sometimes appeared in the solution over time. In addition, recovery of an attractive signal after charge inversion had occurred in the $\epsilon = 54$ solvent with $La^{3+}$ took three times longer than usual. This indicates a reaction involving $La^{3+}$ in which small quantities of $H^+$ ions (less than one per 100 $La^{3+}$ ions) are released [3]. This behavior was never observed with ions other than $La^{3+}$.

## 3.6 Surface-charge density $\sigma_{\text{bare}}$

We have measured the influence of the bare surface-charge density of the amine-terminated surface on the charge-inversion concentration by changing the amount of chargeable sites on the surface. This was achieved using mixtures of 1-trichlorosilyl-11-cyanoundecane and undecyltrichlorosilane (Gelest) during the preparation of the positively charged surfaces. Undecyltrichlorosilane has a $CH_3$ end group that is uncharged. Reducing the amount of chargeable groups on the surface correspondingly reduces $\sigma_{\text{bare}}$. The exact charge ratio on the surface could not be determined reliably because the ratio of charged:uncharged chlorosilanes in the bulk solution cannot be assumed to correspond to the ratio ultimately deposited on the surface. In addition, the preparation of the amine-terminated surfaces is lengthy, and small differences such as the amount of residual water in the solutions and the age of the stock solutions can lead to significant variations in the observed charge-inversion concentration. Here we only compare surfaces with different ratios of charged:uncharged chlorosilane that were prepared simultaneously from the same stock solutions, hence an increase in the charged:uncharged ratio is certain to correspond to an increase in $\sigma_{\text{bare}}$.

Figures 3.6(a-d) show an experiment where three positively charged surfaces with different $\sigma_{\text{bare}}$ were charge inverted using the same bead and the quadrivalent ion $[Fe(CN)_6]^{4-}$. Positively charged surfaces were prepared using only 1-trichlorosilyl-11-cyanoundecane (1:0) and ratios of 1-trichlorosilyl-11-cyanoundecane:undecyltrichlorosilane of 1:3 and 1:9. In this particular experi-

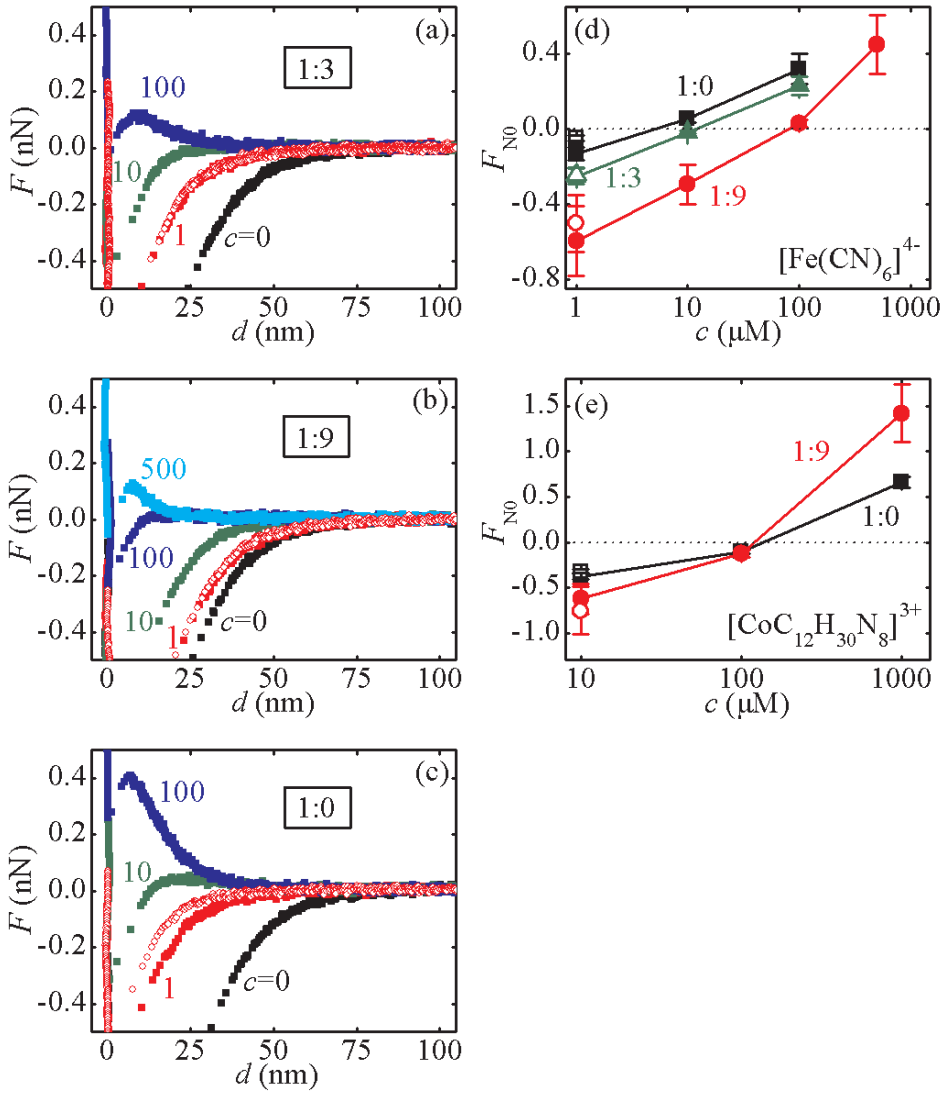


**Figure 3.6:** Force versus separation measurements with the same bead and multivalent ion $[Fe(CN)_6]^{4-}$ on three positively charged surfaces prepared with different ratios of 1-trichlorosilyl-11-cyanoundecane:undecyltrichlorosilane, (a) 1:3, (b) 1:9 and (c) 1:0. Solutions also contained 0.5 mM KCl at pH 6.0±0.5. (d) Normalized force $F_{N0}$ versus multivalent-ion concentration $c$ for all three measurements. Measurements on the 1:0, 1:3 and 1:9 surfaces are shown as squares, triangles and circles, respectively. (e) $F_{N0}(c)$ for measurements with a 1:0 and a 1:9 surface using the multivalent ion $[CoC_{12}H_{30}N_8]^{3+}$ in solutions also containing 0.5 mM KCl at pH 7.0±0.5.

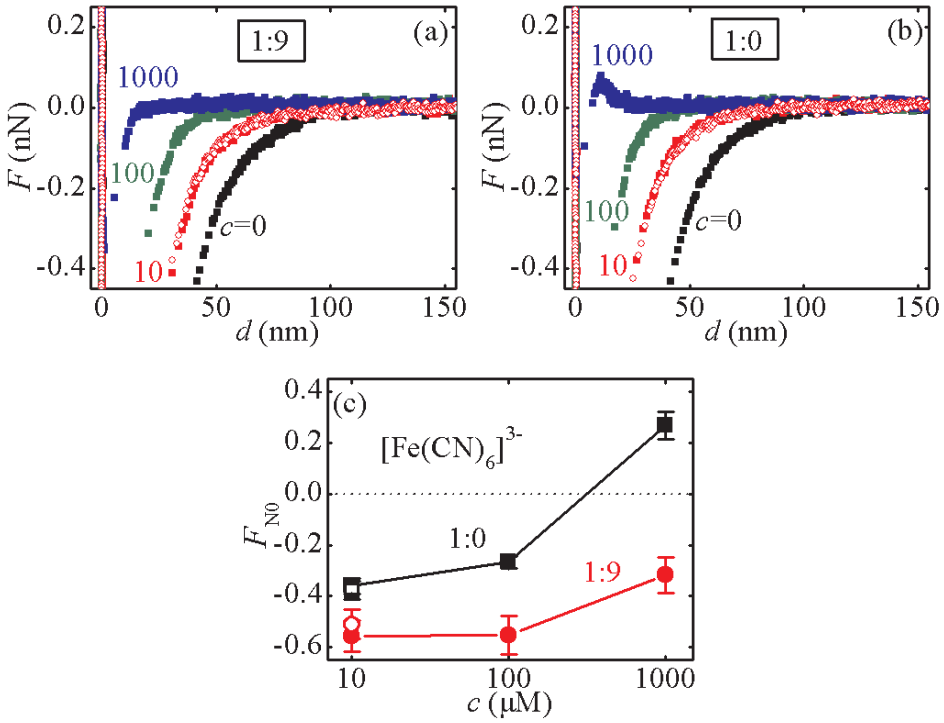


**Figure 3.7:** Force versus separation measurements with the same bead and multivalent ion $[Fe(CN)_6]^{3-}$ on two amine-terminated surfaces prepared with different ratios of 1-trichlorosilyl-11-cyanoundecane:undecyltrichlorosilane, (a) 1:9, (b) 1:0. (c) $F_{N0}$ versus $c$ for both measurements. Measurements on the 1:9 and 1:0 surfaces are shown as circles and squares, respectively. Solutions also contained 0.5 mM KCl at pH 6.0±0.5.

ment, measurements were first done with a 1:3 surface (Fig. 3.6(a)), then with a 1:9 surface (Fig. 3.6(b)) and finally with a 1:0 surface, (Fig. 3.6(c)). The order of the measurements rules out that the observed trend is due to aging of the surfaces. Figure 3.6(d) shows the fitted values of $F_{N0}(c)$ for all three surfaces, showing that decreasing $\sigma_{\text{bare}}$ hinders charge inversion. The values obtained for $c_0$ are 5, 17 and 74 $\mu$M for the 1:0, 1:3 and 1:9 surface respectively.

Figure 3.6(e) shows the results of a control experiment where two different, nominally identical silica beads were charge inverted with $[CoC_{12}H_{30}N_8]^{3+}$ and probed using a 1:9 and a 1:0 surface. The measured charge-inversion concentrations are 140 and 120 $\mu$M using the 1:0 and 1:9 surfaces, respectively. This confirms that the value of $\sigma_{\text{bare}}$ of the positively charged surface has no significant influence on $c_0$ of a silica bead and that this surface indeed acts as a constant probe.

A similar experiment where 1:9 and 1:0 surfaces were charge inverted using the same bead and the trivalent negative ion $[Fe(CN)_6]^{3-}$ is shown in Fig. 3.7. The

value of $c_0$ obtained for the 1:0 surface is 320 $\mu$M. The 1:9 surface did not exhibit charge inversion at 1 mM $[Fe(CN)_6]^{3-}$. Thus if the 1:9 surface can be charge inverted with $[Fe(CN)_6]^{3-}$ ions, $c_0$ is higher than 1 mM. Higher concentrations were not probed because $\lambda$ becomes too short.

## 3.7 Discussion

We first compare our experimental observations with the specific-binding description as summarized by Eq. (3.2). Assuming constant $\Delta\mu^{0*}$, Eq. (3.2) predicts that $c_0 \sim |\sigma_{\text{bare}}/Z|$ and is independent of $\epsilon$. None of these trends agrees with the experiments. We instead observe a decrease of more than an order of magnitude in $c_0$ when increasing $Z$ from 3 to 4 [2], a decrease in $c_0$ with increasing $\sigma_{\text{bare}}$ instead of the predicted increase, and a sharp decrease in $c_0$ with decreasing $\epsilon$.

To reconcile the observations with Eq. (3.2) it is necessary to let the adsorption energy $\Delta\mu^{0*}$ depend on $Z$, $\epsilon$ and $\sigma_{\text{bare}}$ and empirically fit its value for each individual measurement. While this approach lacks predictive power, some of the trends observed in the experiment could be rationalized in this way. For example, a more negative $\Delta\mu^{0*}$ might be expected for all ions when the dielectric constant is decreased since this affects ion solubility. The dielectric constant might similarly influence the hydrolysis of metal ions. Two aspects of the data call for a more universal explanation, however.

First, $\Delta\mu^{0*}$ is expected to depend critically on the specific chemical composition of the ions. Although some differences were observed with $La^{3+}$, the measured $c_0$ and its dependence on $\epsilon$ was similar for three chemically very distinct ions with the same valence.

Second, the observed dependence of $c_0$ on $\sigma_{\text{bare}}$ implies that binding of the multivalent ions to the surface is cooperative: increasing the density of surface charges facilitates charge inversion. This behavior is not captured by a simple chemical binding picture. This remains true even if a more sophisticated description of the surface is introduced. For example, the surface can be modelled as consisting of discrete sites where multivalent ions compete with other charge-determining ions. Such a model yields an equation similar to Eq. (3.2) but with a prefactor that is independent of $\sigma_{\text{bare}}$. That is, it still does not exhibit cooperativity.

We now compare the observations with the ion correlation theory of Eqs. (3.3)-(3.5). The latter predicts that $\mu_c \propto -\sqrt{|\sigma_{\text{bare}} Z^3|}/\epsilon$ approximately, and this expression captures very well the direction (increase or decrease) and relative magnitude of the dependence of $c_0$ on these parameters.

**Table 3.1:** Important parameters for the ion-correlation model calculated using Eqs. (3.3)-(3.5) and the measured values of $c_0$ (also shown) for the same ion with different values of $\epsilon$. Units are $\mu$M for $c_0$, e/nm$^2$ for $\sigma_{\rm bare}$ and $kT$ for $\Delta\mu^0$ and $\mu_c$.

| ion | $c_0$ $\epsilon = 80$ | $c_0$ $\epsilon = 68$ | $c_0$ $\epsilon = 54$ | $\sigma_{\rm bare}$ | $\Delta\mu^0$ | $\mu_c$ $\epsilon = 80$ | $\mu_c$ $\epsilon = 68$ | $\mu_c$ $\epsilon = 54$ |
|---|---|---|---|---|---|---|---|---|
| $[Fe(CN)_6]^{4-}$ | 12 | 5 | | 0.11 | -4.1 | -4.3 | -5.2 | |
| $[Fe(CN)_6]^{4-}$ | 12 | | 1 | 0.12 | -4.0 | -4.4 | | -6.9 |
| $[Fe(CN)_6]^{4-}$ | | 5 | 1 | 0.11 | -3.9 | | -5.4 | -7.0 |
| $[Fe(CN)_6]^{3-}$ | 120 | | 18 | 0.17 | -3.5 | -3.3 | | -5.2 |
| $[CoC_{12}H_{30}N_8]^{3+}$ | 220 | 88 | | -0.28 | -2.2 | -4.5 | -5.4 | |
| $[CoC_{12}H_{30}N_8]^{3+}$ | 220 | | 14 | -0.34 | -1.9 | -4.9 | | -7.7 |
| $[CoC_{12}H_{30}N_8]^{3+}$ | | 88 | 14 | -0.37 | -1.6 | | -6.2 | -8.0 |
| $[CoC_{12}H_{30}N_8]^{3+}$ | 300 | | 10 | -0.50 | -0.8 | -6.2 | | -9.6 |
| $[Ru(NH_3)]^{3+}$ | 520 | | 23 | -0.43 | -0.8 | -5.6 | | -8.8 |
| $La^{3+}$ | 280 | | 6 | -0.63 | -0.3 | -7.0 | | -10.9 |

The experimental data permit a more quantitative self-consistency test of this theory. Two unknown parameters enter the model: the surface-charge density at charge inversion, $\sigma_{\rm bare}(c_0)$, and the residual chemical interaction, $\Delta\mu^0$. Two measurements carried out under slightly different conditions can be used for extracting values for these parameters. We previously showed in this manner that varying $Z$ while keeping the chemical structure constant yields results consistent with $\Delta\mu^0 \approx 0$ [2].

A similar procedure can be used for the measurements at different values of $\epsilon$ presented here. Assuming that $\sigma_{\rm bare}$ and $\Delta\mu^0$ do not depend on $\epsilon$, their values can be deduced from consecutive measurements using the same ion and solvents with different $\epsilon$. The numerical results of this procedure are summarized in Table 3.1, together with the corresponding calculated values of $\mu_c$. In those cases where three values of $\epsilon$ were measured, fits were performed pairwise to extract separate estimates of $\sigma_{\rm bare}$ and $\Delta\mu^0$; the results are consistent within experimental scatter.

We first focus on the results for charge inversion of a silica bead by trivalent positive ions. The fitted values of $\Delta\mu^0$ are in the range $-0.3kT$ to $-2.2kT$. For comparison, the corresponding values of $\mu_c$ are in the range $-4.5kT$ to $-10.9kT$. This implies that spatial correlations between multivalent ions are largely sufficient to account for charge inversion. Results for the three different trivalent positive ions are similar, re-iterating that, in spite of anomalies observed with $La^{3+}$, the chemical composition of these ions does not appear to play a dominant role in determining $c_0$. Figure 3.8(a) plots the measured values of $c_0$ as a function

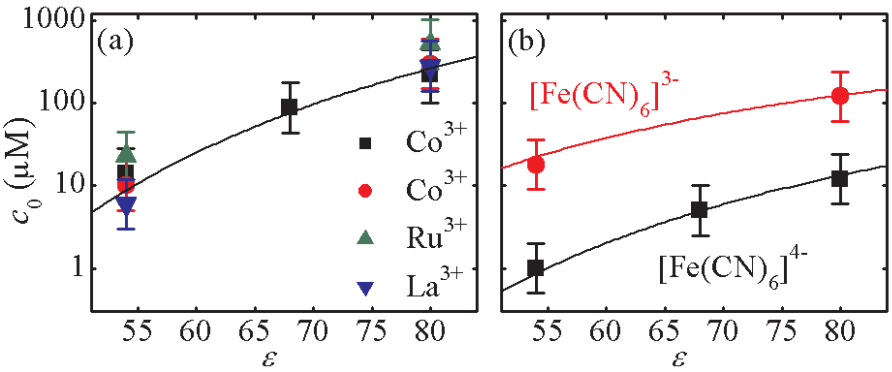


**Figure 3.8:** (a) Charge-inversion concentration $c_0$ versus dielectric constant $\epsilon$ for the data shown in Fig. 3.4(f) and 3.5. The lines are the predicted $c_0$ versus $\epsilon$ according to Eq. (3.3) with $\sigma_{\text{bare}} = 0.5$ e/nm$^2$, $\Delta\mu^0 = -1kT$ and a typical value $r = 0.4$ nm for the radius of the ions. The error bars represent a factor of two, which corresponds to the scatter in the data for measurements with the same ion using different, nominally identical beads and amine-terminated surfaces. (b) Same as (a) for the data of Fig. 3.3 and 3.4(c). The fitted curves use $\sigma_{\text{bare}} = 0.14$ e/nm$^2$, $\Delta\mu^0 = -3.6kT$ and the real radius of the ions.

of $\epsilon$ for the different experiments, and shows that all of our measurements for silica surfaces are consistent with $\sigma_{\text{bare}} = -0.5$ e/nm$^2$ and $\Delta\mu^0 = -1kT$. Taken together, these observations lend further support to the proposal that a spatial interactions between multivalent ions are the driving mechanism behind charge inversion.

Results for the amine-terminated surfaces are not as clear-cut. The calculated values of $\Delta\mu^0$ for charge inversion of the amine-terminated surface by trivalent and quadrivalent negative ions are significantly larger than $kT$ and comparable in magnitude to $\mu_c$. Figure 3.8(b) shows that the values of $c_0$ for these measurements can be described by Eq. (3.3) using $\sigma_{\text{bare}} = 0.14$ e/nm$^2$ and $\Delta\mu^0 = -3.6kT$. In terms of Eq. (3.3), this suggests that spatial correlations between multivalent ions do not fully account for the observed charge inversion in this case, and that specific binding also plays a role.

One possible reason for this discrepancy is that the calculated values of $\sigma_{\text{bare}}$ of the amine-terminated surfaces correspond to the lower end of the range of validity of the inequality $\Gamma \gg 1$. A similar trend was observed in measurements where $Z$ was varied with low surface-charge densities [2]. Another possible reason is that in the theoretical descriptions discussed here, the charge on the surface is modelled as being continuously distributed whereas real surfaces consist of discrete chemical groups. This disorder can potentially facilitate charge inversion [28, 29]. The relative important of this disorder is expected to increase with

decreasing $\sigma_{\rm bare}$.

Some caution is necessary in drawing conclusions from the quantitative analysis above, however. If regulation of the surface charge plays a significant role, $\sigma_{\rm bare}$ depends on the ion concentrations and thus on $c_0$. The analysis instead assumes that $\sigma_{\rm bare}$ remains constant. Similarly, both $\sigma_{\rm bare}$ and $\Delta\mu^0$ can depend on $\epsilon$ [30], introducing errors in the quantitative comparison. The degree of consistency between the three calculated values of $\sigma_{\rm bare}$ and $\Delta\mu^0$ for the measurements with three values of $\epsilon$ suggests that treating $\sigma_{\rm bare}$ and $\Delta\mu^0$ as constants is at least approximately valid, however. To describe the behavior of $F_0$ away from $c_0$, regulation of the surface charge has to be considered within the theory. Elucidating the interplay between disorder, regulation and correlations remains an important theoretical challenge.

In summary, we have performed a systematic study of charge inversion by multivalent ions using atomic force spectroscopy. At long range this technique gives a direct, unambiguous measurement of the polarity of the surface being probed. Measurements at shorter range show an additional attractive component of the force, corresponding to constant-potential boundary conditions. We measured the dependence of the charge-inversion concentration on valence, chemical composition, dielectric constant and surface-charge density, the latter indicating that multivalent ion adsorption is cooperative. These observations are remarkably consistent with a very straightforward description of charge inversion in terms of spatial interactions between multivalent ions in the Stern layer [16]. To our knowledge, no existing description based on specific adsorption provides a similar degree of agreement, even at a qualitative level. A direct experimental proof of the correlation mechanism, via direct determination of the spatial correlations between multivalent ions at the surface, would be highly desirable.

**Acknowledgement:** We thank J. Lyklema, H. A. Heering and B. Shklovskii for useful discussions and C. Dekker for general support.

# Bibliography

[1] V. A. Bloomfield, Biopolymers **44**, 269 (1997).

[2] K. Besteman, M. A. G. Zevenbergen, H. A. Heering, and S. G. Lemay, Phys. Rev. Lett. **93**, 170802 (2004).

[3] R. O. James and T. W. Healey, J. Colloid Interface Sci. **40**, 42 (1972); **40**, 53 (1972); **40**, 65 (1972).

[4] A. Martín-Molina, M. Quesada-Pérez, F. Galisteo-González, and R. Hidalgo-Álvarez, J. Chem. Phys. **118**, 4183 (2003).

[5] R. Messina, C. Holm, and K. Kremer, Phys. Rev. Lett. **85**, 872 (2000).

[6] M. Tanaka and A. Y. Grosberg, Eur. Phys. J. E. **7**, 371 (2002).

[7] R. M. Pashley, J. Colloid Interface Sci. **102**, 23 (1984).

[8] K. B. Agashe and J. R. Regalbuto, J. Colloid Interface Sci. **185**, 174 (1996).

[9] V. Vithayaveroj, S. Yiacoumi, and C. Tsouris, J. Dispersion Sci. Technol. **24**, 517 (2003).

[10] For comprehensive reviews see A. Yu. Grosberg, T. T. Nguyen, and B. I. Shklovskii, Rev. Mod. Phys. **74**, 329 (2002); Y. Levin, Rep. Prog. Phys. **65**, 1577 (2002); M. Quesada-Pérez, E. González-Tovar, A. Martín-Molina, M. Lozada-Cassou, and R. Hidalgo-Álvarez, Chem.Phys.Chem. **4**, 234 (2003).

[11] E. S. Reiner and C. J. Radke, Adv. Colloid Interface Sci. **47**, 59 (1993).

[12] S. H. Behrens and D. G. Grier, J. Chem. Phys. **115**, 6716 (2001).

[13] J. Lyklema and J. F. L. Duval, Adv. Colloid Interface Sci. **114**, 27 (2005).

[14] R. Zhang and B. I. Shklovskii, Phys. Rev. E **72**, 021405 (2005).

[15] R. Pericet-Camara, G. Papastavrou, S. H. Behrens, and M. Borkovec, J. Phys. Chem. B **108**, 19467 (2004).

[16] B. I. Shklovskii, Phys. Rev. E **60**, 5802 (1999).

[17] H. Totsuji, Phys. Rev. A **17**, 399 (1977).

[18] I. Rouzina and V. A. Bloomfield, J. Phys. Chem. **100**, 9977 (1996).

[19] J. Ennis, S. Marcelja, and R. Kjellander, Electrochim. Acta **41**, 2115 (1996).

[20] W. A. Ducker, T. J. Senden, and R. M. Pashley, Langmuir **8**, 1831 (1992).

[21] Sum of metal ion radius and ligand ($H_2O$, $NH_3$, $CN^-$) diameter. The radii are comparable (within 4 %) to crystallographic data.

[22] R. D. Shannon, Acta Crystallogr., Sect A: Cryst. Phys., Diffr., Theor. Gen. Crystallogr. **A32**, 751 (1976).

[23] Y. Marcus, *Ion properties* (Marcel Dekker Inc., New York, 1997), Chap. 3.

[24] Measurements were done at pH less than the first hydrolysis constant of $La^{3+}$; J. Burgess, *Metal ions in solution* (Ellis Horwood, Chichester, England, 1979), Chap. 9.

[25] From crystal structure with van der Waals radii; A. Bacchi, F. Ferranti, and G. Pelizzi, Acta Crystallogr., Sect. C: Cryst. Struct. Commun **C49**, 1163 (1993).

[26] G. Telléz and E. Trizac, Phys. Rev. E **70**, 011404 (2004).

[27] G. Arscott and V. A. Bloomfield, Biopolymers **36**, 345 (1995).

[28] A. G. Moreira and R. R. Netz, Europhys. Lett. **57**, 911 (2002).

[29] M. L. Henle, C. D. Santangelo, D. M. Patel, and P. A. Pincus, Europhys. Lett. **66**, 284 (2004).

[30] F. A. Rodrigues, P. J. M. Monteiro, and G. Sposito, J. Colloid Interface Sci. **211**, 408 (1999).

# Chapter 4

# Influence of charged surfaces on the morphology of DNA condensed with multivalent ions

**K. Besteman, K. van Eijk, I. D. Vilfan, and S. G. Lemay**

DNA in solution can be condensed into dense aggregates by multivalent counterions. Atomic Force Microscopy has been widely used to study DNA condensation, but this requires adsorbing the condensates on a surface. Here we investigate the effect of this nearby surface on the morphology of DNA condensates. We show that, contrarily to what has often been assumed, interactions between DNA condensates and the surface can strongly influence the observed morphology.

## 4.1 Introduction

DNA in solution can condense into compact structures in the presence of a sufficiently high concentration of multivalent cations [1]. This multivalent-ion-induced DNA condensation was first observed with the naturally occurring polyamine spermidine [2] which, together with other polyamines, is involved in several cellular processes including DNA compaction in vivo [3]. DNA compaction by polycations has also been identified as a promising system for gene delivery [4].

It is mostly believed that the short range interaction leading to DNA condensation results from an inhomogeneous distribution of counterions causing oscillations of the polarity of the charge along the length of the DNA [5–10]. Proposals for the origin of this charge modulation include dynamic fluctuations of the counterion distribution [6, 7], the intrinsic helicity of DNA [8], and the formation a strongly correlated liquid (SCL) of multivalent counterions [9, 10]. Directly probing the microscopic interaction between DNA molecules experimentally has however proven difficult due to the short length scales involved.

One of the main approaches being pursued to infer the microscopic mechanism behind DNA condensation consists in investigating the morphology of DNA condensates and its evolution over time. Several imaging techniques have been applied to this problem. Using electron microscopy, toroidal, rod-like and sphere-like structures were reported for DNA condensed with the trivalent ions spermidine and cobalt hexamine and the quadrivalent ion spermine [2, 11, 12]. In these measurements, the DNA was condensed in solution and deposited on a hydrophobic carbon grid, then stained to obtain contrast, and finally fixed on the surface with ethanol. Most of the observed structures were three-dimensional and appeared largely undistorted by the presence of the imaging surface. Considerable further support for the hypothesis that the observed structures resemble those in bulk solution was given by the cryoelectron microscopy work of Hud and Downing [13].

Another powerful imaging technique frequently used for the study of the morphology of condensed DNA is Atomic Force Microscopy (AFM) [14]. A variety of morphologies, including toroid-like, rod-like and so-called flower-like structures have been observed using AFM for DNA condensed with spermine and spermidine [15–17], cobalt hexamine [18] and several other multivalent cations [19, 20]. Although some of the observed morphologies resemble those observed with electron microscopy, most observations with AFM show more poorly defined structures that are often relatively flat. It has been argued that the flower-like structures are early intermediates in the condensation pathway [16]. Similar structures were also observed for DNA condensed using several polycations considered promising

for gene delivery [21–25]. Finally, DNA has been observed to condense in the presence of mobile cationic surface groups [26–28].

Advantages of AFM are that no staining is required to observe the condensates and that imaging can be performed in liquid without drying the sample (although most existing AFM studies of DNA condensation have nonetheless been done in air for practical reasons). This technique however requires the condensates to be attached to a surface; most studies use mica as the imaging surface as it is very flat, hydrophilic, and readily binds DNA condensates. It remains unclear to what extent the observed structures reflect those present in bulk or are influenced by the nearby surface, however. Non-trivial interactions can be expected since the same physical mechanism that causes DNA-DNA attraction and condensation can also potentially mediate an attractive interaction between DNA and the negatively charged mica. According to the SCL model, a larger charge density can even enhance the attractive interaction between like-charged objects mediated by multivalent ions [9, 10].

In this study we used AFM imaging to investigate the effect of a nearby surface on the morphology of DNA condensates. We obtained high-quality images of DNA condensates prepared over a broad range of concentrations of different multivalent ions and deposited on surfaces with different properties. We conclude that the morphology of the condensates is strongly influenced by the nearby surface, significantly limiting the applicability of AFM as a probe of the morphology of multivalent-ion-induced DNA condensates in solution. Counter-intuitively, the most negatively charged surface, bare mica, exhibits the strongest attraction for negatively charged DNA. This suggests that the same counterion-mediated interaction responsible for DNA condensation also dominates DNA-surface interactions.

## 4.2 Materials and Methods

We have used four different positively charged multivalent cations to condense DNA. These included the two trivalent ions cobalt sepulchrate ($[CoC_{12}H_{30}N_8]^{3+}$, cosep) and cobalt hexamine ($[Co(NH_3)_6]^{3+}$, cohex), as well as the biologically relevant trivalent and quadrivalent polyamines spermidine ($[C_7N_3H_{22}]^{3+}$) and spermine ($[C_{10}N_4H_{30}]^{4+}$). All ions were ordered from Sigma as chloride salts and used as received.

We present AFM data for three different imaging surfaces, freshly cleaved muscovite mica (bare mica), freshly cleaved graphite, and mica coated with poly-L-lysine (PL). Bare mica is negatively charged in water and DNA does not adsorb

to it in the absence of multivalent ions. Graphite is very hydrophobic with a slight negative charge at neutral pH. Uncondensed DNA binds only weakly to graphite and therefore cannot be imaged well; condensed DNA does get sufficiently immobilized on the graphite to obtain reliable images. Finally, adsorbing poly-L-lysine on mica yields a positively charged surface and thus allows DNA to bind even in the absence of multivalent ions. This surface is commonly employed to image DNA with AFM. We prepared PL-coated mica surfaces by incubating a 5 $\mu$L droplet of 0.1% PL (molecular weight 70000-150000) in deionized, milli-Q-filtered water (milli-Q water) on freshly cleaved muscovite mica for 30 sec, after which the droplet was flushed off with milli-Q water and the surface was blown dry in a stream of nitrogen. Using AFM force spectroscopy, we experimentally verified that the PL-coated mica was positively charged.

DNA samples were prepared in an identical manner for all measurements. Double-stranded 1.5 kbp DNA fragments were produced by PCR using $\lambda$-DNA as a template and primer sequences 5′- GTAAAGCGCCACGCTCC and 5′-TGATATTGCCAAAACAGAGCTG, and purified using gel extraction. Solutions containing 1 ng/$\mu$L DNA, 10 mM TRIS buffer with pH 7.5, and a concentration of multivalent ions in the range between $10^{-6}$ and 1 M were prepared. After a 5 min incubation time, 5 $\mu$L of solution was deposited on the surface. Imaging was done both in air and in liquid environment. For imaging in air the droplet was flushed off after 1 min with milli-Q water and dried in a stream of nitrogen. For imaging in liquid the droplet was flushed off after 1 min with a solution containing 10 mM TRIS and the same concentration of multivalent ions as the condensing solution. Subsequently the dry or wet substrates were imaged with a Digital Instrument NanoScope IV AFM using tapping mode. For dry imaging Olympus Micro cantilevers (OMCL-AC160TS) with a spring constant of 42 N/m (as indicated by the manufacturer) were used. Wet imaging was done using Veeco Microlever probes (MLCT-AUHW) with a spring constant of 0.03 N/m (as indicated by the manufacturer).

Multivalent cations from the DNA solution also participate in screening the negative surface charge of bare mica and graphite. For low bulk concentrations of multivalent ions, this accumulation of multivalent ions at the surface lowers the bulk concentration and could thereby hinder condensation [29]. Depletion of the solution by a charged surface should be considered in any study using low concentrations of multivalent ions. We verified that this was not a significant factor in this experiment at 100 $\mu$M spermidine by pre-treating bare mica with 100 $\mu$M spermidine in 10 mM TRIS solution to saturate the mica with multivalent ions before depositing a droplet containing the DNA and 100 $\mu$M spermidine. No change in behavior was observed, indicating that depletion of the bulk solution

does not play a major role in our experiments.

Dynamic light scattering (DLS) measurements were performed using a Zetasizer Nano ZS apparatus (Malvern Instruments) to independently determine the hydrodynamic diameter of the DNA condensates in solution. Volumes of 1 mL of the same solutions as used for AFM were prepared. After a variable incubation time the DLS measurement was performed in a disposable cuvette.

Transmission Electron Microscopy (TEM) was performed using a Philips CM300 UT FEG high-tension instrument with 300 kV electron-beam energy. TEM samples were prepared by depositing 5 $\mu$L of solution as used for AFM on a carbon-coated grid, incubating for 10 min and staining for 1 min with uranyl acetate (Sigma) after which the sample was dipped in ethanol and blotted dry.

## 4.3 Results and Discussion

Figure 4.1a-g shows AFM images in air of DNA condensed with spermidine and deposited on bare mica. The morphology of the DNA changes dramatically with increasing multivalent-ion concentration. In zero or a very low concentration of spermidine (1 $\mu$M, data not shown), DNA does not adsorb to negatively charged mica. In contrast, at 10 $\mu$M (not shown) and 100 $\mu$M (Fig. 4.1a) spermidine, individual uncondensed molecules are seen to adsorb to the surface. The multivalent ions thus mediate a net attraction between negatively charged mica and DNA. At 1 mM, 10 mM and 100 mM (Fig. 4.1b, 4.1c and 4.1d, respectively), large multimolecular condensates are observed. The structures are disordered and do not resemble toroids or rods, but rather the previously reported flower-like structures. They are also very flat, consisting for the most part of individual DNA molecules or bundles of a few molecules lying in direct contact with the surface. A higher three-dimensional core is also observed. At 900 mM spermidine (Fig. 4.1e), the highest concentration investigated, the condensates had dissolved and we again observed loose DNA. This well-known reentrant behavior was first reported by Pelta *et al* [30].

Figure 4.1h-j shows characteristic images of DNA condensates prepared in the same manner with spermidine but adsorbed on graphite instead of mica. Uncondensed DNA binds only weakly to the hydrophobic graphite and can therefore not be imaged well. Condensed DNA does get sufficiently immobilized on the graphite to obtain reliable images. Condensates are observed on the surface from above 0.1 mM spermidine to about 100 mM, a range of concentrations similar to that for bare mica. On the other hand, the morphology of the condensates is very different from that observed on bare mica: the core of the condensates

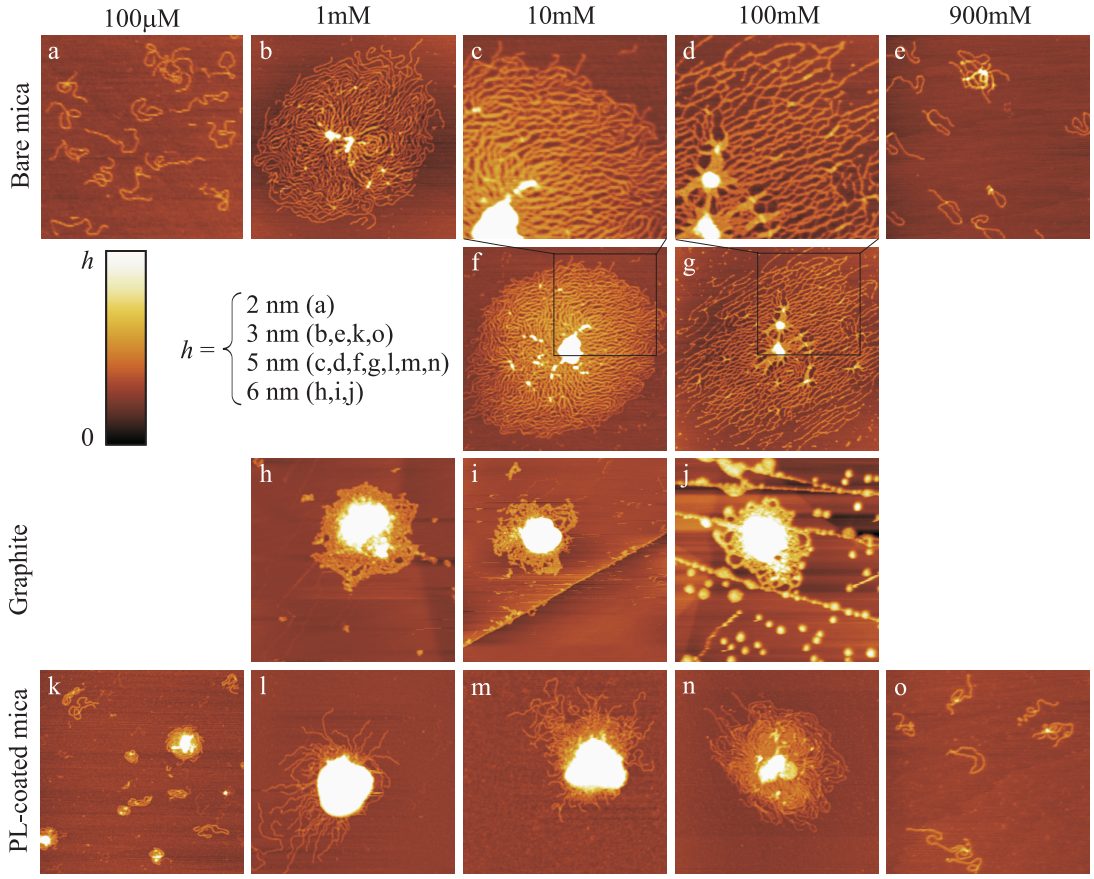


**Figure 4.1:** AFM images in air of DNA condensates prepared with different concentrations of spermidine as indicated above the images on bare mica (a-g), graphite (h-j) and PL-coated mica (k-o). Images (a-e) and (h-o) are 1 $\mu$m by 1 $\mu$m. Images (f) and (g) are 2 $\mu$m by 2 $\mu$m. Images (c) and (d) show additional details of the condensates in images (f) and (g), respectively.

appears globular, with greater height (up to ∼20 nm) and a smaller width than on mica. A flat disk structure is still observed surrounding the central globular core, but it does not extend as far from the core.

For comparison, Fig. 4.1k-o shows corresponding images for PL-coated mica. As expected for this positively charged surface, uncondensed DNA molecules adsorb to PL-coated mica at low concentrations of spermidine (not shown). Small condensates are already visible on the surface at 10 $\mu$M (similar-looking to the smallest condensates in Fig. 4.1k) and 100 $\mu$M (Fig. 4.1k) spermidine, whereas condensates are not yet visible on bare mica at 100 $\mu$M. Finally, the condensates on PL-coated mica are 3-dimensional with flat edges reminiscent of condensates observed on graphite, as seen in Figs. 4.1l, 4.1m and 4.1n for 1 $\mu$M, 10 $\mu$M and 100 $\mu$M spermidine, respectively. Since PL is a known condensing agent [23],

traces of PL coming (partly) off the surface might assist in the condensation and could cause the lower threshold for condensation on PL-coated mica. Because of this potential influence of PL, the results on this surface cannot be directly compared to the two other surfaces. Nonetheless, the similarities between graphite and PL-coated mica indicate that the net influence of these surfaces on condensate morphology is comparable.

The condensates on all three surfaces have comparable volumes as measured by AFM, confirming that they correspond to the same bulk structures before adsorption to the surface.

In order to ascertain to what extent the imaging surfaces disturb the three-dimensional structure of the condensates in solution, we performed dynamic light scattering (DLS) measurements on the same solutions as used for AFM imaging. Figure 4.2a shows the measured hydrodynamic-diameter distribution of DNA condensates prepared with 1, 10 and 100 mM spermidine after a 5 min incubation time. A well defined, reproducible peak in the distribution is observed at 300 nm. The hydrodynamic diameter became larger with incubation time, indicating slow growth and/or aggregation of the condensates (Fig. 4.2b). The measured hydrodynamic diameters are in agreement with those obtained from comparable studies in the literature [17], and the hydrodynamic diameter measured after 5 min incubation time is similar to the width of the DNA condensates observed on graphite and on PL-coated mica. For spermidine concentrations up to 0.1 mM and from 300 mM we did not obtain a well defined and reproducible size distribution, suggesting that DNA condensation did not occur.

To further investigate the morphology of the condensates in solution, we performed TEM imaging of DNA condensed with 1 mM spermidine. TEM mainly showed small aggregates of torroidal structures (Fig. 4.2d-f), consistent in size with the DLS measurement. Three-dimensional, well condensed particles were thus present in solution. Individual torroids were also observed (Fig. 4.2c).

As a further check of the existence of torroids in the solutions used for AFM imaging, we obtained AFM data on a graphite surface treated with an oxygen plasma. The treatment was performed at 100 mTorr ($\sim$80% oxygen) for 15 sec. This created a rough surface that is comparable to that of a standard TEM grid. Torroidal structures could occasionally be observed on this carefully tuned surface with 0.25 mM spermidine as condensing agent, as shown in Fig. 4.2g.

The spectrum of observations on the various surfaces together with the independent characterization of the samples by DLS and TEM directly demonstrate that the morphology of DNA condensates is significantly distorted by adsorption to a surface. Counter-intuitively, the negatively charged bare mica surface perturbs the three-dimensional structure of the condensates the most and results in

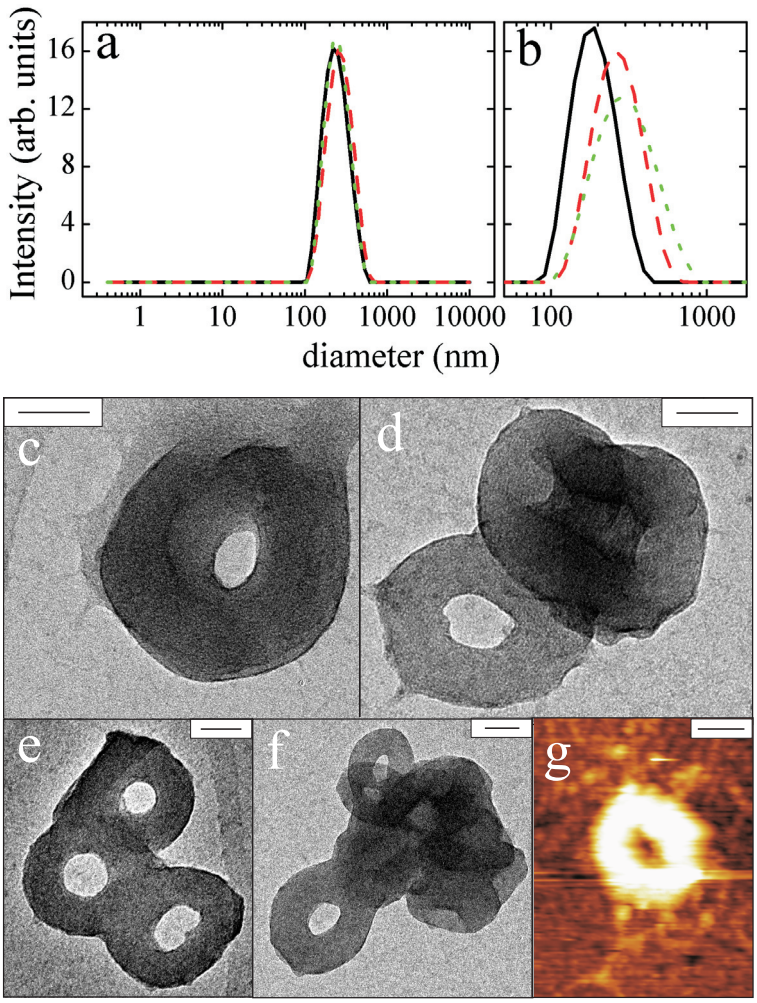


**Figure 4.2:** (a) Distribution of the hydrodynamic diameter of condensates in a solution containing 1 ng/$\mu$L DNA, 10 mM TRIS, and spermidine concentrations of 1 mM (solid line), 10 mM (dashed line), and 100 mM (dotted line) after 5 min incubation time measured with DLS. (b) Similar measurements for a solution containing 1 ng/$\mu$L DNA, 10 mM spermidine and 10 mM TRIS after 2 min (solid line), 5 min (dashed line) and 8 min (dotted line) incubation time. Intensity is normalized to the area under the curve. (c-f) TEM images of DNA condensed with 1 mM spemidine in 10 mM TRIS. (g) AFM image of a torroidal DNA condensate on graphite treated with oxygen plasma. The color scale is the same as in Fig. 4.1, with $h = 6$ nm. All scalebars represent 50 nm.

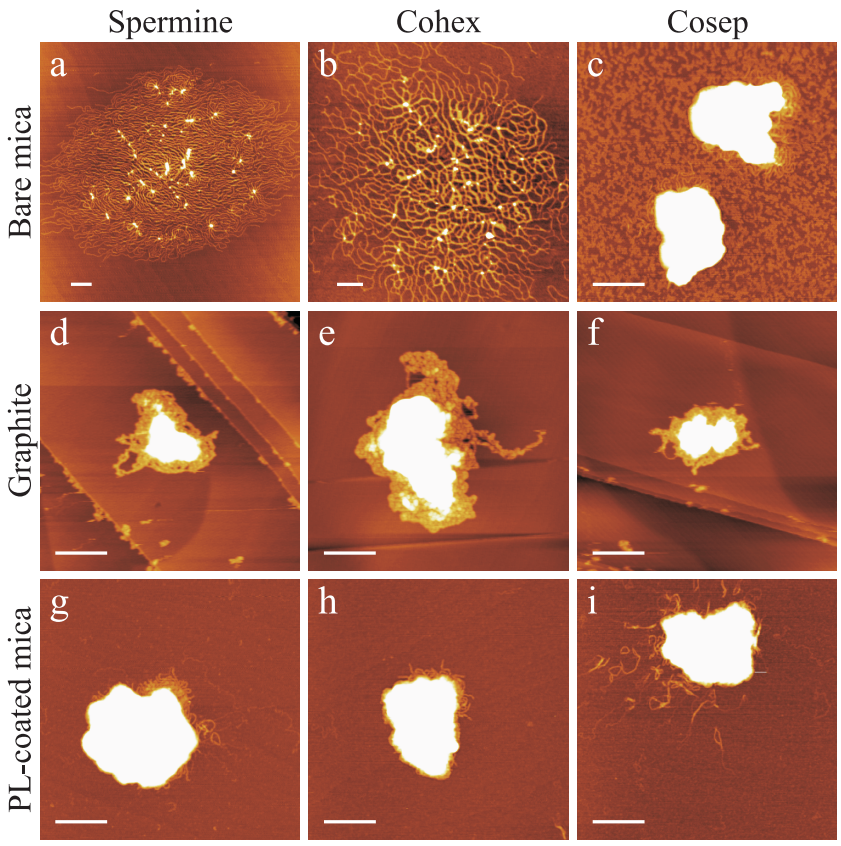


**Figure 4.3:** AFM images in air of DNA condensates prepared with 10 mM spermine (a,d,g), cohex (b,e,h), and cosep (c,f,i) on bare mica (a-c), on graphite (d-f) and on PL-coated mica (g-i). The cosep, and to a lesser extend the cohex, left behind a residue on bare mica at concentrations above 0.1 mM; this is the origin of the surface roughness in (c). All scalebars represent 200 nm. The color scale is the same as in Fig. 4.1, with $h = 3$ nm for images (a) and (b) and 5 nm for images (c)-(i).

the flattest morphologies, indicating a strong attraction with negatively charged DNA. This attraction, like DNA condensation itself, is mediated by multivalent cations since no adhesion of DNA is observed in their absence. It is therefore likely that the same microscopic mechanism is responsible for both effects. It is however difficult to draw strong conclusions from simple images bout the nature of this mechanism. In particular, we cannot ascertain the relative importance of charge inversion of the surfaces [31, 32] and of short-range attraction due to inhomogeneous distributions of counterions [5–7, 9, 10].

We repeated these experiments using three other multivalent ions. Figure 4.3 shows results for 10 mM multivalent ions. The results for spermine and cohex were very similar to those for spermidine, including the difference in the morphology of the condensates on bare mica, on graphite and on PL-coated mica

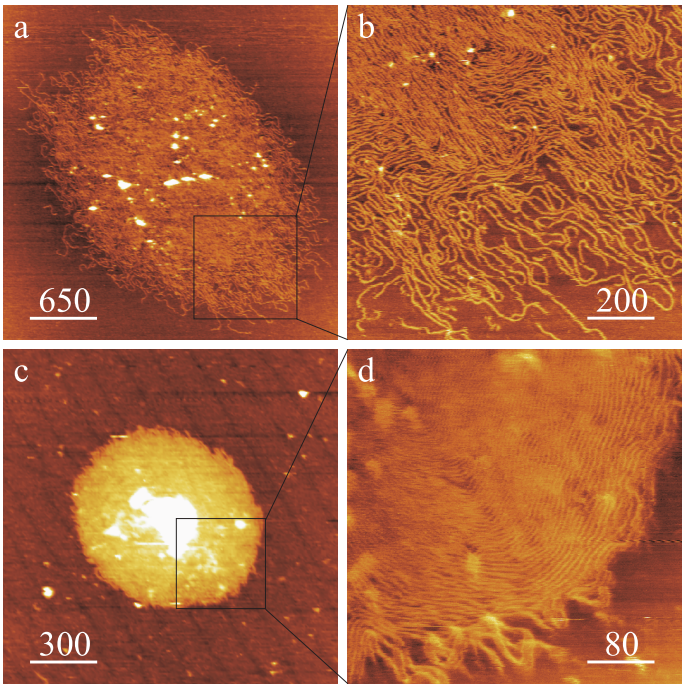


**Figure 4.4:** AFM images in liquid of DNA condensates on bare mica (a,b) and on PL-coated mica (c,d). All images were obtained in a solution containing 1 mM spermidine and 10 mM TRIS buffer. The color scale is the same as in Fig. 4.1, with $h = 3$ nm. Images (b) and (d) show zooms of the condensates in images (a) and (c) respectively. Size of scalebars is given in nm.

(Fig. 4.3a,b,d,e,g,h). In contrast, the condensates prepared with cosep were similar for these three surfaces and resembled the structures observed on graphite and on PL-coated mica for the other ions (Fig. 4.3c,f,i). This indicates that the influence of the surface on the observed morphology can be ion specific. Whether this specificity results from ion-specific DNA-DNA interactions or DNA-surface interactions cannot be deduced from these imaging experiments.

The measurements discussed above were performed in air, leaving open the possibility that the observed surface dependence is an artifact resulting from the drying process. To investigate the influence of drying we have performed AFM imaging in liquid. Figure 4.4 shows representative results for DNA condensed with 1 mM spermidine using bare mica and PL-coated mica as the imaging surfaces. Again a clear difference between condensates on bare mica (Fig. 4.4a,b) and on PL-coated mica (Fig. 4.4c,d) is observed, with similar trends in liquid as in air. On bare mica, the condensates are flat and often consist of only a DNA monolayer, indicating that the surface has a large influence on the morphology. On the PL-coated mica the condensates consist of a 3-dimensional core

surrounded by a flat disk.

Additional fine details of the condensates can be observed in liquid, in particular the arrangement of individual DNA molecules in the monolayer-thick region near the edges of the condensates. Further differences between condensate structures on the two surfaces exist at this more microscopic level. On PL-coated mica, DNA strands tend to be highly ordered, with adjacent molecules running parallel to each other. The spacing between strands is larger than that corresponding to tight packing (∼2.4 nm [13]). For example, the spacing between parallel molecules in Fig. 4.4d is 4 nm near the center of the condensate and 7 nm near the edges. On bare mica the DNA is less ordered and the spacing between individual molecules is larger than on PL-coated mica. Crossings of two DNA molecules are relatively rare, suggesting substantial relaxation of the condensate structure following adsorption.

## 4.4 Conclusions

We have imaged DNA condensed with different concentrations of four multivalent ions adsorbed on three chemically distinct surfaces. The flattened morphology of the condensates is indicative of strong DNA-surface interactions. We further observed significant systematic differences in the morphology of condensates adsorbed on different surfaces. Surprisingly, the negatively charged bare-mica surface results in the most flattened condensates. Graphite still perturbs the condensate structure somewhat, however, as can be seen from the flat edges adhering to the surface around the central globular condensates.

This study directly demonstrates that AFM imaging on surfaces is an unreliable probe of the morphology of condensates in bulk solution, limiting the usefulness of AFM for the study of DNA condensation with multivalent ions. DNA compaction near a charged surface is biologically very relevant and worthy of study in its own right [14]. Our measurements however show that in such study it is crucial to use the precise surface of interest since the choice of surface influences the condensate structure.

**Acknowledgement:** We thank U. Ziese for obtaining the electron-microscopy images, H. W. Zandbergen for providing access to the TEM, and C. Dekker for general support.

# Bibliography

[1] V. A. Bloomfield, Biopolymers **44**, 269 (1997).

[2] L. C. Gosule and J. A. Schellman, Nature **259**, 333 (1976).

[3] T. Thomas and T. J. Thomas, Cell. Mol. Life Sci. **58**, 244 (2001).

[4] V. Vijayanathan, T. Thomas, and T. J. Thomas, Biochemistry **41**, 14085 (2002).

[5] W. M. Gelbart, R. F. Bruinsma, P. A. Pincus, and V. A. Parsegian, Physics Today **53**, 38 (2000).

[6] F. Oosawa, Biopolymers **6**, 1633 (1968).

[7] R. Golestanian and T. B. Liverpool, Phys. Rev. E **66**, 051802 (2002).

[8] A. A. Kornyshev and S. Leikin, Phys. Rev. Lett. **82**, 4138 (1999).

[9] I. Rouzina and V. A. Bloomfield, J. Phys. Chem. **100**, 9977 (1996).

[10] B. I. Shklovskii, Phys. Rev. Lett. **82**, 3268 (1999).

[11] D. K. Chattoray, L. C. Gosule, and J. A. Schellman, J. Mol. Biol. **121**, 327 (1978).

[12] J. Widom and R. L. Baldwin, J. Mol. Biol. **144**, 431 (1980).

[13] N. V. Hud and K. H. Downing, Proc. Natl. Acad. Sci. USA **98**, 14925 (2001).

[14] H. G. Hansma, Annu. Rev. Phys. Chem. **52**, 71 (2001).

[15] Z. Lin, C. Wang, X. Feng, M. Liu, J. Li, and C. Bai, Nucleic Acids Res. **26**, 3228 (1998).

[16] Y. Fang and J. H. Hoh, J. Am. Chem. Soc. **120**, 8903 (1998).

[17] V. Vijayanathan, T. Thomas, T. Antony, A. Shirahata, and T. J. Thomas, Nucleic Acids Res. **32**, 127 (2004).

[18] D. Liu, C. Wang, Z. Lin, J. Li, B. Xu, Z. Wei, Z. Wang, and C. Bai, Surf. Interface Anal. **32**, 15 (2001).

[19] V. Andrushchenko, Z. Leonenko, D. Cramb, H. van de Sande, and H. Wieser, Biopolymers **61**, 243 (2002).

[20] J. C. Sitko, E. M. Mateescu, and H. G. Hansma, Biophys. J. **84**, 419 (2003).

[21] M. J. Allen, E. M. Bradbury, and R. Balhorn, Nucleic Acids Res. **25**, 2221 (1997).

[22] D. D. Dunlap, A. Maggi, M. R. Soria, and L. Monaco, Nucleic Acids Res. **25**, 3095 (1997).

[23] H. G. Hansma, R. Golan, W. Hsieh, C. P. Lollo, P. Mullen-Ley, and D. Kwoh, Nucleic Acids Res. **26**, 2481 (1998).

[24] S. Danielsen, K. M. Vårum, and B. T. Stokke, Biomacromolecules **5**, 928 (2004).

[25] Y. T. A. Chim, J. K. W. Lam, Y. Ma, S. P. Armes, A. L. Lewis, C. J. Roberts, S. Stolnik, S. J. B. Tendler, and M. C. Davies, Langmuir **21**, 3591 (2005).

[26] Y. Fang and J. Yang, J. Phys. Chem. B **101**, 441 (1997).

[27] Y. Fang and J. H. Hoh, Nucleic Acids Res. **26**, 588 (1998).

[28] M. Y. Ono and E. M. Spain, J. Am. Chem. Soc. **121**, 7330 (1999).

[29] For example, to screen the charge of a surface with a diameter of 1 cm and a surface charge of 1 electron/nm$^2$, about $3*10^{13}$ trivalent counterions are needed. This number is similar to the total amount of ions present in a 10 $\mu$M solution with a volume of 5 $\mu$L.

[30] J. Pelta, F. Livolant, and J.-L. Sikorav, J. Biol. Chem. **271**, 5656 (1996).

[31] K. Besteman, M. A. G. Zevenbergen, H. A. Heering, and S. G. Lemay, Phys. Rev. Lett. **93**, 170802 (2004).

[32] K. Besteman, M. A. G. Zevenbergen, and S. G. Lemay, Phys. Rev. E. **72**, 061501 (2005).

# Chapter 5

# The role of tension and twist in single-molecule DNA condensation

**K. Besteman, S. Hage, N. H. Dekker and S. G. Lemay**

Using magnetic tweezers, we study in real time the condensation of single DNA molecules under tension. We find that DNA condensation occurs via discrete nucleated events. By measuring the influence of an imposed twist, we show that condensation is initiated by the formation of plectonemic supercoils in the DNA. This demonstrates a strong interplay between the condensation transition and externally imposed mechanical constraints.

This chapter is under review with Physical Review Letters

## 5.1 Introduction

Despite its stiffness and high charge density, double-stranded DNA is condensed *in vivo* into highly compact structures by positively charged proteins. Morphologies and packing densities similar to those observed in sperm nuclei and in certain viruses [1, 2] can be reproduced *in vitro* using a broad array of simple tri- or quadrivalent cations [3]. This represents an ideal experimental system for testing theoretical ideas on like-charge attraction in electrolytes [4–9]. Elucidating the microscopic mechanism for DNA condensation by multivalent ions further marks an important step toward understanding more complex forms of DNA packaging since multivalent polyamines are associated with stages of the cell cycle where chromatin is highly compact [10].

Most physical studies of DNA condensation to date have concentrated on free molecules in bulk solution. This neglects the biologically relevant influence of mechanical constraints such as DNA supercoiling and forces exerted by the cellular machinery [11, 12]. For example, while the force exerted by a DNA molecule as a function of its end-to-end distance was recently measured under condensation conditions using optical tweezers [13–15], the consequences of the imposed tension on the condensation transition were not explored.

Here we investigate DNA condensation by multivalent ions at the single-molecule level using magnetic tweezers. This technique allows applying a constant pulling force on a DNA molecule while measuring its elongation in real time. Importantly, a controlled, sign-specific twist can be applied to the molecule to study the role of torsion in DNA-condensation dynamics. We show that condensation occurs via a series of force-dependent nucleation events initiated by the formation of plectonemic supercoils (loops) in the DNA.

## 5.2 Materials and Methods

Our experimental setup consisted of a single 8 kbp double-stranded DNA (dsDNA) molecule tethered between a glass surface and a 2.8 $\mu$m paramagnetic bead using digoxigenin/anti-digoxigenin and biotin/streptavidin, respectively. Nearby magnets exerted a force $F$ on the bead, pulling it away from the surface and stretching the DNA molecule. Translating and rotating the magnets allowed tuning the magnitude of $F$ and rotating the bead in the plane parallel to the surface, respectively. The extension of the DNA was monitored by measuring the position $z$ of the bead above the surface. Further details are available in Ref. [16].

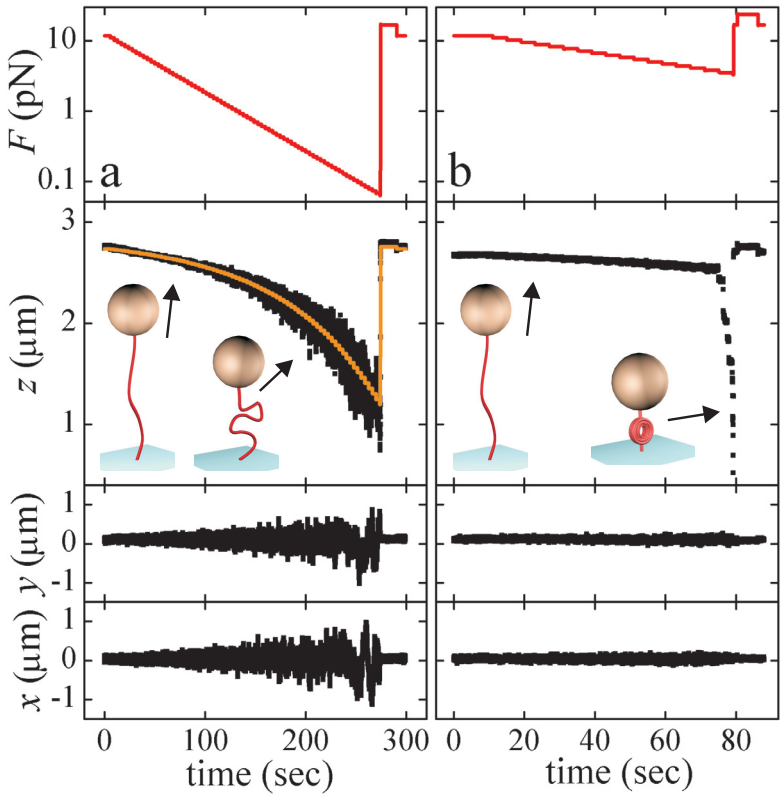


**Figure 5.1:** Measurement of DNA extension $z$ and bead position in the horizontal plane $(x, y)$ while gradually lowering the force $F$ in (a) a monovalent buffer and (b) in the same buffer with 1 mM cosep added. The solid line through the $z(t)$ data in (a) is a fit to the WLC model. All data were obtained with the same 8 kbp nicked DNA molecule.

## 5.3 Results and Discussion

### 5.3.1 Observing DNA condense in real time

A typical experiment is shown in Fig. 5.1. Starting from a large applied force $F$, we measured the DNA extension $z$ and the bead position in the horizontal plane $(x, y)$ as a function of time $t$ while gradually lowering $F$. The measurements were performed in TRIS buffer (10 mM Tris Hydroxymethylaminoethane) with pH 7.5 and a variable concentration $c$ of multivalent salt. Figure 5.1a shows that for $c = 0$ M (no multivalent ions), the DNA acted as an entropic spring. A fit to the worm-like-chain (WLC) model [17] (solid line in Fig. 5.1a) yields a persistence length $p = 52$ nm and a contour length $L = 2.85$ $\mu$m, as expected for 8 kbp nicked DNA in monovalent-salt buffer.

Figure 5.1b shows the force-extension curve of the same DNA molecule in a concentration $c = 1$ mM of the trivalent-cation cobalt sepulchrate ($[CoC_{12}H_{30}N_8]^{3+}$, cosep). At high forces this curve was similar to the data without multivalent ions, but at $F =$ 3-4 pN a sudden, rapid drop in $z$ occurred. No changes in $(x, y)$ were observed during this drop. We tentatively interpret this behavior as condensation of the DNA molecule, consistent with the previous finding by imaging individual fluorescently-labeled DNA molecules that condensation is an abrupt transition between two stable states [18]. We define the condensation force $F_c$ as the force at which the first sharp step is observed in $z(t)$, $F_c = 3.5$ pN in Fig. 5.1b.

### 5.3.2 Control experiment: DNA-surface interactions

Another possible cause for the sudden collapse, however, is sticking of the DNA to the magnetic bead or to the nearby glass surface. Multivalent ions mediate an attractive interaction between like-charged DNA strands, and could similarly result in attraction between DNA and the negatively charged, nearby surfaces. This potential experimental artefact has not been thoroughly addressed in previous studies [13–15].

To test whether sticking plays a role, we performed measurements on ds-DNA kept away from the bead and surface by stiff, rod-like spacers that consist of RecA-coated single-stranded DNA (ss-DNA). RecA is a DNA-binding protein that promotes DNA strand exchange during homologous recombination in bacteria [19]. It can polymerize on ss-DNA and ds-DNA, but the rate of binding to ds-DNA is negligible compared to that to ss-DNA at pH 7.5 [19, 20]. Figure 5.2a shows an Atomic Force Microscope (AFM, Digital Instrument NanoScope IV) image of a DNA molecule consisting of single-stranded ends of length 1.7 kb and 1.9 kb and a double-stranded middle of length 7 kbp (ss-ds-ss-DNA) on mica [see Appendix for preparation method]. Figure 5.2b-d shows ss-ds-ss-DNA on poly-L-lysine coated mica after RecA-filament formation on the ss ends, showing stiff filaments with RecA-free ds-DNA in between.

Figure 5.2e shows the results of a condensation experiment in 1 mM cosep using ss-ds-ss-DNA without RecA. For $15 > F > 8$ pN, $z$ decreased progressively with decreasing $F$. This decrease corresponds to that of a 3.6 kb (1.7 + 1.9 kb ends) ss-DNA molecule (data not shown), as expected since $z(F)$ for ds-DNA is almost constant over this range of forces. From $F = 8$ to 3.6 pN, $z$ was $\sim$2.4 $\mu$m, corresponding to the length of the 7 kbp ds-DNA. At 3.6 pN, $z$ dropped suddenly as for ds-DNA condensation. The ss-ds-ss-DNA thus behaved as the independent superposition of a 3.6 kb ss-DNA molecule and a 7 kbp ds-DNA molecule attached end to end.

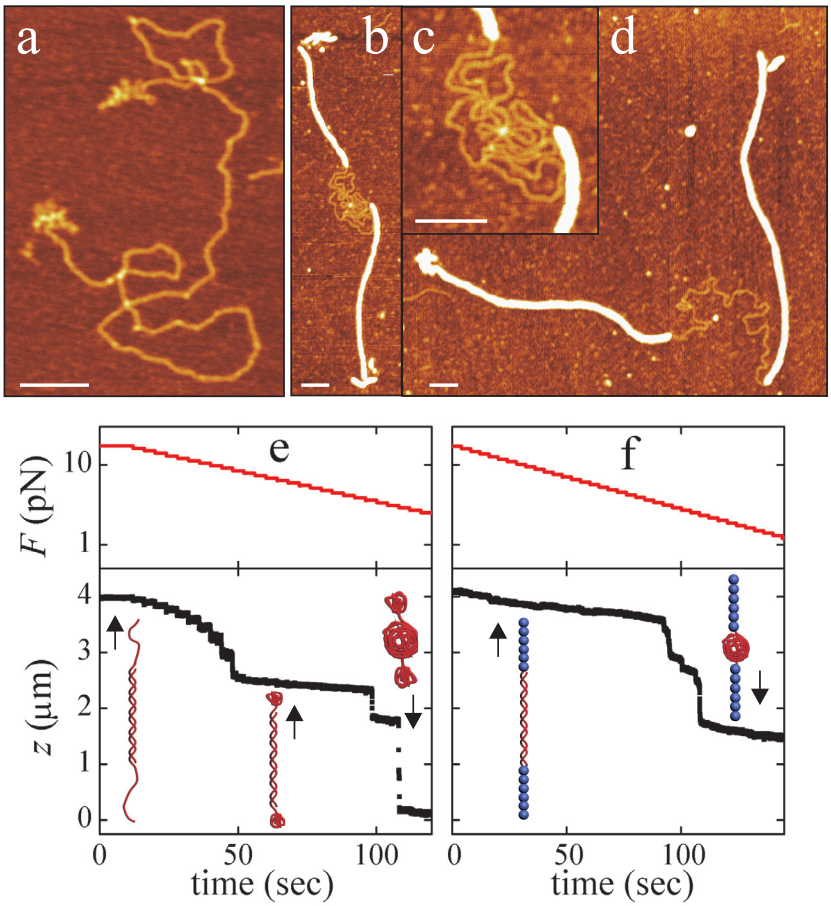


**Figure 5.2:** Tapping-mode AFM images of the ss-ds-ss-DNA (a) before and (b)-(d) after coating the single-stranded ends with RecA. (c) is a magnification of (b). Due to the large flexibility of ss-DNA, the ss ends in (a) appear as small globular structures. Scale bars represent 100 nm. Extension in 1 mM cosep of ss-ds-ss-DNA before (e) and after (f) RecA-filament formation (different molecules).

Figure 5.2f shows $z(F)$ for a RecA-modified ss-ds-ss-DNA with 1 mM cosep. The contraction of the ss-DNA from 15 to 8 pN was now absent. At $F = 3.1$ pN there was an abrupt reduction in $z$ that resembled the behavior of a pure ds-DNA molecule. Experiments on four such constructs gave an average $F_c$ of $2.9 \pm 0.4$ pN, in good agreement with $F_c$ of nicked ds-DNA molecules under the same conditions ($F_c = 3.2 \pm 0.4$ pN). Condensation stopped when the bead was about 1.8 $\mu$m from the surface, corresponding to the total length of the RecA filaments (0.85 and 0.95 $\mu$m for fully-coated 1.7 and 1.9 kb ss-DNA molecules, respectively [19, 20]). We conclude that under the conditions investigated, the observed collapse of DNA was not due to multivalent-ion-induced DNA-surface

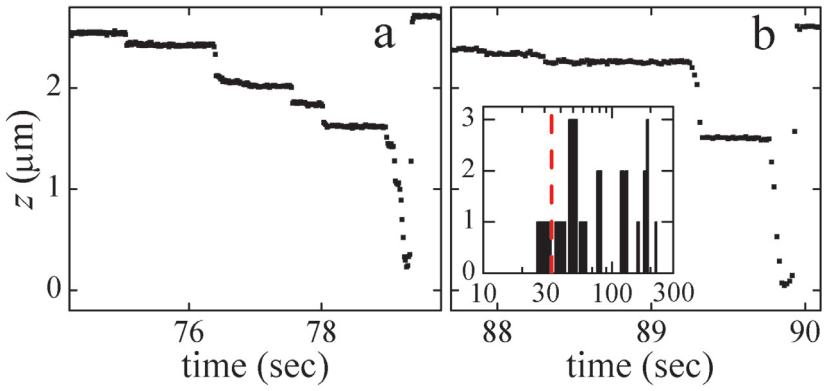


**Figure 5.3:** (a) Magnification of Fig. 1b. (b) Repeated measurement on the same molecule. Inset shows a histogram of the observed step sizes (in nm) for both measurements and a third consecutive measurement, where the dashed line indicates the size of a single loop at $F = 3.5$ pN.

interactions.

### 5.3.3 Transition state

Having established that our experiment probes intrinsic DNA condensation, we further investigated the dynamics of this process. Figure 5.3a shows the rapid $z(t)$ transient of Fig. 5.1b in more detail. Rather than a single abrupt transition, the decrease in $z$ consisted of several sudden steps separated by $\sim$1 sec plateaus. Condensation could also be reversed so as to repeat the experiment with the same molecule. De-condensation was hysteretic, typically requiring a force $\geq$15 pN to return the molecule to its original state. No backward steps were observed unless such high forces were applied. The pattern of the steps for a given molecule was slightly different each time that it was measured, as illustrated in Fig. 5.3b, but $F_c$ typically varied by no more than 20% between measurements on the same molecule. Similar results were obtained using cobalt hexamine ($[Co(NH_3)_6]^{3+}$) and spermine ($[C_{10}N_4H_{30}]^{4+}$) as condensing agent. These condensation dynamics and hysteresis indicate that DNA condensates are formed via a first-order process [18] in which activation through an energetically unfavorable transition state limits the rate of condensation.

Determining the nature of the transition state is a key step in understanding the condensation dynamics. Based on the influence of intrinsic DNA bending on the size of toroid-shaped DNA condensates, it has been proposed that condensates nucleate as loops [21]. Although bending the DNA molecule into such conformations costs energy, it permits attractive short-range electrostatic inter-

actions to come into play. The transition state has not been probed directly, however.

An important difference between our experiments and bulk studies is that a tension force $F$ is applied to the DNA molecule. The force-dependent energy for forming a plectonemic supercoil of radius $R$ is $U_{\rm loop} = \pi k_b T p/R + 2\pi RF$, where $k_b T$ is the thermal energy. The first term represents the energy needed to bend the DNA into a circle and favors large loops while the second term represents work done against the external force and favors small loops. The energetically most favorable loop radius is $R_0 = \sqrt{k_b T p/2F}$ [16]. Note that $R_0$ only characterizes the transition state for nucleation: it does not necessarily dictate the ultimate size of the condensate, nor does it imply that the condensate will be a toroid once fully formed. For the conditions in Fig. 5.3, the smallest expected steps are $2\pi R_0 = 34$ nm (using $p = 50$ nm and $F_c = 3.5$ pN). This is consistent with the observed step size distribution, as shown in the inset to Fig. 5.3b.

The rotational capabilities of magnetic tweezers permit a stringent test of the loop hypothesis for a DNA molecule under tension. The above discussion of loop formation holds for nicked DNA molecules (as used for Figs. 5.1-5.3), which are torsionally unconstrained. For unnicked molecules with fixed ends, forming a loop also implies twisting the molecule by an angle $2\pi$. The free energy associated with introducing this twist is $U_{\rm tw} = -4\pi^2 C|n|/L$, where $C$ is the torsional modulus of the DNA and $2\pi n$ is the twist angle already present in the molecule [16]. The negative sign corresponds to a loop that relieves existing twist; loops of the opposite sign are energetically unfavorable and are neglected here.

Assuming that condensation starts with loop formation, condensation is observed within our experimental time scale when the free-energy barrier for condensation $G^{\ddagger} = U_{\rm loop} + U_{\rm tw} + G_{\rm add}$ is below a critical value $G_{\rm crit}$. Here $G_{\rm add}$ represents any additional contribution to the energy barrier arising from, e.g., electrostatic repulsion between the two parts of the molecule being brought into contact. Twisting the DNA prior to condensation (increasing $|n|$) makes $U_{\rm tw}$ more negative and allows condensation at larger values of $U_{\rm loop}$ and $F$. Solving $U_{\rm loop}(F_c(n)) - U_{\rm loop}(F_c(n=0)) = |U_{\rm tw}|$ yields the expected dependence of the condensation force $F_c$ on $n$,

$$F_c(n) = F_c(n=0)\left(1 + \frac{2\pi C}{L\sqrt{2k_b T p F_c(n=0)}}|n|\right)^2. \tag{5.1}$$

The actual transition state is presumably more complex than an ideal circular plectonemic supercoil with a single contact point. In our simple description, these additional details and the values of $G_{\rm crit}$ and $G_{\rm add}$ enter into the experimentally determined parameter $F_c(n=0)$. This calculation assumes that $G_{\rm add}$

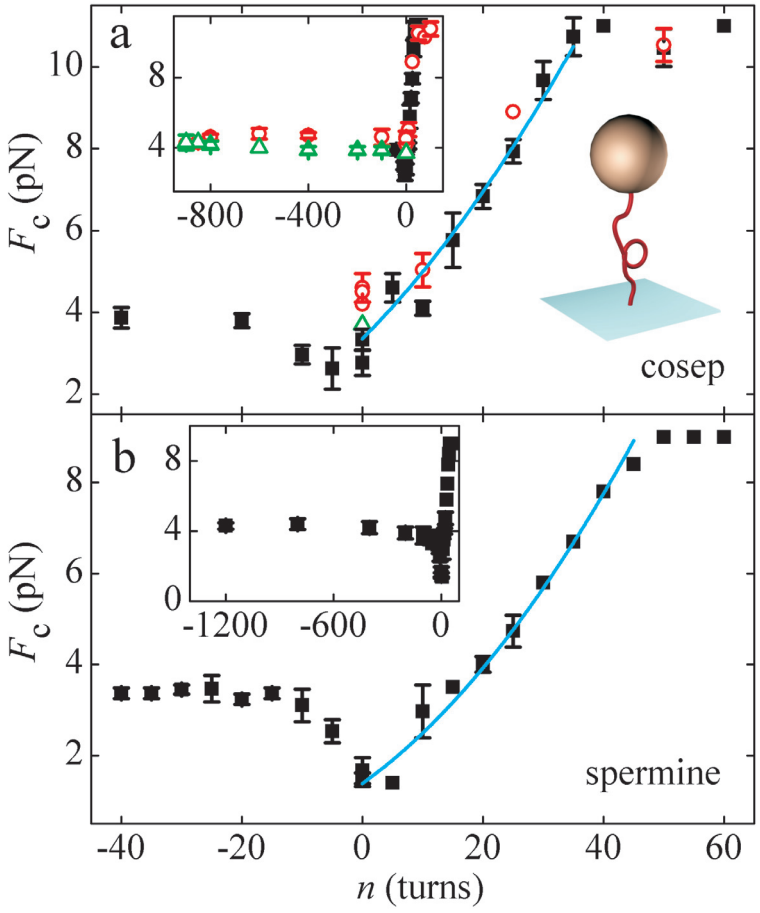


**Figure 5.4:** Condensation force $F_c$ versus rotations $n$ in 1 mM cosep (a) and spermine (b) solutions. The different symbols in (a) correspond to different molecules. The solid lines are fits to Eq. 5.1. The insets show data at large negative $n$.

is independent of $n$ and $F$. Insofar as this approximation is valid, Eq. 5.1 makes a non-trivial, experimentally testable prediction that must hold if the transition state contains a loop.

We have performed an experimental test of Eq. 5.1 using 8 kbp unnicked DNA molecules. Before each condensation measurement, the molecule was prepared by rotating the magnet $n$ times under an applied force $\geq$15 pN. No plectonemic supercoils were introduced at such high forces. Figure 5.4 shows the resulting $F_c$ as a function of $n$ for 1 mM cosep and 1 mM spermine. At $n = 0$, both the value of $F_c$ and the condensation dynamics were similar for torsionally constrained and unconstrained molecules, as expected. For non-zero values of $n$, three different regimes were observed. (i) For negative $n$, $F_c$ was practically independent of $n$ except for a slight increase between $n = 0$ and $n = -20$. (ii) For small positive

$n$, $F_c$ increased monotonically with $n$. (iii) Around $n = 35$ for cosep and 45 for spermine, $F_c$ reached a plateau and became independent of $n$.

It has previously been established that imposing a negative twist with $F > 0.3$ pN [regime (i)] does not elastically deform the DNA, but transforms regions of the molecule from B-form DNA into an alternate structure in which the bases are more exposed to solution [22]. Similarly, regime (iii) can be explained by the transition of part of the DNA to P-DNA, that has about 2.6 bases per turn. This has been observed before to occur at $F \geq 3$ pN and a degree of supercoiling $+0.037$ [22], corresponding to $n = 30$ for an 8 kbp DNA molecule [23].

In regime (ii), B-DNA retains its structural integrity, the molecule can be described as an elastic rod, and Eq. 5.1 is expected to apply. Figure 5.4 shows fits to Eq. 5.1 using $T = 293$ K, $C = 86$ nm$\times k_bT$ [16], $L = 2.7$ $\mu$m, and $p = 50$ nm (values of $p$ from 40 to 60 nm were consistent with the data). $F_c(n = 0)$ was the sole fitting parameter. The good quantitative agreement between Eq. 5.1 and the data provide strong evidence that condensation is indeed limited by the formation of plectonemic supercoils.

It has been proposed that the short-range attraction responsible for condensation is a consequence of the helical structure of ds-DNA [5]. We however observed that the condensation force is essentially independent of negative twist, even if sufficient twist is introduced as to completely transform the molecule from B-form DNA to an alternate structure ($n \approx -800$ for our 8 kbp DNA, see insets to Fig. 5.4). This suggests that the helicity of ds-DNA does not play a fundamental role in its condensation, contrary to the assumption of this model.

Other microscopic mechanisms based on spatial correlations between multivalent ions [8, 9] have mostly focused on DNA condensation as a transition between equilibrium phases. In particular, optical tweezers experiments [15] were interpreted by assuming that condensates form in a continuous, reversible process and that the applied force exactly opposes a "condensation force" equal to the condensation free energy per unit length $g_{\mathrm{cond}}$ [8, 15]. An analytical model for $F_c(c)$ based on the Strongly Correlated Liquid (SCL) hypothesis [8] was found to be consistent with the optical tweezers study of Ref. [15]. Our experiments however show that condensation of DNA under tension is an activated process that is irreversible on experimental time scales. The simple reversibility assumption $F_c = |g_{\mathrm{cond}}|$ thus does not hold under experimental conditions. Instead, decreasing $F$ lowers the barrier for nucleation and the measured $F_c$ represents the applied force at which nucleation becomes fast enough to be detected. The measured $F_c$ thus cannot be directly compared to theoretical models for $g_{\mathrm{cond}}$ [8, 9]. The condition $|g_{\mathrm{cond}}| > F$ remains a prerequisite for condensation to be energetically favorable, however, and the measured $F_c$ thus represents a lower

bound for $|g_{\mathrm{cond}}|$. This might partly explain why the simple equilibrium SCL model still provides an adequate qualitative description of the data of Ref. [15]. A more likely explanation, however, is that multivalent ions, by affecting the effective charge of the DNA, modify the barrier height for condensation through the term $G_{\mathrm{add}}$ as discussed above.

**Acknowledgement:** We thank T. van der Heijden, I. D. Vilfan and R. Seidel for useful discussions and C. Dekker for general support.

# Bibliography

[1] N. V. Hud, M. J. Allen, K. H. Downing, J. Lee, and R. Balhorn, Biochem. Biophys. Res. Commun. **193**, 1347 (1993).

[2] M. E. Cerritelli, N. Cheng, A. H. Rosenberg, C. E. McPherson, F. P. Booy, and A. C. Steven, Cell **91**, 271 (1997).

[3] V. A. Bloomfield, Biopolymers **44**, 269 (1997).

[4] For a general review see W. M. Gelbart, R. F. Bruinsma, P. A. Pincus, and V. A. Parsegian, Physics Today **53**, 38 (2000).

[5] A. A. Kornyshev and S. Leikin, Phys. Rev. Lett. **82**, 4138 (1999).

[6] I. Rouzina and V. A. Bloomfield, J. Phys. Chem. **100**, 9977 (1996).

[7] F. Oosawa, Biopolymers **6**, 1633 (1968).

[8] R. Zhang and B. I. Shklovskii, Physica A **349**, 563 (2005).

[9] R. Golestanian and T. B. Liverpool, Phys. Rev. E **66**, 051802 (2002).

[10] T. Thomas and T. J. Thomas, Cell. Mol. Life Sci. **58**, 244 (2001).

[11] W. S. Ward and D. S. Coffey, Biol. Reprod. **44**, 569 (1991).

[12] M. G. Poirier and J. F. Marko, J. Muscle Res. Cell Motil. **23**, 409 (2002).

[13] C. G. Baumann, S. B. Smith, V. A. Bloomfield, and C. Bustamante, Proc. Nat. Acad. Sci. USA **94**, 6185 (1997).

[14] C. G. Baumann, V. A. Bloomfield, S. B. Smith, C. Bustamante, M. D. Wang, and S. M. Block, Biophys. J. **78**, 1965 (2000).

[15] Y. Murayama, Y. Sakamaki, and M. Sano, Phys. Rev. Lett. **90**, 018102 (2003).

[16] T. R. Strick, J.-F. Allemand, V. Croquette, and D. Bensimon, Prog. Biophys. Mol. Biol. **74**, 115 (2000).

[17] C. Bouchiat, M. D. Wang, J.-F. Allemand, T. R. Strick, S. M. Block, and V. Croquette, Biophys. J. **76**, 409 (1999).

[18] K. Yoshikawa, M. Takahashi, V. V. Vasilevskaya, and A. R. Khokhlov, Phys. Rev. Lett. **76**, 3029 (1996).

[19] A. I. Roca and M. M. Cox, Prog. Nucl. Acid Res. Mol. Biol. **56**, 129 (1997).

[20] M. Hegner, S. B. Smith, and C. Bustamante, Proc. Nat. Acad. Sci. USA **96**, 10109 (1999).

[21] C. C. Conwell, I. D. Vilfan, and N. V. Hud, Proc. Nat. Acad. Sci. USA **100**, 9296 (2003).

[22] J.-F. Allemand, D. Bensimon, R. Lavery, and V. Croquette, Proc. Nat. Acad. Sci. USA **95**, 14152 (1998).

[23] Regime (iii) could also occur if $F$ exceeds the free energy of condensation per unit length $g_{\mathrm{cond}}$ at these high forces. This would be consistent with $F_c$ being close to the de-condensation force and the occasional occurrence of backward steps in this regime.

# Appendix

To prepare the ss-ds-ss-DNA construct, a plasmid was first nicked in both strands with 7028 bp between the nicks. The plasmid was then dephosphorylated and linearized with XhoI (New England BioLabs) to create a 5' protruding end 1945 bp from the closest nick on the same strand as the protruding end. This end was filled with biotin-labeled dUTP (Roche) using Klenow polymerase (Promega), creating a blunt end. Using SpeI (New England BioLabs) and Klenow, a digoxygenin-labeled blunt end was created 1712 bp from the second nick. Finally, Lambda Exonuclease (New England BioLabs) was used to remove part of each strand starting from the 5' end and ending at the nick on that strand. The ss-ds-ss-DNA for the AFM study was prepared in the same manner using unlabeled nucleotides.

The single-stranded ends of the ss-ds-ss-DNA molecule were coated with RecA in the magnetic-tweezers cell by flowing in 50 $\mu$L TRIS buffer with 1 mM $MgCl_2$, 33 $\mu$g/mL RecA protein (Roche) and 1.3 mM Adenosine-5'-0-(3-thitriphosphate) ($\gamma$-S-ATP, Roche), incubating for about 100 sec at $F \approx 15$ pN, and rinsing with 0.6 mL TRIS buffer. For AFM imaging, this was done by incubating TRIS buffer

with 1 mM $MgCl_2$, 50 $\mu$g/mL RecA, 1 mM $\gamma$-S-ATP and $\sim$ 2 $\mu$g/mL ss-ds-ss-DNA for 15 min at 37 °C, after which the solution was diluted 10$\times$ in TRIS with 1 mM EDTA to remove the free $Mg^{2+}$ and thereby stop the reaction.

# Chapter 6

# DNA condensation and charge inversion

**K. Besteman, K. van Eijk and S. G. Lemay**

DNA is condensed by multivalent ions into densely packed structures. We use dynamic light scattering to measure the electrophoretic mobility and show for the first time that these condensates can acquire a positive effective charge at large concentrations of multivalent ions. We further show that the multivalent-ion concentration at which charge inversion occurs coincides with the maximum in the applied force at which single-molecule DNA condensation first occurs. These observations are consistent with the prediction that DNA condensation is caused by spatial correlations between multivalent counterions.

## 6.1 Introduction

Electrostatics play a fundamental role in a variety of cellular processes that form the basis of life, yet key aspects of the physics of room-temperature electrolytes remain poorly understood. For example, highly charged DNA molecules can be densely packed *in vivo* by small, positively-charged proteins [1], and similar packing densities and morphologies can be obtained *in vitro* with small concentrations of naturally occurring multivalent ions [2–5]. The mechanism by which multivalent ions mediate an attractive interaction between highly charged DNA strands has however not been identified experimentally.

Several mechanisms have been proposed to explain DNA condensation and, more generally, like-charge attraction in multivalent electrolytes. An element common to most of these mechanisms is an inhomogeneous distribution of counterions that results in oscillations of the polarity of the charge along the length of the DNA [6–12]. Proposals for the origin of this inhomogeneous distribution include van der Waals-like fluctuations of the counterion distribution [7, 8], the intrinsic helicity of DNA [9], and the formation of a Wigner-crystal-like strongly correlated liquid (SCL) of multivalent counterions [10–12]. A direct experimental determination of the correct mechanism is however proving extremely challenging due to the short length scales involved.

One aspect of DNA condensation that can readily be accessed experimentally is so-called reentrant condensation: at very high concentrations of multivalent ions, DNA re-dissolves into individual molecules [13]. The SCL mechanism [10, 12] provides a compelling explanation for this effect. DNA condensation is predicted to be accompanied by charge inversion of the DNA at high multivalent-ion concentrations [14]; the electrostatic repulsion caused by this charge inversion ultimately renders the condensed phase energetically unfavorable [15].

Reentrant condensation has recently been observed on the single molecule level using optical tweezers in the presence of spermidine [16], where it manifests itself as a maximum in the force exerted by the DNA when condensing. SCL theory predicts that this maximum corresponds to the charge inversion concentration $c_0$ [15], the bulk concentration of multivalent ions at which the surface charge is exactly canceled by ions in the Stern layer [17, 18]. The optical-tweezers results were interpreted as corresponding to the equilibrium condensation free energy per unit length $g_{\mathrm{cond}}$ and found to be in agreement with a SCL calculation based on this assumption [16, 19]. On the other hand, charge inversion of DNA by multivalent ions has not been observed experimentally [20, 21], even though it was explicitly checked by simulations that charge inversion should result in a sign reversal of the electrophoretic mobility [22, 23].

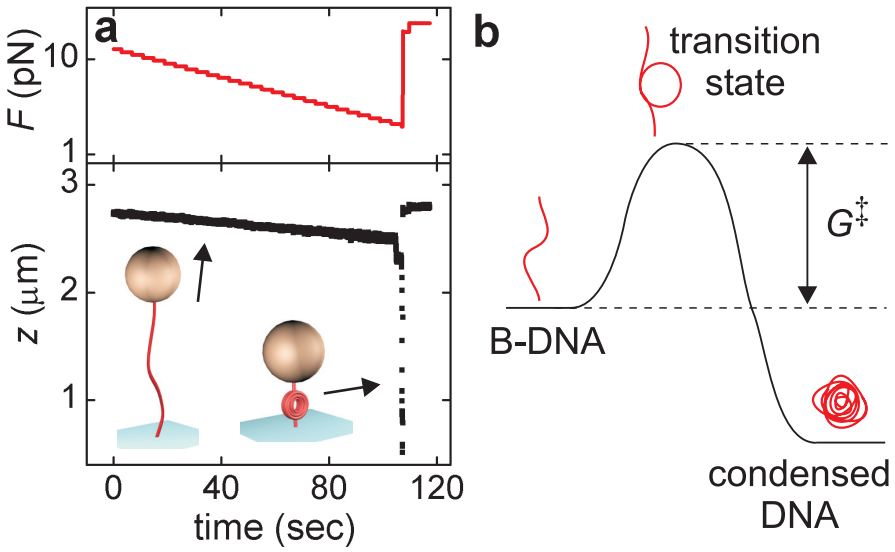


**Figure 6.1:** (a) Measurement of DNA extension $z$ while gradually lowering the force $F$ on an 8 kbp nicked DNA molecule in a 10 mM TRIS buffer with 1 mM spermine. (b) Schematic representation of the energy barrier $G^{\ddagger}$ for the nucleation of single-molecule DNA condensation under tension.

Here we present real-time observations of the condensation of single DNA molecules by multivalent ions. We show that condensation is a nucleation-limited process at all concentrations. This implies that the equilibrium model used until now to describe single-molecule condensation experiments is unsuitable. We propose an alternative model, also based on SCL theory, which quantitatively explains the data. We then present measurements of the effective charge of DNA condensates by electrophoresis and show for the first time that charge inversion of DNA does occur at sufficiently low ionic strength. The concentration at which charge inversion occurs coincides with the signature of reentrant concentration in the single-molecule experiments, consistent with the predictions of the SCL model.

## 6.2 Results and Discussion

In magnetic tweezers a single DNA molecule is tethered between a surface and a magnetic bead [24]. A nearby magnet permits applying a controlled force $F$ and twist to the molecule. Starting from large $F$, we measured the DNA extension $z$ in time $t$ while lowering $F$ in discrete steps of 7% every 4 sec (Fig. 6.1a). In a monovalent electrolyte, $z(F)$ follows the worm-like-chain model. In the

presence of multivalent ions on the other hand, a rapid, step-like decrease in $z$ is observed below a certain applied force (Fig. 6.1a). We attribute this decrease to the condensation of the single DNA molecule, and call the force at which it occurs the condensation force $F_c$.

To investigate reentrant condensation on the single-molecule level we measured $F_c$ as a function of multivalent-ion concentration $c$ for 8 kbp nicked DNA in the presence of spermine ($[C_{10}N_4H_{30}]^{4+}$), cobalt sepulchrate ($[CoC_{12}H_{30}N_8]^{3+}$, cosep), cobalt hexamine ($[Co(NH_3)_6]^{3+}$, cohex), and spermidine ($[C_7N_3H_{22}]^{3+}$) in a 10 mM monovalent TRIS buffer (Fig. 6.2). For all of these ions the measured $F_c(c)$ increased with increasing $c$ at low $c$, reached a maximum for $c = 10^{-3} - 10^{-2}$ M, and decreased again with increasing $c$ at high $c$. The dependence on $c$ was approximately parabolic in $\ln(c)$. For all ions the dynamics of the condensation over the entire concentration range consisted of discrete steps similar to the 1 mM case investigated in detail earlier (chapter 5). This implies that, over the whole range of concentration, the value of $F_c(c)$ is not set by variations in the condensate free energy $g_{\mathrm{cond}}$, but rather by modulation of the barrier height for nucleation $G^{\ddagger}$ (Fig. 6.1b).

We introduce a simple model to describe these results. The model assumes that condensation is initiated by the formation of a loop in the DNA molecule (chapter 5) and that a SCL of multivalent ions exists at the DNA surface. For condensation of a torsionally unconstrained molecule to occur, an energy barrier $G^{\ddagger} = U_{\mathrm{loop}} + G_e + G^*_{\mathrm{add}}$ must be overcome (chapter 5). Here $U_{\mathrm{loop}}$ is the mechanical energy required to bend the DNA molecule into a loop, $G_e$ is the electrostatic free energy for bringing different parts of the DNA molecule into contact, and $G^*_{\mathrm{add}}$ is an additional unknown constant independent of $F$ and $c$. The energetically most favorable loop has a force-dependent radius $R = \sqrt{k_b T p/2F}$ and a corresponding formation energy $U_{\mathrm{loop}} = \sqrt{8\pi^2 F p k T}$, where $p$ the persistence length and $k_b T$ the thermal energy [24].

The term $G_e$ appears because loop formation and subsequent condensation requires two parts of the DNA to come into close contact. Before the short-range attraction responsible for condensation can come into action, the electrostatic repulsion between like-charged objects that exists on the scale of the Debye length $\lambda_d$ must first be overcome. We estimate the magnitude of this contribution to the free-energy barrier by considering the approach of two like-charged cylinders of length $L_c$ and radius $R_c$. In the presence of multivalent ions, the DNA together with a SCL of multivalent ions at its surface can effectively be described as a cylinder with constant surface potential [25]

$$\varphi_0 = \frac{k_b T}{Ze} \ln \frac{c}{c_0}, \tag{6.1}$$

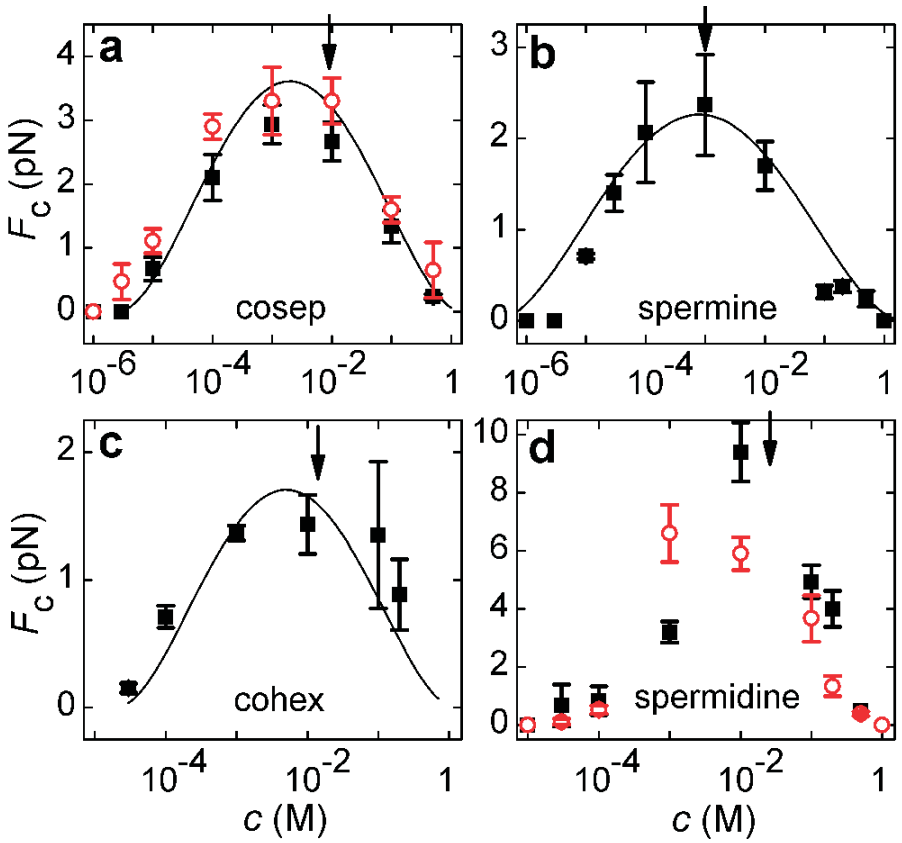


**Figure 6.2:** Condensation force $F_c$ for an 8 kbp nicked DNA molecule as a function of multivalent-ion concentration $c$ for the ions cosep (a), spermine (b), cohex (c) and spermidine (d) in a 10 mM TRIS buffer. Each data point is the average of 3 consecutive measurements with the corresponding standard deviation as the error. Each concentration series was obtained on the same molecule. In (a) and (d), data for two different molecules are shown as squares and open circles. Lines are fits to Eq. 6.3. Arrows indicate obtained values of $c_0$ from DLS measurements.

where $Z$ is the valence of the multivalent ions, $-e$ the electron charge, and $c_0$ the charge-inversion concentration. The corresponding energy for bringing the two parallel cylinders into contact is [25]

$$G_e = \frac{4\pi\epsilon\epsilon_0 L_c}{\ln \frac{\lambda_d}{R_c}} \varphi_0^2, \tag{6.2}$$

where $\epsilon$ is the dielectric constant and $\epsilon_0$ the permittivity of free space. This equation holds for $L_c > \lambda_d > R$.

Condensation is observed when $G^{\ddagger} \leq G_{\text{crit}}$, where $G_{\text{crit}}$ is the barrier that can be overcome on the time scale of our experiment. Changing the multivalent-ion concentration away from $c_0$ increases the electrostatic barrier to condensation

$G_e(c)$, and this is compensated by a corresponding decrease of the loop-formation energy $U_{\rm loop}(F)$. Equating these contributions yields the predicted concentration dependence of the condensation force,

$$F_c(c) = F_{c,\max}\left[1 - (L_c/a)\ln^2(c/c_0)\right]^2, \tag{6.3}$$

where

$$a = \frac{(Ze)^2\sqrt{pF_{c,max}/2}}{\epsilon\epsilon_0(kT)^{3/2}}\ln\left(\frac{\lambda_d}{R_c}\right). \tag{6.4}$$

For $c$ near $c_0$, Eq. (6.3) predicts a parabolic form for $F_c(c)$.

Figure 6.2a-c shows fits to Eq. (6.3). The length $L_c$ was taken as constant for all three ions, while $c_0$ and $F_{c,\max}$, which correspond to the position of the peak in $F_c(c)$, were fitted separately for each ion. The fits use $p = 50$ nm, $R_c = 1.5$ nm (complex of DNA with multivalent ions is larger than bare DNA diameter of 1 nm) and $\lambda_d = 4.3$ nm (the value in the monovalent buffer without multivalent ions [15]). The good agreement with the data in Fig. 6.2 indicate that $F_c(c)$ for spermine, cosep and cohex are well described by the model using $L_c = 9$ nm. The corresponding fitted values of $c_0$ for spermine, cosep and cohex are 0.8, 2 and 5 mM, respectively. The fitted value for the strand overlap $L_c$ is reasonable since it is a small fraction of the loop circumference $2\pi R \geq 34$ nm. This calculation indicates that the electrostatic barrier $G_e$ as derived from the SCL model has the correct dependence on $c$ and the right order of magnitude to explain our observations.

Some features of the data are not fully consistent with the simple SCL theory, however. First, the concentrations for the onset of condensation and for the maximum in $F_c$ varied between cosep and cohex, consistent with bulk measurements. This indicates that ion-specific interactions also contribute a free energy of order $kT$ per ion to condensation. Second, the ion spermidine showed different behavior from the other ions: the maximum in $F_c(c)$ was significantly higher, the spread in values of $F_c$ between different molecules was larger than with the other ions (as illustrated in Fig. 6.2d), the condensation dynamics exhibited more steps with longer time between steps, and the sharply peaked form of $F_c(c)$ could not be fitted using reasonably small values of $L_c$. This suggests that for this ion our simple model does not hold and that the transition state is more complex, or that specific interactions play a larger role.

A prediction of the model described above for spermine, cosep and cohex is that at concentrations $c$ greater than the peak concentration $c_0$ the DNA should be charge inverted. This prediction can be tested by measuring the sign of the electrophoretic mobility $\mu$ of DNA condensates. This measurement is complicated

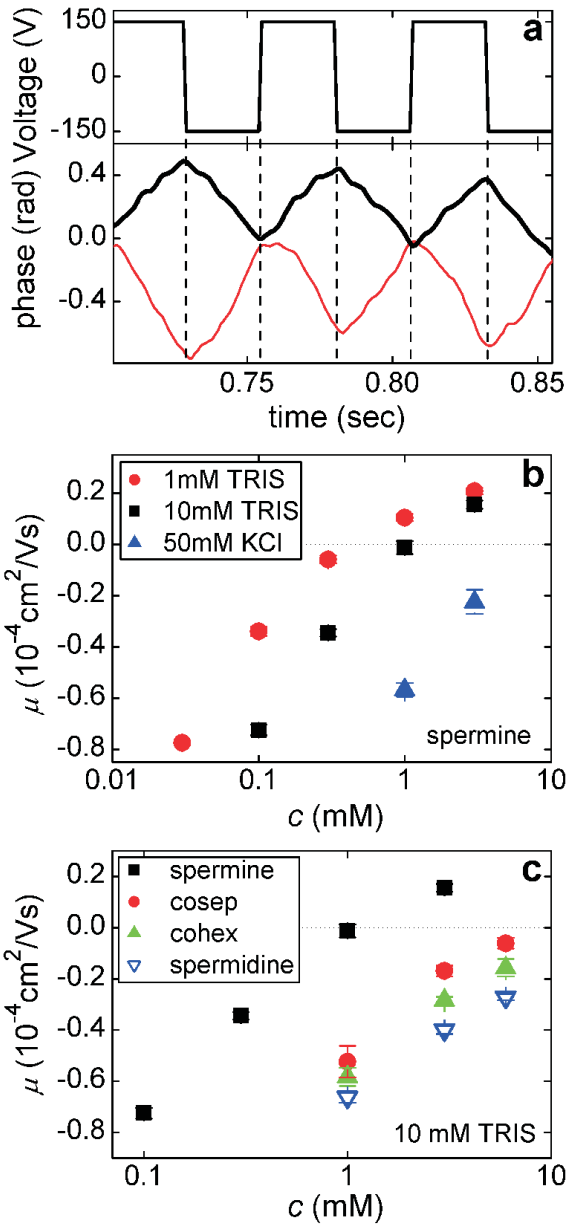


**Figure 6.3:** (a) Small part of a DLS time trace showing the applied voltage and the measured phase as a function of time in solutions containing 5 ng/$\mu$L DNA, 1 mM TRIS, and 0.1 mM (thin line) and 3 mM (thick line) spermine. (b) Electrophoretic mobility $\mu$ of condensed DNA as a function of the spermine concentration in a buffer containing 1 mM TRIS (circles), 10 mM TRIS (squares) and 10 mM TRIS plus 50 mM KCl (triangles). (c) Electrophoretic mobility $\mu$ of condensed DNA as a function of $c$ in 10 mM TRIS for spermine (squares), cosep (circles), cohex (closed triangles) and spermidine (open triangles). Each data point is the average of 3 consecutive measurements with the corresponding standard deviation as the error. DNA concentration and length are 5 ng/$\mu$L and 8 kbp, respectively.

by the fact that standard gel electrophoresis cannot be employed since the DNA condensates become immobilized in the small pores of the gel. An alternative is electrophoresis in bulk solution, but this is also difficult since the mobilities are small and easily masked by electroosmotic flows. A solution is to measure the DNA velocity while rapidly alternating the polarity of the applied voltage, thus eliminating contributions from electroosmosis. This measurement can be performed using dynamic light scattering (DLS), in which laser light scattered from the condensates and the original beam are combined and the phase of this signal is monitored over time. Condensates drifting at constant velocity in an electric field give a phase that evolves linearly in time, the rate of change being proportional to their velocity.

Figure 6.3a shows the phase signal obtained from DNA condensates in solutions containing 0.1 and 3 mM spermine. The rate of change of the phase as a function of time has opposite signs for these two concentrations, directly demonstrating that the DNA has become charge inverted at 3 mM.

Figure 6.3b shows the measured electrophoretic mobility $\mu$ of condensed DNA as a function of spermine and monovalent-ion concentrations. In a solution containing 1 mM TRIS buffer, charge inversion is observed to occur at 0.5 mM spermine concentration. Increasing the TRIS concentration to 10 mM causes the charge-inversion concentration to increase to 1 mM. Further adding 50 mM monovalent KCl salt to the 10 mM TRIS solution causes charge inversion to disappear entirely at spermine concentrations below 3 mM. Higher spermine concentrations are not accessible in our experiment since they result in large electrochemical currents causing bubbles to form at the electrodes and reaction products that influence the measurement over time. This dependence on salt concentration is reminiscent of the disappearance of charge inversion at glass surfaces at high monovalent-salt concentrations [26]. The observation that charge inversion is increasingly hindered when approaching physiological conditions may be the reason why charge inversion of DNA has not been reported earlier.

Figure 6.3c shows results for spermine, cosep, cohex and spermidine in 10 mM TRIS, the buffer concentration at which the magnetic-tweezers data of Figs. 6.1 and 6.2 were obtained. For all three ions the mobility becomes less negative with increasing $c$ at a similar rate as with spermine, but reversal of its polarity is not yet observed at the maximum concentration that is experimentally accessible. Extrapolating the observed trend by fitting a straight line on the lin-log scale between the two points closest to $\mu = 0$ yields expected charge-inversion concentrations of 9, 14 and 26 mM for cosep, cohex and spermidine, respectively.

The measured (spermine) and extrapolated (cosep, cohex and spermidine) charge inversion concentrations are compared to $F_c(c)$ obtained by magnetic

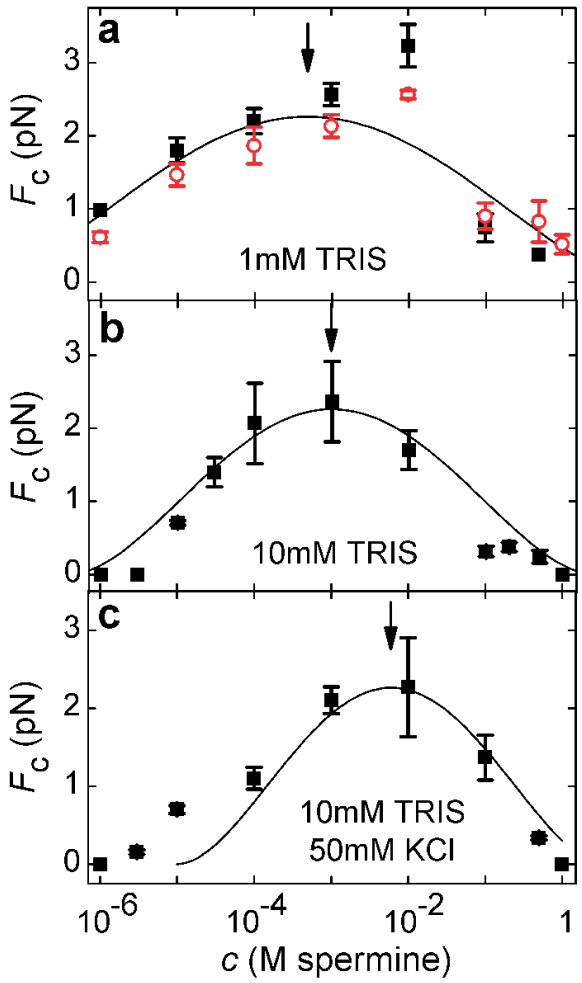


**Figure 6.4:** Condensation force $F_c$ for an 8 kbp nicked DNA molecule as a function of spermine concentration in 1 mM TRIS buffer (a), 10 mM TRIS buffer (b), and in a buffer containing 10 mM TRIS and 50 mM KCl (c). Lines are fits to Eq. 6.3 using the measured charge-inversion concentrations from Fig. 6.3b. Each data point is the average of 3 consecutive measurements with the corresponding standard deviation as the error. Different symbols in (a) are for two different molecules. Arrows indicate obtained values of $c_0$ from DLS measurements.

tweezers in Fig. 6.2, where they are represented by arrows. For all four ions the charge-inversion concentration coincides with or is slightly above the maximum in $F_c(c)$. This good agreement between these two a priori independent quantities provides strong evidence that the observed decrease in $F_c(c)$ at high concentrations is caused by the DNA becoming increasingly positively charged.

We further tested the link between charge inversion and the condensation force

by performing magnetic-tweezers measurements at different salt concentrations. Figure 6.4 shows measurements of $F_c(c)$ for the same three buffer conditions as were used for the electrophoretic-mobility measurements shown in Fig. 6.3b. In all three cases $F_c(c)$ is concave, and the overall curve shifts to higher multivalent-ion concentration with increasing monovalent ionic strength. The lines show fits to Eq. (6.3) using $c_0$ as determined from the electrophoretic measurement of Fig. 6.3b (taking $F_{c,max}$ and $L_c$ same as in Fig. 6.2b, and using $\lambda_d$ as a free parameter for Fig. 6.4c to bypass break down of Eq. (6.2) with the calculated value of $\lambda_d$ for 10 mM TRIS 50 mM KCl). The data are well describe by the $\ln^2(c/c_0)$ dependence, indicating that the shift in $c_0$ indeed translates into a corresponding shift of $F_c(c)$. The only major discrepancy is the unexpectedly large force in 1 mM TRIS and 10 mM spermine, which may result from the low salt concentration but which we do not understand at this time.

Two cautionary notes are in order. First, we measured the mobility of condensates containing multiple molecules while the condensation force was measured for single molecules. This may introduce a small systematic error in the comparison. Second, it has been argued that high ionic strength can destroy charge inversion due to incomplete dissociation of the ions [27]. We cannot rule out that this effect also plays a role at multivalent-ion concentration much greater than $c_0$.

## 6.3 Conclusions

In summary, we have demonstrated charge inversion of DNA condensates by multivalent ions and investigated condensation on the single-molecule level. The observed $c_0$ coincides with the maximum in $F_c(c)$, suggesting that charge inversion is responsible for the shape of the $F_c(c)$ curve and giving considerable support to the SCL theory of DNA condensation. A simple model based on the SCL picture and nucleation-limited condensation describes the data for several ions very well. The observed ion specificity however indicates that the structural composition and chemical affinity of the ions for DNA have to be considered before a complete understanding of DNA condensation can be obtained.

## 6.4 Materials and Methods

In our magnetic tweezers a DNA molecule with biotin-labeled nucleotides at one side and digoxigenin-labeled nucleotides at the other end was tethered between an anti-digoxigenin-coated glass surface and a 2.8 mm streptavidin-coated para-

magnetic bead (Dynabeads, M-280 Streptavidin). The glass surface formed one of the walls of a 50 $\mu$L liquid cell. The height of the bead above this surface (DNA extension, $z$) and the displacement of the bead parallel to the surface ($x$, $y$) were monitored optically. A 3.2 mm polystyrene bead (Bangs Laboratories, Inc.) bound to the surface was used as a reference for position tracking. Further details are available in Ref. [24].

Unnicked 8 kbp DNA constructs for the tweezers setup were prepared by ligating biotin- and digoxigenin-labeled fragments (∼500 bp) to a 7922 bp DNA fragment. The nicked version was prepared by dephosphorylating the biotin-labeled fragment prior to ligation.

Phosphate buffer saline (PBS) containing 10 mM phosphate, 137 mM NaCl and 2.7 mM KCl at pH 7.4, was used for reference bead attachment to the surface. Standard buffer (SB) containing 10 mM phosphate, 10 mM $NaN_3$, 10 mg/mL Bovine serum albumin (BSA) and 0.1 % Tween at pH 7.5 was used for attaching the DNA molecules to the surface. Measurements were done in a Tris Hydroxymethylaminoethane buffer (monovalent) at pH 7.5 (TRIS) with different concentrations of multivalent ions $c$ and KCl. All ions were ordered at Sigma and used as received. Solutions were changed by flushing at least 1 mL of the new solution through the flowcell. Prior to condensation measurements, the SB was removed by rinsing with 2 mL PBS, 1 mL 0.5 M KCl in TRIS, and 3 mL TRIS. This was done because BSA influenced the condensation dynamics, presumably due to BSA clustering and adhering to DNA in the presence of multivalent ions.

Electrophoretic-mobility measurements were carried out using a Malvern ZetasizerNano ZS apparatus. Equal volumes (0.5 mL) of solutions containing 8 kbp DNA fragments and multivalent ions were mixed to a final concentration of 5 ng/$\mu$L DNA and a concentration $c$ of multivalent ions. Measurements were performed after a 10 min of incubation time.

**Acknowledgement:** We thank C. Dekker for general support.

# Bibliography

[1] W. S. Ward and D. S. Coffey, Biol. Reprod. **44**, 569 (1991).

[2] V. A. Bloomfield, Biopolymers **44**, 269 (1997).

[3] N. V. Hud, M. J. Allen, K. H. Downing, J. Lee, and R. Balhorn, Biochem. Biophys. Res. Commun. **193**, 1347 (1993).

[4] T. Thomas and T. J. Thomas, Cell. Mol. Life Sci. **58**, 244 (2001).

[5] D. Hougaard, Int. Rev. Cytol. **138**, 51 (1992).

[6] W. M. Gelbart, R. F. Bruinsma, P. A. Pincus, and V. A. Parsegian, Physics Today **53**, 38 (2000).

[7] F. Oosawa, Biopolymers **6**, 1633 (1968).

[8] R. Golestanian and T. B. Liverpool, Phys. Rev. E **66**, 051802 (2002).

[9] A. A. Kornyshev and S. Leikin, Phys. Rev. Lett. **82**, 4138 (1999).

[10] I. Rouzina and V. A. Bloomfield, J. Phys. Chem. **100**, 9977 (1996).

[11] N. Grønbech-Jensen, R. J. Mashl, R. F. Bruinsma, and W. M. Gelbart, Phys. Rev. Lett. **78**, 2477 (1997).

[12] B. I. Shklovskii, Phys. Rev. Lett. **82**, 3268 (1999).

[13] J. Pelta, F. Livolant, and J.-L. Sikorav, J. Biol. Chem. **271**, 5656 (1996).

[14] B. I. Shklovskii, Phys. Rev. E **60**, 5802 (1999).

[15] T. T. Nguyen, I. Rouzina, and B. I. Shklovskii, J. Chem. Phys. **112**, 2562 (2000).

[16] Y. Murayama, Y. Sakamaki, and M. Sano, Phys. Rev. Lett. **90**, 018102 (2003).

[17] K. Besteman, M. A. G. Zevenbergen, H. A. Heering, and S. G. Lemay, Phys. Rev. Lett. **93**, 170802 (2004).

[18] K. Besteman, M. A. G. Zevenbergen, and S. G. Lemay, Phys. Rev. E **72**, 061501 (2005).

[19] R. Zhang and B. I. Shklovskii, Physica A **349**, 563 (2005).

[20] E. Raspaud, I. Chaperon, A. Leforestier, and F. Livolant, Biophys. J. **77**, 1547 (1999).

[21] Y. Yamasaki, Y. Teramoto, and K. Yoshikawa, Biophys. J. **80**, 2823 (2001).

[22] M. Tanaka, J. Phys.: Condens. Matter **16**, S2127 (2004).

[23] M. Tanaka and A. Y. Grosberg, Eur. Phys. J. E **7**, 371 (2002).

[24] T. R. Strick, J.-F. Allemand, V. Croquette, and D. Bensimon, Prog. Biophys. Mol. Biol. **74**, 115 (2000).

[25] T. T. Nguyen and B. I. Shklovskii, Phys. Rev. E **65**, 031409 (2002).

[26] F. H. J. van der Heyden, D. Stein, K. Besteman, S. G. Lemay, and C. Dekker, Phys. Rev. Lett. **96**, 224502 (2006).

[27] J. Yang and D. C. Rau, Biophys. J. **89**, 1932 (2005).

# Chapter 7

# Dynamics of protamine-induced single-molecule DNA condensation

**K. Besteman and S. G. Lemay**

The DNA found in spermatozoa is in a highly compact, transcriptionally inactive state which is induced by small basic nuclear proteins known as protamines. Here we study the dynamics of protamine-induced DNA condensation on the single-molecule level using magnetic tweezers. We observe a single DNA molecule condense in real time, investigate the influence of twist and protamine concentration on the condensation, and establish a link between these and bulk measurements of the electrophoresis of condensed DNA. These results are qualitatively similar to those obtained with simple multivalent ions as condensing agents, except that the pathway for the nucleation of condensates in the absence of torsion appears to be different.

## 7.1 Introduction

During spermiogenesis, histones are replaced by small basic nuclear proteins named protamines to form a chromatin structure that is highly condensed and transcriptionally inactive [1, 2]. Although protamines evolved rapidly and differ significantly among species, all protamines have in common a large amount of positively charged arginine [1, 3]. For example salmon protamine (salmine) contains 21 arginine of a total of 32 amino acids. In several vertebrates such as fish, protamines are small and replace histones spontaneously [1, 4]. In mammals, protamines contain in addition to arginine several cysteine that can form intra- and interprotamine disulfide bonds. Here histone replacement occurs via dedicated transition proteins [4–6].

The morphology of protamine-DNA condensates has been widely studied both by extracting chromatin from sperm [7–13] and by mixing protamines with DNA *in vitro* [4, 10, 14–16]. Protamines from a wide range of organisms condense DNA into many small particles 50-100 nm in diameter, with DNA strands running alongside each other and protamines bound in the major groove. The DNA interhelical distance is about 2.7 nm, close to the maximum packing density, and the condensate structure resembles that induced *in vitro* by multivalent cations [17].

The dynamics of the DNA-protamine condensation process are still virtually unknown due to the fast condensation rates. Recently developed single-molecule techniques allow for the study of these dynamics *in vitro*. Protamine-DNA binding was investigated on the single-molecule level by observing the condensation of a fluorescently labelled single DNA molecule stretched in a flow in the presence of protamines [18]. In this study the condensation dynamics were limited by the protamine binding to the DNA, thereby yielding values for the binding and dissociation rates of different protamines and their constituents [18–21].

Here we employ magnetic tweezers to investigate the real-time dynamics of DNA condensation by salmine *in vitro* under conditions where the dynamics are not limited by protamine binding to DNA. This technique allows us to apply a constant pulling force on the DNA molecule and observe its elongation as a function of time. In addition, we can apply a controlled, sign-specific twist to the DNA molecule and investigate its influence on the condensation dynamics. We show that the condensation process is nucleation limited and that the nature of the transition state depends on an imposed twist: at large twist it is a loop, but at small twist it is a different, achiral structure. We also investigate the influence of the protamine concentration on the condensation force in magnetic tweezers and on the electrophoretic mobility of condensed DNA. We compare these results with our earlier studies on DNA condensation by multivalent ions

(chapters 5 and 6) to establish whether the same physical principles are at work.

This chapter reports on ongoing work. The data and the conclusions that can be drawn from them are included here as a guide for future additional work.

## 7.2 Materials and Methods

In the magnetic-tweezers setup a DNA molecule containing biotin-labeled nucleotides on one side and digoxigenin-labeled nucleotides on the other end was tethered between a 2.8 $\mu$m streptavidin-coated paramagnetic bead (Dynabeads, M-280 Streptavidin) and an anti-digoxigenin-coated glass surface. The glass surface formed one of the walls of a 50 $\mu$L liquid cell. The height of the bead above this surface (which corresponds to the DNA extension $z$) and the displacement of the bead parallel to the surface ($x$, $y$) were optically monitored. A 3.2 $\mu$m polystyrene bead (Bangs Laboratories, Inc.) attached to the glass surface was used as a reference for position tracking. A nearby magnet allowed applying a controlled force $F$ and imposing a twist on the paramagnetic bead, and hence on the DNA. Further details are available elsewhere [22, 23].

Unnicked 8 kbp DNA constructs for the magnetic tweezers were prepared by ligating biotin- and digoxigenin-labeled fragments (∼500 bp) to a 7922 bp DNA fragment. The nicked version was prepared by dephosphorylating the biotin-labeled fragment prior to ligation.

Several buffer solutions were employed in the experiments. Phosphate buffer saline (PBS) containing 10 mM phosphate, 137 mM NaCl and 2.7 mM KCl at pH 7.4, was used for reference-bead attachment to the surface. Standard buffer (SB) containing 10 mM phosphate, 10 mM $NaN_3$, 0.2 mg/mL Bovine serum albumin (BSA) and 0.1 % Tween at pH 7.5 was used for attaching the DNA molecules to the surface. Measurements were done in a 10 mM Tris Hydroxymethylaminoethane buffer (monovalent) at pH 7.5 (TRIS) with different concentrations of salmon protamine $c_p$. Salmine was ordered from Sigma and used as received. Solutions were changed by flushing at least 1 mL of the new solution through the liquid cell.

Dynamic light scattering was also performed to measure the electrophoretic mobility of the protamine-DNA condensates using a Zetasizer Nano ZS apparatus (Malvern Instruments). For this purpose, equal volumes of a solution (0.5 mL) containing 1.5 kbp DNA and a solution containing salmine were mixed and incubated for 15 min prior to the measurement. The 1.5 kbp DNA fragments were produced by PCR using lambda-DNA as a template and purified using NucleoSpin.

## 7.3 Results and Discussion

### 7.3.1 Condensation experiments with magnetic tweezers

In a typical magnetic-tweezers measurement, the extension $z$ of a single DNA molecule and the displacement of the bead parallel to the surface ($x$, $y$) were measured as a function of time $t$ while lowering the applied force $F$ in steps of $\sim$7% (corresponding to a movement of 50 $\mu$m in the magnet position away from the bead) every 4 sec. Such measurements on an 8 kbp nicked DNA molecule are shown in Fig. 7.1. At $c_p = 0$ the DNA molecule acted as an entropic spring and the extension decreased gradually with decreasing force (Fig. 7.1a). The worm-like-chain (WLC) model [24] yielded a good fit with persistence length $p$ of 57 nm and a contour length $L$ of 2.8 $\mu$m, in reasonable agreement with expected values.

In the presence of 0.1 ng/$\mu$L ($\sim$0.02 $\mu$M) salmine, a very different behavior was observed, as shown in Fig. 7.1b. Already at high force, in this case around 5 pN, the extension started to deviate from the WLC behavior and a rapid decrease in $z$ was observed. A magnification of this part of the time trace is shown in Fig. 7.1c that exhibits a step-like pattern. We interpret this sudden decrease as the condensation of the single DNA molecule by protamines. The displacement of the bead parallel to the surface ($x$, $y$) did not change while the molecule was condensing. When $z$ dropped below a predetermined value, $F$ was rapidly increased so as to prevent the DNA molecule from pulling the bead all the way to the surface where it could adhere irreversibly.

The condensation process could be reversed as to repeat the experiment with the same molecule. De-condensation was hysteretic, typically requiring a force $\gtrsim$ 15 pN. No backward stepping was observed unless such high forces were applied. Figure 7.1c-e shows consecutive measurements on the same molecule. Details of the transient $z(t)$ are different every time. These results resemble our observations with multivalent ions (chapters 5 and 6), except that for protamines the transient $z(t)$ often contains time intervals in which a gradual decrease was observed in which individual steps could not be distinguished. Nonetheless, the condensation dynamics and hysteresis suggest that condensation by protamines also occurs via a first order process in which activation through an energetically unfavorable transition state is rate-limiting.

In what follows we concentrate on the condensation force $F_c$, which we define as the force at which the first sharp step in $z(t)$ was observed. For example, Fig. 7.1c-e yields values of $F_c = 5.3$, 5.7, and 4.3 pN, respectively.

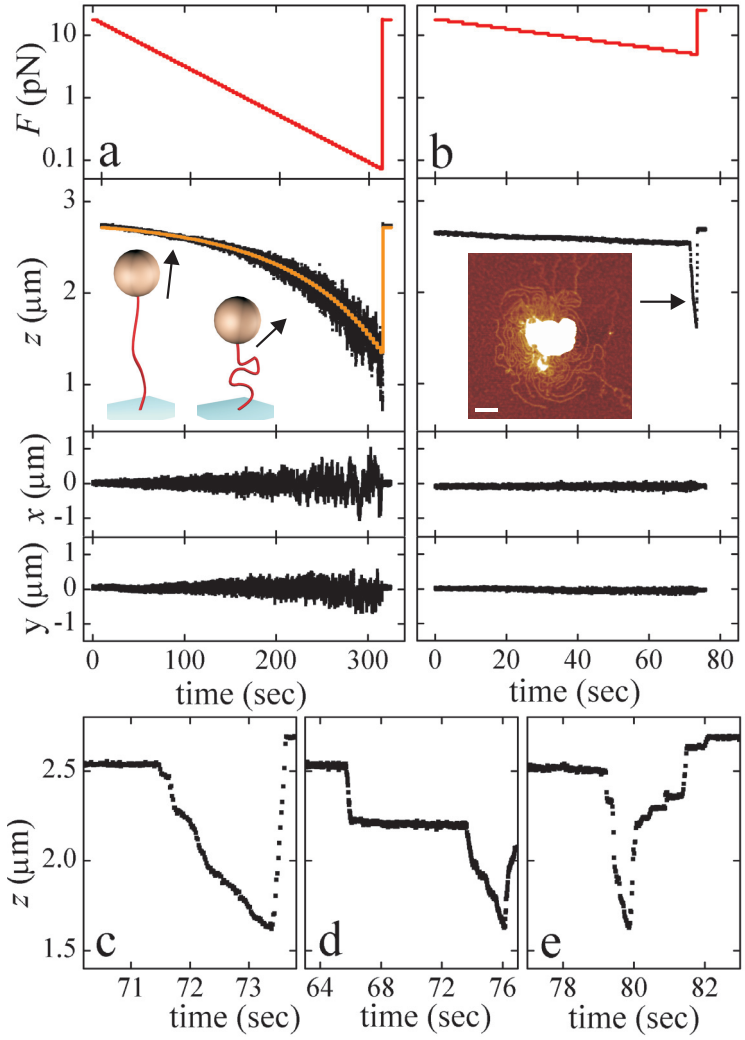


**Figure 7.1:** Measurement of DNA extension $z$ and bead position in the horizontal plane ($x$,$y$) while gradually lowering the force $F$ in (a) a monovalent buffer of pH 7.5 (TRIS) and (b) in the same buffer with 0.1 ng/$\mu$L protamine added. The solid line through the $z(t)$ data in (a) is a fit to the WLC model. Inset in (b) shows an Atomic Force Microscopy image (Digital Instruments NanoScope IV) in air on mica (scalebar represents 100 nm) of a DNA condensate prepared by mixing equal volumes of a DNA and a salmine solution to a final concentration of 1 ng/$\mu$L 1.5 kbp DNA and 3 ng/$\mu$L salmine in TRIS. (c) Magnification of (b). (d,e) Subsequent measurements on the same molecule. All data was obtained with the same 8 kbp nicked DNA molecule.

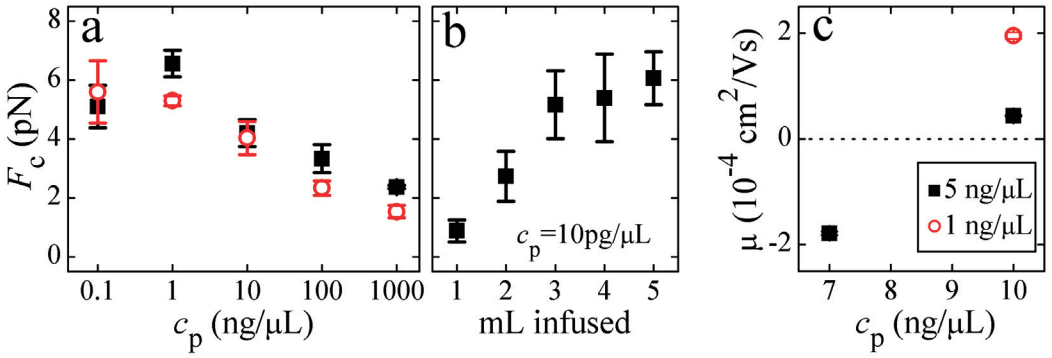


**Figure 7.2:** (a) $F_c(c_p)$ for an 8 kbp nicked DNA molecule. Each data point was taken after infusing 1 mL of the specific solution. Filled squares and open symbols show data for two different DNA molecules. (b) Condensation force as function of amount of 10 pg/$\mu$L salmine solution infused. (c) Electrophoretic mobility $\mu$ of 1.5 kbp DNA condensed with salmine at concentrations 5 ng/$\mu$L DNA (filled squares) and 1 ng/$\mu$L DNA (open circle). All data points are the average of three consecutive measurements with the standard deviation as the error. All measurements were performed in the presence of 10 mM TRIS.

### 7.3.2 Reentrant condensation and charge inversion

We measured the influence of the protamine concentration $c_p$ on the condensation force $F_c$ in 10 mM TRIS, as shown in Fig. 7.2a. $F_c$ was maximal for $c_p \approx 1$ ng/$\mu$L and decreased with increasing concentration for higher $c_p$. The maximum value $F_c \approx 6$ pN is larger than that observed for many multivalent ions, instead resembling the anomalously large value for spermidine (chapter 6). Below $c_p = 0.1$ ng/$\mu$L, $F_c$ was observed to increase with the amount of infused solution, as shown in Fig. 7.2b. This indicates that depletion of the protamine solution plays an important role at these concentrations. We have not investigated this regime further.

Although condensation does not vanish entirely, the decrease in $F_c$ with increasing $c_p$ above 1 ng/$\mu$L is very reminiscent of reentrant condensation observed with multivalent ions as condensing agents. Indeed, fully developed reentrant condensation in which condensates redissolve has recently been reported for very short DNA segments (150 bp) by salmon protamine in a bulk study using sedimentation [25]. In that same study reentrant condensation was not observed for the much longer (48 kbp) lambda DNA [25]. Our observation of a decrease in $F_c$ shows that condensation is nonetheless hindered at higher $c_p$ for long DNA.

It has been suggested that reentrant condensation is a consequence of charge inversion of the DNA [26], and this picture has received experimental support

for condensation by multivalent ions (chapter 6). In the study by Raspaud *et al*, charge inversion of protamine-induced condensates of short DNA segments was also reported for a sufficiently high protamine-DNA ratio [25]. Using the same dynamic light scattering technique, we have performed electrophoretic-mobility measurements on protamine-induced DNA condensates for 1.5 kbp DNA. First results are shown in Fig. 7.2c. Unambiguous charge inversion is observed for $c_p = 10$ ng/$\mu$L protamine. The degree of charge inversion depends on DNA concentration, however, indicating that binding of protamine to DNA is decreasing the bulk protamine concentration. As a result, the charge-inversion concentration estimated from light scattering cannot easily be compared with the concentration where $F_c(c_p)$ starts to decrease, and more extensive titration curves will be needed in the future. Nevertheless, the observation of both reentrant condensation and charge inversion is suggestive that the decrease in $F_c(c_p)$ above $c_p = 1$ ng/$\mu$L is a consequence of charge inversion of DNA by salmine, similar to the case of multivalent ions (chapter 6).

### 7.3.3 Twisting the DNA

Using the rotational capabilities of the magnetic tweezers, we showed in chapter 5 that the condensation of a single DNA molecule under tension by the multivalent-cations cobalt sepulchrate and spermine starts with the formation of a plectonemic supercoil (loop) in the DNA. Here we test whether the nucleation state for protamine-induced DNA condensation also contains a loop.

The energy cost for the formation of a loop in a torsionally unconstrained (nicked) DNA molecule under tension is $U_{\text{loop}} = \pi k_b T p/R + 2\pi RF$, where $k_b T$ is the thermal energy and $R$ is the loop radius. The first term corresponds to the energy associated with bending the DNA and favors large loops, while the second term corresponds to the work against the force and favors small loops. Minimizing $U_{\text{loop}}$ with respect to $R$ gives the energetically most favorable loop radius, $R_0 = \sqrt{k_b T p/2F}$ with the corresponding energy $U_{\text{loop}} = 2\pi\sqrt{2k_b T p F}$ [23].

In a torsionally constrained (unnicked) DNA molecule, looping also implies inducing a twist of $2\pi$ in the molecule. The free energy associated with introducing this twist is $U_{\text{tw}} = -4\pi^2 C|n|/L$, where $C$ is the torsional modulus of the DNA and $2\pi n$ is the twist angle already present in the molecule prior to loop formation [23]. The negative sign of $U_{\text{tw}}$ corresponds to a loop that relieves the twist already present in the molecule. Here we ignore loops of the opposite sign since they are energetically unfavorable.

Assuming that condensation starts with the formation of a loop, condensation is observed within the experimental timescale when the free energy barrier for

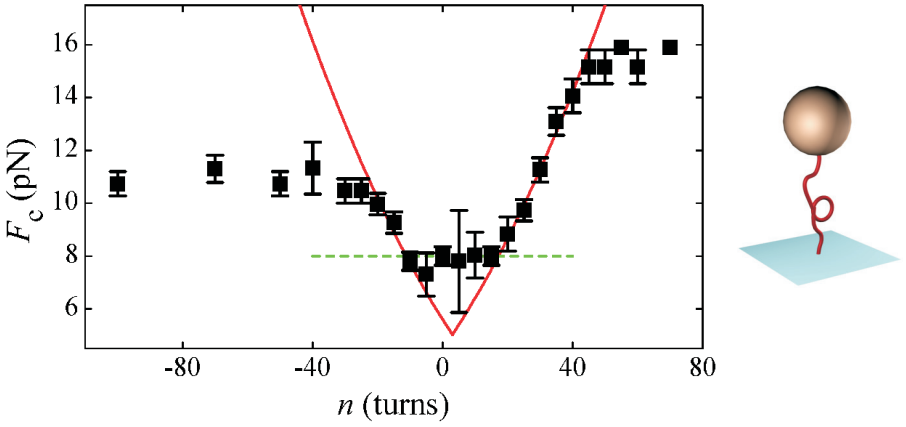


**Figure 7.3:** $F_c(n)$ of an unnicked 8 kbp DNA molecule in the presence of 0.1 ng/$\mu$L salmine. The solid line is a fit of Eq. (7.1) to the data for $20 \leq n \leq 40$, from which we obtain $p = 47$ nm.

condensation $G^{\ddagger} = U_{\text{loop}} + U_{\text{tw}} + G_{\text{add}}$ is lower than some critical value, where $G_{\text{add}}$ represents any additional contribution to the energy barrier. This results in the following equation for the condensation force $F_c(n)$ as a function of the applied twist $n$ (chapter 5):

$$F_c(n) = F_c(n=0)\left(1 + \frac{2\pi C}{L\sqrt{2k_bTpF_c(n=0)}}|n|\right)^2. \tag{7.1}$$

Figure 7.3 shows a measurement of $F_c(n)$ for an unnicked DNA molecule in the presence of 0.1 ng/$\mu$L protamine in TRIS. Several distinct regimes were observed. When applying positive rotations, the condensation force $F_c(n)$ was constant up to $n = 15$, increased with increasing $n$ for $15 < n < 45$, and was again constant for $n \geq 45$. For negative $n$, $F_c(n)$ was constant up to $n = -10$, increased for $-10 < n < -25$ and was constant for $n < -25$.

It has been demonstrated previously that negative twist at high forces ($>$ 0.3 pN) does not elastically twist the DNA, but instead causes a transformation of regions of the DNA from the B-form into an alternate structure where the bases are more exposed to the solution [27]. The plateau at $n < -25$ is consistent with this transition. The increase in $F_c$ for negative $n$ however indicate that for $0 < n < -25$ this transition does not take place for forces up to 10 pN, suggesting that salmine stabilizes the B-form of DNA.

A similar transition of the B-form structure to a different structure, P-DNA, can explain the plateau in $F_c$ for $n > 45$. P-DNA has about 2.6 bases per turn with its bases exposed to solution [27]. This transition has been observed to

occur at $F > 3$ pN and a degree of supercoiling $\sigma > +0.037$, which corresponds to $n = 30$ for an 8 kbp DNA molecule [27]. Another possible explanation for the constant, high $F_c$ at large positive $n$ is that the condensation free energy per unit length becomes smaller than the value of $F$ were looping can occur, preventing condensation despite the occurrence of loop formation.

For small positive $n$, where no transition to a different DNA structure is expected and the DNA is elastically twisted upon rotating the magnet, Eq. (7.1) is expected to hold. Eq. (7.1) predicts a continuous increase of $F_c$ with positive $n$, while we instead observe a constant $F_c$ for $n < 20$. Despite this discrepancy, we fitted that part of the data where $F_c$ does increase with $n$ ($20 \leq n \leq 40$) to Eq. (7.1) using $p$ and $F_c(n = 0)$ as fitting parameters. This resulted in a good fit to the data with $p = 47 \pm 1$ pN, in good agreement with the expected value $p = 50$ nm (solid line in Fig. 7.3). This strongly suggests that for $20 \leq n \leq 40$, the condensation starts with the formation of a loop.

Our data indicates that also at small negative $n$ the DNA is elastically twisted since a dependence of $F_c$ on $n$ was observed. $F_c(n)$ is then expected to be symmetric around $n = 0$, provided that salmine does not change the helical pitch of the DNA, and Eq. (7.1) should be applicable at negative $n$ as well. For the data in Fig. 7.3, $F_c(n)$ appears symmetric around $n = 3$, which suggests that that salmine changes the helical pitch by only a small amount, $\sim 0.4$ %. Assuming a small rotational offset of 3, the fit of Eq. (7.1) to the data at positive $n$ also describes the increase in $F_c(n)$ at negative $n$ (Fig. 7.3).

While the $n$-dependent parts of $F_c(n)$ follow Eq. (7.1) (solid line in Fig. 7.3), the observed value of $F_c$ remains approximately constant for $-10 \leq n \leq 15$ (dashed line in Fig. 7.3). This indicates that the transition state at $-10 \leq n \leq 15$ is not a loop, but rather a structure that does not involve twist and is thus insensitive to $n$. In this interpretation the loop only becomes the favored transition state when its free energy has been sufficiently reduced by twisting at $|n| \gtrsim 15$.

## 7.4 Conclusions

We have measured protamine-induced condensation of a single DNA molecule under tension in real time. The condensation dynamics reveal a nucleation-limited process. The condensation force decreases at high protamine concentrations, and the measured charge inversion of protamine-DNA condensates suggests that this decrease in $F_c$ is due to electrostatic self-repulsion of the charge-inverted DNA. The observations also suggest that salmine stabilizes the B-form of DNA and

does not significantly change its helical pitch.

These first results indicate that DNA condensation by protamines can be understood based on the same physical concepts as DNA condensation by multivalent ions, with one important difference: in the absence of torsion (ie. for nicked molecules or $n = 0$), the main mechanism for nucleation does not entail the formation of a loop in the molecule. This suggests that other structures, such as hairpins, 'tennis racquets' or kinks become dominant. It remains unclear whether this alternative condensation pathway is somehow advantageous biologically.

# Bibliography

[1] J. D. Lewis, Y. Song, M. E. de Jong, S. M. Bagha, and J. Ausió, Chromosoma **111**, 473 (2003).

[2] W. S. Ward and D. S. Coffey, Biol. Reprod. **44**, 569 (1991).

[3] J. M. Eirín-López, L. J. Frehlick, and J. Ausió, J. Biol. Chem. **281**, 1 (2006).

[4] I. D. Vilfan, C. C. Conwell, and N. V. Hud, J. Biol. Chem. **279**, 20088 (2004).

[5] M. L. Meistrich, B. Mohapatra, C. R. Shirley, and M. Zhao, Chromosoma **111**, 483 (2003).

[6] R. Balhorn, M. Corzett, and J. A. Mazrimas, Arch. Biochem. Biophys. **296**, 384 (1992).

[7] M. Loir, D. Bouvier, M. Fornells, M. Lanneau, and J. A. Subirana, Chromosoma **92**, 304 (1985).

[8] W. S. Ward, A. P. Partin, and D. S. Coffey, Chromosoma **98**, 153 (1989).

[9] M. J. Allen, C. Lee, J. D. Lee, G. C. Pogany, M. Balooch, W. J. Siekhaus, and R. Balhorn, Chromosoma **102**, 623 (1993).

[10] N. V. Hud, M. J. Allen, K. H. Downing, J. Lee, and R. Balhorn, Biochem. Biophys. Res. Commun. **193**, 1347 (1993).

[11] M. J. Allen, E. M. Bradbury, and R. Balhorn, J. Struct. Biol. **114**, 197 (1995).

[12] N. S. Blanc, A. Senn, A. Leforestier, F. Livolant, and J. Dubochet, J. Struct. Biol. **134**, 76 (2001).

[13] P. Gimenez-Bonafé, E. Ribes, P. Sautière, A. Gonzalez, H. Kasinsky, M. Kouach, P. E. Sautière, J. Ausió, and M. Chiva, Eur. J. Cell Biol. **81**, 341 (2002).

[14] P. Suau and J. A. Subirana, J. Mol. Biol. **117**, 909 (1977).

[15] M. J. Allen, E. M. Bradbury, and R. Balhorn, Nucleic Acids Res. **25**, 2221 (1997).

[16] N. V. Hud, F. P. Milanovich, and R. Balhorn, Biochemistry **33**, 7528 (1994).

[17] V. A. Bloomfield, Biopolymers **44**, 269 (1997).

[18] L. R. Brewer, M. Corzett, and R. Balhorn, Science **286**, 120 (1999).

[19] R. Balhorn, L. Brewer, and M. Corzett, Mol. Reprod. Dev. **56**, 230 (2000).

[20] L. Brewer, M. Corzett, and R. Balhorn, J. Biol. Chem. **277**, 38895 (2002).

[21] L. Brewer, M. Corzett, E. Y. Lau, and R. Balhorn, J. Biol. Chem. **43**, 42403 (2003).

[22] T. R. Strick, J.-F. Allemand, D. Bensimon, A. Bensimon, and V. Croquette, Science **271**, 1835 (1996).

[23] T. Strick, J.-F. Allemand, V. Croquette, and D. Bensimon, Prog. Biophys. Mol. Biol. **74**, 115 (2000).

[24] C. Bouchiat, M. D. Wang, J.-F. Allemand, T. Strick, S. M. Bloch, and V. Croquette, Biophys. J. **76**, 409 (1999).

[25] E. Raspaud, J. Pelta, M. de Frutos, and F. Livolant, Phys. Rev. Lett. **97**, 068103 (2006).

[26] T. T. Nguyen, I. Rouzina, and B. I. Shklovskii, J. Chem. Phys. **112**, 2562 (2000).

[27] J. F. Allemand, D. Bensimon, R. Lavery, and V. Croquette, Proc. Natl. Acad. Sci. USA **95**, 14152 (1998).

# Summary

The inside of a cell is a very crowded environment containing a high density of highly charged macromolecules such as nucleic acids and proteins in an electrolyte with diverse mobile ions. The electrostatic interactions between these macromolecules determine in large part their function, and hence the vitality of the organism. The description of electrostatics in liquids is thus one of the pillars on which detailed physical understanding of complex cellular processes must be built.

In electrolytes, mobile ions screen the charge of an object from its surroundings. Two charged objects thus only "feel" each other electrostatically when the layers of screening ions surrounding them (the electric double layers) overlap. Historically, mean-field theories have predominantly been used to describe the electric double layer. In many situations, such as an object with low charge in a monovalent salt, the mean-field approach provides a good description of the electric double layer. But it fails to rationalize several counterintuitive observations such as charge inversion and like-charge attraction that occur in the presence of multivalent ions and highly-charged objects. Recent theoretical work suggests that these systems can only be correctly described if spatial correlations between discrete multivalent screening ions are explicitly taken into account.

Charge inversion is a phenomenon where the effective charge of an object screened by multivalent counterions reverses its polarity. It has traditionally been explained by specific binding of ions: when counterions have an additional affinity for a charged surface, more will accumulate at the surface than is expected from a purely electrostatic mean-field approach. More recently, it has been pointed out that charge inversion can also occur in the absence of specific binding. In this alternate mechanism, spatial correlations between multivalent counterions at the surface lower their free energy and drive charge inversion.

We investigated the phenomenon of charge inversion by multivalent ions using atomic force spectroscopy. The force between a negatively charged silica sphere and a positively charged amine-terminated surface was measured in an electrolyte containing multivalent ions of one polarity. The interaction between

these oppositely charged surfaces changed from attractive to repulsive at high multivalent-ion concentration, directly demonstrating charge inversion of one of the surfaces.

We performed extensive measurements using chemically different multivalent ions with the same valence, as well as using the same multivalent ion in different charge states. We also measured the influence of the bare surface-charge density and of the dielectric constant of the medium. Our measurements show that charge inversion is very sensitive to the valence of the ion and the dielectric constant of the medium, but not to its exact chemical composition, indicating that charge inversion is an electrostatic effect. Charge inversion is enhanced with increasing bare surface-charge density, which implies that the ions bind cooperatively to the charged surface. These results are difficult to explain using specific binding only, but can be rationalized very well by the ion-correlation theory.

A related effect is like-charge attraction, in which two charged objects with the same polarity attract each other in the presence of multivalent counterions. A dramatic example of like-charge attraction is DNA condensation, in which negatively charged DNA molecules are condensed into compact structures. This process is relevant biologically: for example, every human cell contains $\sim$2 m DNA that must be fitted in a nucleus with a diameter of order 10 $\mu$m. *In vivo* the compaction of DNA is mainly carried out by small basic proteins, but simple multivalent ions also play a role.

Beside lowering the electrostatic repulsion between the like-charged DNA, a short-range attraction must be induced to cause DNA condensation. It is widely believed that positional correlations of multivalent ions at the DNA surface, resulting in an alternating charge along the DNA molecule, are responsible for this short-range attraction. Several possible causes for these positional correlations have been proposed. It is however experimentally difficult to directly probe the microscopic mechanism responsible for DNA condensation due to the short length scales involved (order 1 nm).

One particularly promising model of DNA condensation is once again based on the inclusion of spatial correlations beyond the mean field. This model makes an experimentally testable prediction: DNA condensation should be accompanied by charge inversion. Indeed, it was suggested that this charge inversion of the DNA is responsible for the observed de-condensation of DNA at high multivalent-ion concentration (reentrant condensation). In this scenario, charge inversion eventually becomes so pronounced as to overcome the short-range correlation-induced attraction, leading to reentrant condensation.

We measured DNA condensation on the single-molecule level using magnetic tweezers. In magnetic tweezers, a DNA molecule is tethered between a mag-

netic bead and a macroscopic surface. Nearby magnets allow applying a force and imposing a twist on the DNA molecule. We observed a single DNA molecule condense in real time by multivalent ions and protamines (proteins that condense DNA *in vivo* in sperm cells). Our observations indicate that a DNA molecule under tension condenses via a nucleation-driven process. Using the rotational capabilities of the magnetic tweezers, we demonstrated quantitatively that for several multivalent ions the nucleation state consists of a loop of DNA. We also measured the applied force at which DNA condensation first occurs, the so-called condensation force, as a function of the multivalent-ion concentration. We observed that reentrant condensation manifests itself on the single-molecule level as a maximum in the condensation force with concentration, above which the condensation force decreases with increasing concentration.

Using dynamic light scattering we also measured the electrophoretic mobility of DNA condensates. For the first time we report charge inversion of DNA by multivalent ions. We could only observe the effect at salt concentrations much lower than those relevant biologically, however, which explains why such a basic property was not observed previously. The concentration where we first observed charge inversion correlated with the concentration where the condensation force was maximal. This confirms that charge inversion accompanies the peak in the condensation force, as predicted by the ion-correlation theory.

In summary, we have experimentally investigated the significance of spatial interactions between multivalent screening ions at the surface of a charged object by investigating the phenomena of charge inversion and DNA condensation. Our observations indicate that including ion correlations in the model for the electric double layer captures much of the physics observed in these systems.

Koen Besteman
Delft, October 2006

# Samenvatting

Het binnenste van een cel bevat een hoge dichtheid aan sterk geladen macromoleculen zoals DNA en eiwitten, in een oplossing waarin zich diverse soorten mobiele ionen bevinden. De elektrostatische interactie tussen deze macromoleculen bepaalt voor een groot deel hun functie, en daarmee de vitaliteit van het organisme. De beschrijving van elektrostatica in vloeistoffen is dus een van de pilaren waarop ons fysisch begrip van complexe processen in de cel gebouwd dient te worden.

In een elektrolyt wordt de lading van een object afgeschermd van zijn omgeving door mobiele ionen. Twee geladen objecten "voelen" elkaar elektrostatisch dus alleen als er overlap is tussen de lagen van afschermende ionen (de elektrische dubbellagen). Historisch zijn voornamelijk mean-field theorieën gebruikt voor de beschrijving van de elektrische dubbellaag. In veel gevallen, zoals voor een object met een kleine lading die afgeschermd wordt door monovalente ionen, geeft mean-field theorie een goede beschrijving van de elektrische dubbellaag. Echter deze theorie faalt in de beschrijving van verscheidene tegen-intuïtieve observaties, zoals ladingsinversie en aantrekking tussen gelijk geladen objecten, die plaatsvinden als objecten met een grote lading afgeschermd worden door multivalente ionen. Recent theoretisch werk suggereert dat dergelijke situaties alleen beschreven kunnen worden als ruimtelijke interacties tussen multivalente ionen expliciet in beschouwing worden genomen.

Ladingsinversie is een fenomeen waarbij de polariteit van de effectieve lading van een object dat afgeschermd wordt door multivalente ionen, omdraait. Ladingsinversie wordt traditioneel beschreven door specifieke binding van ionen: als ionen een additionele affiniteit hebben voor het geladen oppervlak resulteert dat in een grotere hoeveelheid ionen aan het oppervlak dan verwacht wordt op grond van een elektrostatische mean-field theorie. Recentelijk is het gesuggereerd dat ladingsinversie ook zonder specifieke adsorptie kan plaatsvinden. In dit alternatieve mechanisme verlagen ruimtelijke interacties tussen multivalente ionen aan het oppervlak hun vrije energie wat leidt tot ladingsinversie.

Wij hebben het fenomeen ladingsinversie door multivalente ionen onderzocht met behulp van "atomaire kracht spectroscopie". Hiervoor hebben wij de kracht

gemeten tussen een negatief geladen bol en een positief geladen oppervlak in een elektrolyt waarin zich multivalente ionen van één type polariteit bevonden. De interactie tussen deze tegengesteld geladen oppervlakken veranderde van aantrekkend naar afstotend bij een toenemende concentratie van multivalente ionen, wat een directe demonstratie is van ladingsinversie van een van de oppervlakken.

Wij hebben gebruik gemaakt van chemisch verschillende multivalente ionen met dezelfde valentie en van eenzelfde multivalent ion in twee verschillende ladingstoestanden. Ook hebben wij de invloed van de oppervlaktelading en de diëlektrische constante van het medium gemeten. Onze metingen tonen aan dat ladingsinversie erg gevoelig is voor de valentie van het ion en de dieëlektrische constante van het medium, maar niet zozeer voor de exacte chemische structuur van het ion. Dit wijst erop dat ladingsinversie een elektrostatisch effect is. Dat ladingsinversie wordt bevorderd door de oppervlaktelading te verhogen, wijst erop dat de multivalente ionen coöperatief binden aan het geladen oppervlak. Deze resultaten zijn moeilijk te verklaren met enkel specifieke adsorptie, maar kunnen goed gerationaliseerd worden met de ionencorrelatie theorie.

Een gerelateerd effect is de aantrekking tussen gelijk geladen objecten in de aanwezigheid van multivalente ionen. Een dramatisch voorbeeld van dit fenomeen is DNA condensatie, waarbij negatief geladen DNA moleculen condenseren tot compacte structuren. Dit proces is biologisch relevant: bijvoorbeeld, iedere menselijke cel bevat $\sim$2 m DNA dat zich bevindt in een celkern van orde grootte 10 $\mu$m. De compactie van DNA *in vivo* wordt grotendeels veroorzaakt door kleine basische eiwitten, echter multivalente ionen spelen hierin ook een rol.

Buiten het verlagen van de elektrostatische afstoting tussen gelijk geladen DNA moleculen, moet er een aantrekking op korte afstanden plaatsvinden wil DNA condenseren. De meest gangbare theorie is dat positionele correlaties van multivalente ionen aan het DNA oppervlak, resulterend in een periodieke ladingsverdeling, verantwoordelijk zijn voor de attractieve interactie. Verscheidene oorzaken van deze positionele correlaties zijn voorgesteld, maar het is erg moeilijk om het microscopische mechanisme dat leidt tot DNA condensatie direct te meten als gevolg van de korte lengteschalen die hiermee gemoeid zijn (orde grootte 1 nm).

Een veelbelovend model voor DNA condensatie is, net als voor ladingsinversie, gebaseerd op ruimtelijke interacties tussen multivalente ionen. Dit model doet een experimenteel toegankelijke voorspelling, namelijk dat DNA condensatie vergezeld wordt door ladingsinversie van het DNA. Het is voorspeld dat deze ladingsinversie van DNA verantwoordelijk is voor de geobserveerde decondensatie van DNA bij hoge concentraties van multivalente ionen. In dit scenario wordt ladingsinversie zo groot, dat de afstotende elektrostatische interactie het

uiteindelijk wint van de aantrekkende interactie.

Wij hebben DNA condensatie gemeten op het niveau van een enkel molecuul met behulp van een "magnetische pincet". In de magnetische pincet opstelling is een DNA molecuul opgespannen tussen een magnetische bol en een macroscopisch oppervlak. Met magneten kan een kracht en een moment uitgeoefend worden op het DNA molecuul. Wij hebben live de condensatie van een enkel DNA molecuul gevolgd, geïnduceerd door multivalente ionen en protaminen (eiwitten die DNA in spermacellen condenseren). Onze metingen wijzen erop dat de condensatie van een DNA molecuul onder spanning een nucleatie gedreven proces is. Met behulp van de rotationele capaciteiten van de magnetische pincet hebben wij kwantitatief laten zien dat voor verscheidene multivalente ionen de condensatie van DNA begint met de formatie van een lus in het DNA. Ook hebben wij de maximale kracht gemeten waarbij condensatie nog plaatsvindt, de condensatiekracht, als functie van de concentratie multivalente ionen. Onze resultaten laten zien dat decondensatie op het enkel molecuulniveau zich manifesteert als een maximum in de condensatiekracht, waarboven de condensatiekracht afneemt bij een toenemende concentratie van multivalente ionen.

Door gebruik te maken van "dynamische licht verstrooiing", hebben we de elektroforetische mobiliteit van DNA condensaten gemeten. Voor het eerst laten wij zien dat DNA ladingsinversie plaatsvindt door multivalente ionen. Als gevolg van experimentele complicaties hebben wij dergelijke metingen niet kunnen doen bij fysiologische zoutconcentraties, wat kan verklaren dat deze fundamentele eigenschap niet eerder geobserveerd was. De laagste concentratie multivalente ionen waarbij ladingsinversie optreedt, blijkt overeen te komen met het maximum in de condensatiekracht. Dit bevestigt dat ladingsinversie en de piek in de condensatiekracht elkaar vergezellen, zoals voorspeld door de ionencorrelatie theorie.

Samenvattend hebben wij experimenteel onderzoek gedaan naar het belang van ruimtelijke interacties tussen multivalente ionen aan een geladen oppervlak, door de fenomenen ladingsinversie en DNA condensatie te bestuderen. Onze observaties wijzen erop dat door het meenemen van ionencorrelaties in het model voor de elektrische dubbellaag veel van de geobserveerde fysica van dergelijke systemen beschreven kan worden.

Koen Besteman
Delft, oktober 2006

# Acknowledgement

My "Delft life"began about nine years ago with the study Applied Physics. After four years of mostly courses the real work was about to start. I had to make a decision where to do my Master research. The reason for joining the Molecular Biophysics group (MB) at that time was largely supplied by the head of MB, Prof. Cees Dekker. It was his enthusiastic reception and the nice atmosphere he created in his new-born group that made me decide to join MB. During my Master research I was fortunate to work in close contact with Cees. Although he was not directly involved in the daily experimental work during my Ph.D., he contributed a lot to this work by discussions and by creating the perfect environment to do experimental science and have fun.

It was not hard for me to decide to lengthen my stay in MB as a Ph.D. student. I got the opportunity to begin a new line of research with the person that should be acknowledged the most. Serge Lemay at that time was an UD in MB and was shifting his research from low- to room temperature. In addition to heating up his carbon-nanotube research, he started investigating ionic systems at the nanoscale. Over the last four years I got to know Serge as a nice and gentile person. When it comes to science, his quick thinking, large general knowledge and practical approach make him a "lean mean science machine". Serge, thanks for getting me through my Ph.D. and I wish you and your wife all the happiness with your new-born son.

Serge and I were part of several research teams that conducted the research described in this thesis. The "charge inversion of macroscopic surfaces team" consisted of several other members. Marcel Zevenbergen started as a Master student on the project. When he joined the team, the project certainly got a big boost due to his hard and smart work. He is currently doing a Ph.D. in MB and is a very enthusiastic MB member, especially during group outings that involve ice or paint. Dirk Heering was a postdoc at MB and, with an electrochemistry background, was the ion expert of the team. He is largely responsible for the good choice of multivalent ions. Frank van der Heyden initiated a second charge-inversion team, of which I was lucky to be a small part. He brought charge

inversion together with streaming currents in nanochannels, which turned out to be a very fruitful marriage. All of the charge-inversion work has greatly benefitted from discussions with Prof. Lyklema from Wageningen University.

The "DNA condensation team" had several other members beside Serge and me. First of all Koert van Eijk, a Master student who made most of the AFM images on condensates and worked very hard trying to observe whether DNA charge inversion occurs. In addition, he had a large contribution to my table-soccer fun at MB. Nynke Dekker, Daniel Koster, Ralf Seidel, and Thijn van der Heijden all contributed to the magnetic tweezers fun and frustration. Thijn, who is the DNA-repair fanatic of MB (word goes that his own DNA does not contain a single break), was also closely involved in the preparation of the spacers using RecA. The work has benefitted a lot from the help of Igor Vilfan, who is an expert on DNA condensation. Another large contribution came from Susanne Hage. When we came with the "crazy spacer idea", she actually succeeded in making a DNA construct that consisted of a double-stranded middle part with single-stranded ends. Ya-Hui Chien and Peter Veenhuizen also contributed to this nice piece of DNA engineering, as well as to the making of the infinite amount of other DNA constructs that we have used during the past four years. I also want to thank Ulrike Ziese from the electron-microscopy group at Delft for obtaining TEM images of condensed DNA.

A big thanks goes to the Technical staff of MB that consisted of Dick Korbee, Jaap Beekman, and Jelle van der Does. In addition, I want to acknowledge Liset de Legé, Elsemarieke Kuiper, and computer expert Jack Tekelenburg for their general assistance. FOM and NWO are acknowledged for the funding of this research.

I guess that spending such a long time in a research group (or at any other group/company) must be unbearable when going to work is only about working. Fortunately I didn't get into such a situation at MB, especially due to my three officemates that often kept me from my work (and vice versa). Thijn, Martin, and Ralph, in addition to your large contribution to this thesis by the many scientific discussions that we had and all the other help you guys provided, I also want to acknowledge you for all the discussions on unrelated topics from science on which I cannot elaborate here. For the same reasons I want to acknowledge all other members of the "MB Ph.D. team", in particular Daniel (going to miss our many romantic dinners at the Aula) and Frank.

Many postdocs and Master students that contributed a lot to the life in MB have joined and left the group during my stay. These are too many to name personally, so I would like to collectively thank them for the collaborations in science and for the fun we had during normal workdays, coffee breaks with cake,

table-soccer games, group trips, conferences, and borrels. It must be difficult to find another group/company where one can meet so many nice and interesting persons in a Ph.D. time.

Last but certainly not least I want to thank the home team for their support. Debby, Ineke, Koos, Bart, and Karel, thanks for your understanding and support when I got home very late again and neglected all of you. In addition, I want to acknowledge my soccer team (champion for two years in a row!) for giving me the opportunity to get rid of my frustrations in a healthy manner on the field when the tweezers had a day off again.

Koen Besteman
Delft, October 2006

# Curriculum Vitae

Koen Besteman

| | |
|---|---|
| 29-06-1979 | Born in The Hague, The Netherlands. |
| 1991-1997 | V.W.O. at the 'Zandvliet College' in The Hague. |
| 1997-2002 | M.Sc. Applied Physics at Delft University of Technology.<br>Undergraduate research in the Molecular Biophysics group of prof. dr. C. Dekker.<br>Subject: Carbon nanotubes as single-molecule biosensors. |
| 2002-2006 | Ph.D. research at Delft University of Technology in the Molecular Biophysics group of prof. dr. C. Dekker.<br>Subject: Charge inversion and DNA condensation by multivalent ions. |

# List of publications

1. *Enzyme-Coated Carbon Nanotubes as Single-Molecule Biosensors*
   K. Besteman, J.-O Lee, F. G. M. Wiertz, H. A. Heering and C. Dekker.
   Nano Letters **3**, 727 (2003).

2. *Direct Observation of Charge Inversion as a Universal Electrostatic Phenomenon*
   K. Besteman, M. A. G. Zevenbergen, H. A. Heering and S. G. Lemay.
   Physical Review Letters **93**, 170802 (2004).

3. *Charge inversion by multivalent ions: Dependence on dielectric constant and surface-charge density*
   K. Besteman, M. A. G. Zevenbergen, and S. G. Lemay.
   Physical Review E **72**, 061501 (2005).

4. *Charge Inversion at High Ionic Strength Studied by Streaming Currents*
   F. H. J. van der Heyden, D. Stein, K. Besteman, S. G. Lemay, and C. Dekker.
   Physical Review Letters **96**, 224502 (2006).

5. *The role of tension and twist in single-molecule DNA condensation*
   K. Besteman, S. Hage, N. H. Dekker, and S. G. Lemay.
   Under review with Physical Review Letters.

*Articles based on chapters 4 and 6 are being prepared for submission.*